Report No.416

epa Research

Development and Application of Monte Carlo Models for High-purity Germanium Gamma Spectrometry

Authors: Luis León Vintró and Niall Murphy

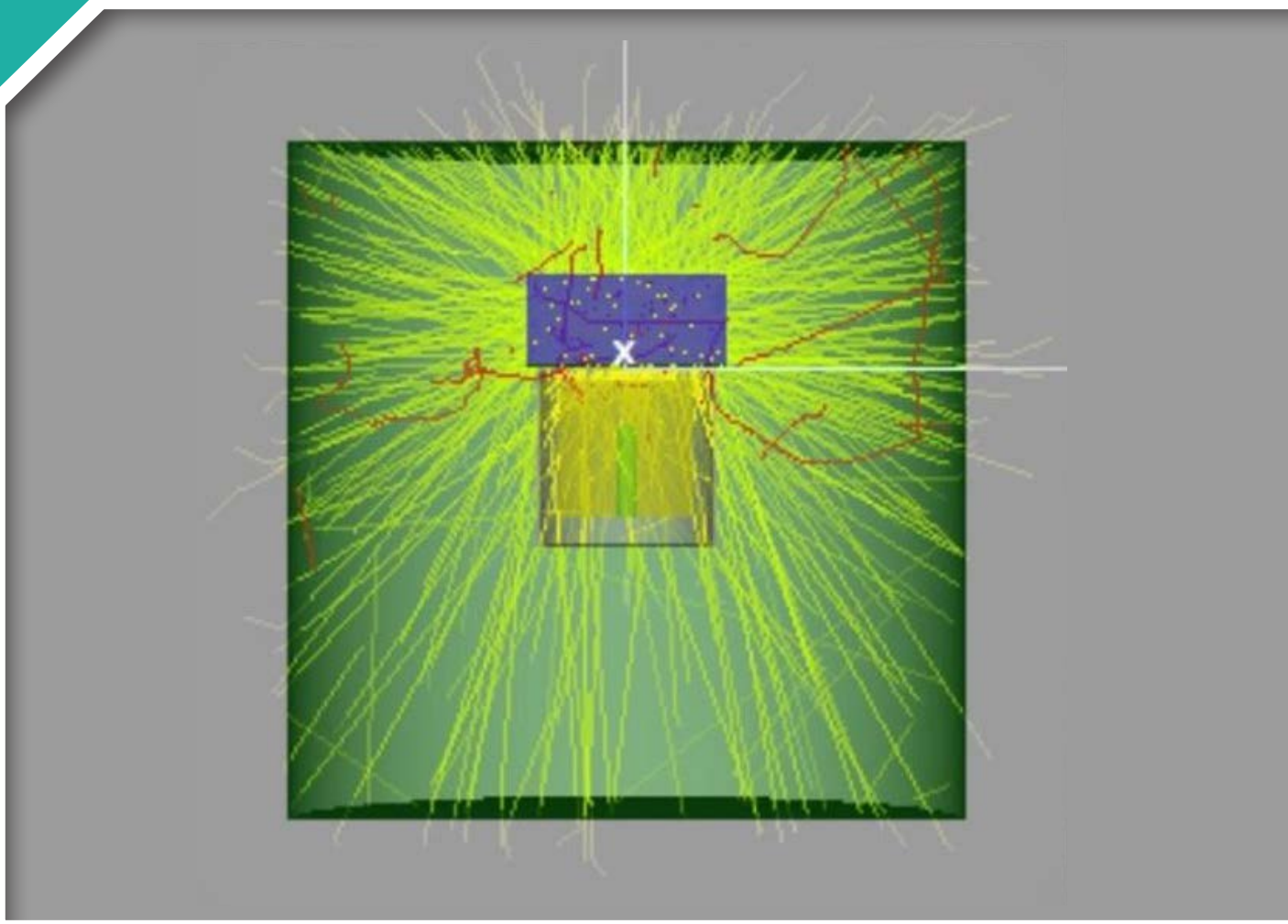

www.epa.ie

Rialtas na hÉireann
Government of Ireland

ENVIRONMENTAL PROTECTION AGENCY

The Environmental Protection Agency (EPA) is responsible for protecting and improving the environment as a valuable asset for the people of Ireland. We are committed to protecting people and the environment from the harmful effects of radiation and pollution.

The work of the EPA can be divided into three main areas:

Regulation: *We implement effective regulation and environmental compliance systems to deliver good environmental outcomes and target those who don't comply.*

Knowledge: *We provide high quality, targeted and timely environmental data, information and assessment to inform decision making at all levels.*

Advocacy: *We work with others to advocate for a clean, productive and well protected environment and for sustainable environmental behaviour.*

Our Responsibilities

Licensing

We regulate the following activities so that they do not endanger human health or harm the environment:

- waste facilities *(e.g. landfills, incinerators, waste transfer stations)*;
- large scale industrial activities (*e.g. pharmaceutical, cement manufacturing, power plants)*;
- intensive agriculture *(e.g. pigs, poultry)*;
- the contained use and controlled release of Genetically Modified Organisms *(GMOs)*;
- sources of ionising radiation *(e.g. x-ray and radiotherapy equipment, industrial sources)*;
- large petrol storage facilities;
- waste water discharges;
- dumping at sea activities.

National Environmental Enforcement

- Conducting an annual programme of audits and inspections of EPA licensed facilities.
- Overseeing local authorities' environmental protection responsibilities.
- Supervising the supply of drinking water by public water suppliers.
- Working with local authorities and other agencies to tackle environmental crime by co-ordinating a national enforcement network, targeting offenders and overseeing remediation.
- Enforcing Regulations such as Waste Electrical and Electronic Equipment (WEEE), Restriction of Hazardous Substances (RoHS) and substances that deplete the ozone layer.
- Prosecuting those who flout environmental law and damage the environment.

Water Management

- Monitoring and reporting on the quality of rivers, lakes, transitional and coastal waters of Ireland and groundwaters; measuring water levels and river flows.
- National coordination and oversight of the Water Framework Directive.
- Monitoring and reporting on Bathing Water Quality.

Monitoring, Analysing and Reporting on the Environment

- Monitoring air quality and implementing the EU Clean Air for Europe (CAFÉ) Directive.
- Independent reporting to inform decision making by national and local government *(e.g. periodic reporting on the State of Ireland's Environment and Indicator Reports)*.

Regulating Ireland's Greenhouse Gas Emissions

- Preparing Ireland's greenhouse gas inventories and projections.
- Implementing the Emissions Trading Directive, for over 100 of the largest producers of carbon dioxide in Ireland.

Environmental Research and Development

- Funding environmental research to identify pressures, inform policy and provide solutions in the areas of climate, water and sustainability.

Strategic Environmental Assessment

- Assessing the impact of proposed plans and programmes on the Irish environment *(e.g. major development plans)*.

Radiological Protection

- Monitoring radiation levels, assessing exposure of people in Ireland to ionising radiation.
- Assisting in developing national plans for emergencies arising from nuclear accidents.
- Monitoring developments abroad relating to nuclear installations and radiological safety.
- Providing, or overseeing the provision of, specialist radiation protection services.

Guidance, Accessible Information and Education

- Providing advice and guidance to industry and the public on environmental and radiological protection topics.
- Providing timely and easily accessible environmental information to encourage public participation in environmental decision-making *(e.g. My Local Environment, Radon Maps)*.
- Advising Government on matters relating to radiological safety and emergency response.
- Developing a National Hazardous Waste Management Plan to prevent and manage hazardous waste.

Awareness Raising and Behavioural Change

- Generating greater environmental awareness and influencing positive behavioural change by supporting businesses, communities and householders to become more resource efficient.
- Promoting radon testing in homes and workplaces and encouraging remediation where necessary.

Management and structure of the EPA

The EPA is managed by a full time Board, consisting of a Director General and five Directors. The work is carried out across five Offices:

- Office of Environmental Sustainability
- Office of Environmental Enforcement
- Office of Evidence and Assessment
- Office of Radiation Protection and Environmental Monitoring
- Office of Communications and Corporate Services

The EPA is assisted by an Advisory Committee of twelve members who meet regularly to discuss issues of concern and provide advice to the Board.

EPA RESEARCH PROGRAMME 2021–2030

Development and Application of Monte Carlo Models for High-purity Germanium Gamma Spectrometry

(2016-HW-MS-7)

EPA Research Report

Prepared for the Environmental Protection Agency

by University College Dublin

Authors:

Luis León Vintró and Niall Murphy

ENVIRONMENTAL PROTECTION AGENCY
An Ghníomhaireacht um Chaomhnú Comhshaoil
PO Box 3000, Johnstown Castle, Co. Wexford, Ireland

Telephone: +353 53 916 0600 Fax: +353 53 916 0699
Email: info@epa.ie Website: www.epa.ie

© Environmental Protection Agency 2022

ACKNOWLEDGEMENTS

This report is published as part of the EPA Research Programme 2021–2030. The EPA Research Programme is a Government of Ireland initiative funded by the Department of the Environment, Climate and Communications. It is administered by the Environmental Protection Agency, which has the statutory function of co-ordinating and promoting environmental research.

The authors would like to acknowledge Lorraine Currivan (Environmental Protection Agency, EPA) and Paul McGinnity (International Atomic Energy Agency, IAEA) for their support and continued advice during this project.

DISCLAIMER

Although every effort has been made to ensure the accuracy of the material contained in this publication, complete accuracy cannot be guaranteed. The Environmental Protection Agency, the authors and the steering committee members do not accept any responsibility whatsoever for loss or damage occasioned, or claimed to have been occasioned, in part or in full, as a consequence of any person acting, or refraining from acting, as a result of a matter contained in this publication. All or part of this publication may be reproduced without further permission, provided the source is acknowledged.

This report is based on research carried out/data from 1 September 2016 to 31 August 2020. More recent data may have become available since the research was completed.

The EPA Research Programme addresses the need for research in Ireland to inform policymakers and other stakeholders on a range of questions in relation to environmental protection. These reports are intended as contributions to the necessary debate on the protection of the environment.

EPA RESEARCH PROGRAMME 2021–2030
Published by the Environmental Protection Agency, Ireland

ISBN: 978-1-80009-054-5 July 2022

Price: Free Online version

Project Partners

Luis León Vintró
School of Physics
University College Dublin
Belfield
Dublin 4
Ireland
Tel.: +353 1 716 2221
Email: luis.leon@ucd.ie

Niall Murphy
School of Physics
University College Dublin
Belfield
Dublin 4
Ireland

Christopher Burbidge
Office of Radiation Protection and
Environmental Monitoring
3 Clonskeagh Square
Dublin 14
Ireland

Contents

List of Figures

List of Tables

Executive Summary

The aim of this Environmental Protection Agency (EPA)-funded project was to develop and implement suitable Monte Carlo calibration methods for the assay of natural and artificial radionuclides using the high-purity germanium (HPGe) gamma spectrometers at the EPA's Office of Radiation Protection and Environmental Monitoring (ORM) analytical laboratory, so that self-attenuation and true coincidence summing effects can be corrected for, and detector efficiencies established for a variety of geometries and sample matrices without the need to carry out multiple, time-consuming and expensive measurements using certified calibration standards.

At the EPA's ORM analytical laboratory, self-attenuation and coincidence summing effects are accounted for using GESPECOR, a dedicated Monte Carlo package specifically developed for the efficiency calibration of HPGe gamma-ray spectrometers. However, as with other Monte Carlo packages, reliable results can be achieved only if accurate models of the detector, counting geometries and shielding are available as inputs to run the simulations. Although nominal parameters for specific detector models can be obtained from manufacturer specifications, significant uncertainties often remain. The lack of accurate knowledge of some detector parameters can result in Monte Carlo computed efficiency values that differ significantly from those determined experimentally; therefore, an optimisation process is normally required to ensure that experimentally determined efficiencies are accurately reproduced by the simulation.

Before the start of this project, optimisation of model parameters at the EPA's ORM analytical laboratory was carried out manually by running GESPECOR and iteratively adjusting the most sensitive detector parameters from their baseline values to get the best possible agreement between experimental and computed efficiencies for a range of counting geometries. Although good agreement could be achieved using this approach, it required continuous manual intervention from the user to guide the optimisation search and was, therefore, a slow and time-consuming process. A key aim of this project was to automate this optimisation process by developing user-friendly, operational software. Initially using a set of nominal (but realistic) input parameters describing an HPGe detector, together with experimentally determined full-energy peak (FEP) efficiencies for a variety of counting geometries, this new, user-friendly software will use GESPECOR to produce an optimised model of the detector by applying suitable optimisation algorithms *without any further user intervention*.

The software application developed during this project acts as a front end for the GESPECOR software to conduct iterative runs and, using an optimisation algorithm based on a covariance matrix adaptation evolution strategy (CMAES), allows the use of several experimental FEP efficiency curves (corresponding to multiple geometries) in parallel, to optimise all (or selected) detector parameters. In this way, an optimised set of parameters is found that simultaneously fits all experimental curves and accounts for the sensitivity of various parameters under different counting geometry arrangements. The final set of optimised parameters and calculated FEP efficiencies for each of the geometries used in the process are saved and the efficiencies displayed in a graphical form in a plot window.

Application of this optimisation approach to each of the HPGe detectors currently in operation at the EPA's ORM has shown that, with relatively little effort from the user, it is possible to achieve excellent agreement between experimental FEP efficiencies and Monte Carlo calculations, with mean absolute deviations between modelled and experimental efficiencies of $< 2\%$ for all geometries, and individual absolute deviation no higher than 4%.

Through a comprehensive set of characterisation and validation experiments, it has been demonstrated that the optimised models obtained can be used to confidently predict FEP efficiencies for arbitrary source geometries by direct Monte Carlo simulation, to perform efficiency transfer from one matrix to another and to compute accurate values for self-attenuation and true coincidence summing correction factors.

Practical methodologies have been developed for the accurate determination of linear attenuation coefficients required for self-attenuation corrections and applied to a number of environmental matrices routinely analysed by the EPA's ORM for the determination of appropriate self-attenuation correction factors. Participation in international environmental radioactivity proficiency test exercises (PTEs) has allowed validation of the accuracy of derived self-attenuation and coincidence summing correction factors. Furthermore, the accuracy of FEP and total efficiencies generated by GESPECOR has also been benchmarked against those obtained by other Monte Carlo codes such as the electron gamma shower (EGSnrc), GEANT4, PENELOPE and MCNP.

1 Introduction

Gamma spectrometry with high-purity germanium (HPGe) detectors remains the technique of choice of most radioanalytical laboratories for analysing natural and artificial radionuclides in environmental samples. The low limits of detection achievable in relatively short times, together with its non-destructive nature and multi-elemental capability, make it a key assessment tool in emergency situations involving the accidental release of radioactive materials. In Ireland, gamma spectrometry has routinely been used since the early 1980s for determining the presence of artificial fission and activation products in environmental samples resulting from authorised liquid and gaseous discharges from the nuclear industry (e.g. Sellafield, La Hague), and fallout from atmospheric nuclear weapons testing (Mitchell *et al.*, 1990; McGinnity *et al.*, 2012a). The deployment of gamma spectrometry systems also enabled extensive monitoring programmes to be put into operation immediately following the Chernobyl accident in April 1986 (Cunningham *et al*., 1987) and, more recently, the Fukushima disaster in March 2011 (McGinnity *et al.*, 2012b). These programmes, which involved the analysis of a wide range of environmental matrices (e.g. rainfall, air filters, foodstuffs, vegetation and soil samples), provided invaluable data to the Radiological Protection Institute of Ireland (now the EPA's Office of Radiation Protection and Environmental Monitoring, ORM) on which to base advice to the government and the public, as well as for assessing the impact and potential radiation exposure of members of the Irish population. Gamma spectrometry has also routinely been used to quantify some naturally occurring primordial nuclides and their progeny (mainly ^{238}U and ^{232}Th series, and ^{40}K), and to determine their contribution to the background radiation dose (O'Connor *et al.*, 2014).

Although the analysis of acquired gamma spectra is relatively straightforward, a number of potential pitfalls and complications must be carefully considered to obtain high-quality results. The determination of radionuclide activities by gamma spectrometry relies primarily on accurate knowledge of the detector's full-energy peak (FEP) efficiency response for a given counting geometry and sample composition. The most common approach to peak efficiency calibration is to experimentally determine the detector's response at various photon energies (typically in the range 40–2000 keV) using appropriate calibration standards containing radionuclides with certified photon emission rates. The measured efficiencies are then used to construct an efficiency curve that is subsequently used by the analysis software to interpolate efficiency values at other energies. Ideally, calibration of a given counting geometry should be carried out for each type of measured sample and density (e.g. soil, water, milk powder, air filter) to reproduce and account for attenuation and self-attenuation effects, i.e. the absorption of photons by inactive layers between the source and the active volume of the detector, and within the sample matrix itself. In practice, given the variations in density and composition encountered in environmental samples, and the time and cost of carrying out these empirical measurements, it is not possible to measure the efficiency response for each geometrical condition and type of matrix. Instead, an energy-dependent *efficiency transfer* correction factor can be computed, defined as the ratio between the efficiency for the geometry under measurement and that for the reference measurement conditions used in calibration (Sima and Arnold, 2002; Lépy *et al*., 2015). The efficiency transfer method provides accurate corrections when only small differences in geometry and composition between the measured and calibration samples are present. For cases in which there is no calibration source similar to the measured sample, Monte Carlo simulation methods can be applied for the direct computation of the efficiency itself (Sima and Dovlete, 1997), taking into account the detailed geometric and composition characteristics of the detector and measuring geometry. The results obtained, however, are quite sensitive to inaccuracies in the parameters describing the detector or to other problems such as incomplete charge collection in the crystal (Hardy *et al.*, 2002; Sima and Arnold, 2002; Budjás *et al.*, 2009; Luís *et al.*, 2010; Hedman *et al.*, 2015) and so it is important to check the computations against experimental data for several test measurements.

The presence of true coincidence summing effects whenever the analysis takes place under high-efficiency, "close geometry" conditions further complicates efficiency calibration procedures, introducing nuclide-specific effects (Hedman *et al.*, 2015). True coincidence summing is encountered in gamma spectra from radionuclides with complex decay schemes and arises when two or more photons from the same decay are emitted in cascade within a short interval and detected within the resolving time of the spectrometer. In these cases, a pulse will be recorded which represents the sum of the energies deposited by the photons in the active volume of the detector. If one of the photons deposits all of its energy and one of the others is also partially or fully absorbed, this will result in a loss of a count from the FEPs corresponding to the former ("summing out"), leading to an apparent loss of efficiency for this nuclide. If more than one photon deposits all of its energy, sum peaks will appear at energies corresponding to the sum of the individual photon energies ("summing in"), potentially increasing the apparent efficiency of a direct transition of that energy. For HPGe detectors sensitive to X-rays, there is an additional probability of simultaneous detection of gamma rays with X-rays emitted following conversion electron emission or from nuclei decaying by electron capture, which can require complex corrections (Lépy *et al*., 2015). The probability of summing effects depends in a complex way on the decay scheme of the nuclide, the detector's full-peak and total efficiencies, the measurement set-up (including the sample, detector and shield) and the sample composition and density. Even when efficiency calibration is carried out by means of single photon-emitting radionuclides (e.g. ^{210}Pb, ^{241}Am, ^{57}Co, ^{137}Cs, ^{54}Mn, ^{65}Zn), to avoid coincidence summing effects, corrections will still be required for the quantification of all frequently encountered nuclides with cascade photon emission.

With the availability of high-efficiency detectors and the tendency of most radioanalytical laboratories to choose close-counting geometries to attain the lowest possible limits of detection, the need for coincidence summing corrections have become increasingly acute, and international metrology institutes and organisations such as the International Commission for Radionuclide Metrology (ICRM) have repeatedly called for the implementation of coincidence correction protocols, often prompted by the disappointing results of international intercomparison runs involving nuclides affected by coincidence summing.

As in the case of attenuation corrections, a number of methods have been developed to compute the coincidence correction factors, varying in complexity and applicability. In the case of high-volume samples, however, numerical evaluation of coincidence correction factors using Monte Carlo simulation is becoming the method of choice, as Monte Carlo methods can be used to provide realistic estimates of the correction factors for complex geometries and nuclide decay schemes. Indeed, the development of sophisticated photon transport models and the increased computing power available at reasonable cost have permitted the development of Monte Carlo codes that are able to simulate the fate of thousands of gamma rays/X-rays emitted from different points within the source. By tracking the individual histories of these photons and their interactions as they move through the detector and its surroundings, it becomes possible to compute the full peak and total efficiencies required for the accurate evaluation of coincidence summing correction factors (García-Talavera *et al.*, 2000; Sima *et al*., 2001; Hurtado *et al*., 2004; Venkataraman *et al*., 2005; Peyres and García-Toraño, 2007; Gasparro *et al.*, 2008; Vidmar *et al.*, 2008; Dababneh *et al*., 2014; Britton and Davies, 2015; Guerra *et al.*, 2015; Maidana *et al.*, 2016; Lutter *et al.*, 2018).

At the EPA's ORM analytical laboratory, self-attenuation and coincidence summing effects are accounted for using GESPECOR (CID Media GmbH), a dedicated Monte Carlo software package specifically developed for the efficiency calibration of HPGe gamma-ray spectrometers. The software allows the determination of self-attenuation and true coincidence summing correction factors, the transfer of efficiency curves between samples of different geometry and composition, and the direct computation of FEP and total efficiencies. As with other Monte Carlo packages, reliable results can be achieved only if accurate models of the detector, counting geometries and shielding are available as inputs to run the simulations. Although nominal parameters for specific detector models can be obtained from the manufacturer, significant uncertainties often remain regarding the active volume of individual detectors, the position of the crystal in relation to the end cap entrance window and the thicknesses of insensitive regions of the detector, particularly those of the dead layers at the

contacts, which can vary depending on the age and history of the detector. The lack of accurate knowledge of some of these detector parameters can result in Monte Carlo computed efficiency values that differ significantly from those determined experimentally; therefore, an optimisation process is normally required to ensure that experimentally determined efficiencies are accurately reproduced by the simulation.

Prior to the commencement of this project, the Radiation Physics Research Laboratory at University College Dublin, in collaboration with the Radiological Protection Institute of Ireland, carried out a pilot study during 2010–11 to test the implementation, accuracy and robustness of the GESPECOR software. Experimentally determined FEP efficiency curves for an n-type HPGe detector using a range of volumetric sources (including cylindrical tubs, Petri dishes and Marinelli beakers) were used to optimise the most important parameters in the detector model used by GESPECOR. The latter were identified by a sensitivity analysis procedure. By varying four parameters (germanium crystal radius and length, crystal-to-end cap distance and front dead layer thickness), it was possible to match all the experimental efficiencies to within approximately 5% for all the geometries considered (McCrory, 2011). Optimisation of model parameters at the EPA's ORM analytical laboratory was carried out manually by running GESPECOR and iteratively adjusting the most sensitive detector parameters from their baseline values to get the best possible agreement between experimental and computed efficiencies for a range of counting geometries. Although good agreement could be achieved using this approach, it required continuous manual intervention from the user to guide the optimisation search and was, therefore, a slow and time-consuming process.

The validity of the resulting correction factors was checked by the analysis of a certified proficiency sample containing a variety of radionuclides affected by coincidence summing. In all cases, corrected activities were found to be within 2% of the assigned activity values. The validated methodology was also used for the quantification of large-volume air samples collected in Belfield (Dublin) over the period 24 March to 16 May 2011. These samples were taken as part of the monitoring effort to assess the impact on Ireland of atmospheric releases from the damaged reactors at the Fukushima Daiichi nuclear power station in north-east Japan following the earthquake and tsunami on 11 March 2011 (McGinnity *et al.*, 2012b*)*. Our results highlighted the importance of true coincidence summing in the quantitative determination of gamma-emitting radionuclides characterised by complex decay schemes, with correction factors of 10–20% being required in some cases (McCrory, 2011).

As required by the research call associated with this specific project (EPA Sustainability Research Call 2015 – Health and Wellbeing Theme – Project 33), the overall aim of this project was to build on the results obtained in previous feasibility studies with a view to developing and implementing suitable Monte Carlo methods for the assay of natural and artificial radionuclides using high-resolution gamma spectrometry with HPGe detectors at the EPA's ORM analytical laboratory, so that self-attenuation and true coincidence summing effects can be corrected for, and detector efficiencies established for a variety of geometries and sample matrices without the need to carry out multiple, time-consuming and expensive measurements using certified calibration standards.

A key aim of this project was to automate this optimisation process by developing user-friendly, operational software that initially uses a set of nominal (but realistic) input parameters describing an HPGe detector, together with experimentally determined FEP efficiencies for a range of radionuclides in a variety of counting geometries, to produce an optimised model of the detector by applying suitable optimisation algorithms without any further user intervention.

To this end, the commercially available Monte Carlo simulation software GESPECOR was used, in combination with traditional efficiency calibration techniques using certified standards, to develop an automated process for the optimisation of detector model input parameters, so that experimentally determined FEP efficiency curves for a number of reference geometries are accurately reproduced by the model simulation. To minimise the risk of arriving at unrealistic estimates for the model input parameters, manufacturer specifications (e.g. crystal dimensions, end cap to detector distance, dead layer thickness) were verified by X-ray/computed tomography (CT) scans for a selection of the HPGe detectors in use by the EPA, so that that realistic tolerance limits/ variations for each of the parameters could be used during the optimisation process. By using GESPECOR

rather than developing in-house Monte Carlo models, the process of detector modelling and calibration was considerably simplified, leaving more time for the testing and validation of the resulting output. The quality of the photon transport models used for the simulations was also guaranteed, as comparisons of GESPECOR with other Monte Carlo codes (GEANT4, MCNP) are well documented in the published literature. GESPECOR was already in use for a range of applications by the EPA's ORM analytical laboratory, which the proposed project sought to expand and optimise.

To achieve the objectives of the project, work was divided into eight separate but related work packages (or major tasks), each containing a specific set of relevant objectives or subtasks. These work packages were:

- **WP1:** HPGe detector characterisation and establishment of reference FEP efficiencies;
- **WP2:** HPGe detector model optimisation;
- **WP3:** self-attenuation corrections;
- **WP4:** true coincidence summing corrections;
- **WP5:** evaluation of uncertainties;
- **WP6:** integration work package;
- **WP7:** testing and application of methodology;
- **WP8:** reporting and dissemination of results.

In the following chapters, a description is given of the main results achieved during the project for each of the tasks carried out to achieve the project objectives. As a key output of the project, we developed an automated optimisation method for the characterisation of HPGe detectors. Starting with a set of nominal (but realistic) input parameters and experimentally determined FEP efficiencies for multiple calibration standard solutions in a variety of counting geometries (which include cylindrical tubs and Marinelli beakers), the GESPECOR software was used to produce an optimised model of the detector by applying suitable optimisation algorithms without any further user intervention.

Application of the method has shown that, with little effort from the user, it is possible to achieve excellent agreement between experimental FEP efficiencies and Monte Carlo calculations, with mean absolute deviations between modelled and experimental efficiencies of $< 2\%$ for all geometries and individual absolute deviation no higher than 4%. Through validation experiments, it has been demonstrated that the optimised models can be used to confidently predict FEP efficiencies for arbitrary source geometries by direct Monte Carlo simulation, to perform efficiency transfer from one matrix to another and to compute accurate values for self-attenuation and true coincidence summing correction factors.

Optimised models for each of the detectors in use at the EPA's ORM have been established and are now being used to determine appropriate self-attenuation and true coincidence summing, as well as for computing FEP detector efficiencies for a variety of geometries and sample matrices without the need to carry out multiple, time-consuming and expensive measurements using certified calibration standards.

2 HPGe Detector Characterisation and Establishment of Reference Full-energy Peak Efficiencies

As a first step towards the development of suitable Monte Carlo methods, each of the HPGe detectors in use at the EPA's ORM analytical laboratory was characterised to obtain the required initial input parameters for detector parameter optimisation.

2.1 Baseline Manufacturer Specifications and Derivation of Appropriate Models for Each Type of Counting Geometry and Shielding

Baseline manufacturer specifications in the form of quality assurance datasheets, detector specification and performance data, and detailed drawings of crystal and detector assemblies (including dimensions and construction materials) were obtained for each of the HPGe detectors currently in use at the ORM. All these parameters are required as input by GESPECOR to perform Monte Carlo calculations of FEP and total efficiencies, and to derive coincidence summing and self-attenuation correction factors. The required input parameters for developing suitable Monte Carlo models in GESPECOR, depending on the type of HPGe detector, are depicted in Figure 2.1.

In addition to the HPGe detector models, GESPECOR requires models for each of the geometries used for counting. Four different types of geometries, placed directly on top of the detector's end cap or in the well of a well-type HPGe detector, are routinely used at the ORM: cylindrical polypropylene tubs filled to 50 mL (50 GEO), 100 mL (100 GEO) or 250 mL (250 GEO), Marinelli beakers filled to 500 mL (500 GEO) or 1000 mL (1000 GEO), small polypropylene vials that fit in the crystal well of well-type HPGe detectors (5 GEO) and polyethylene Petri dishes for counting small filters (1 GEO). All containers were accurately measured (Figure 2.2) and the required dimensions introduced into GESPECOR as input files. The use of add-ons to the GESPECOR software (Sima *et al*., 2001*)*, enabling the addition of concave bases to the cylindrical geometries, allowed a more accurate description of these geometries. Parameters defining these geometries were considered to be well known and were not varied during the optimisation process. A model of the shield associated with each of the detectors (configuration, dimensions relative to the detector, lead thickness) was also included to complete the required inputs for GESPECOR.

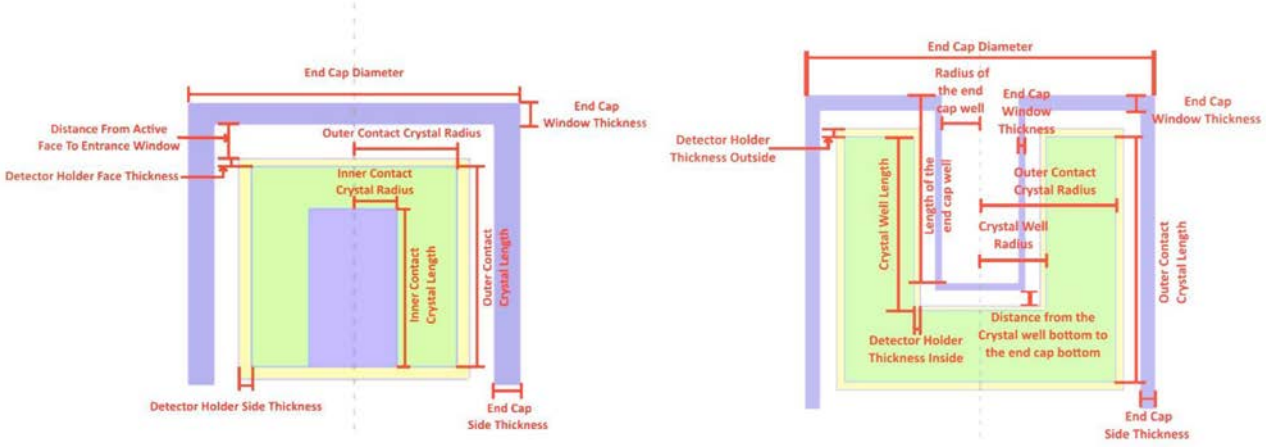

Figure 2.1. HPGe models in GESPECOR, with all the required input parameters defined. Left: model used for n-type, p-type and broad-energy germanium (BEGe) HPGe detectors. Right: model used for well detectors. Reprinted from Murphy *et al*. (2020). Copyright © 2019, with permission from Elsevier.

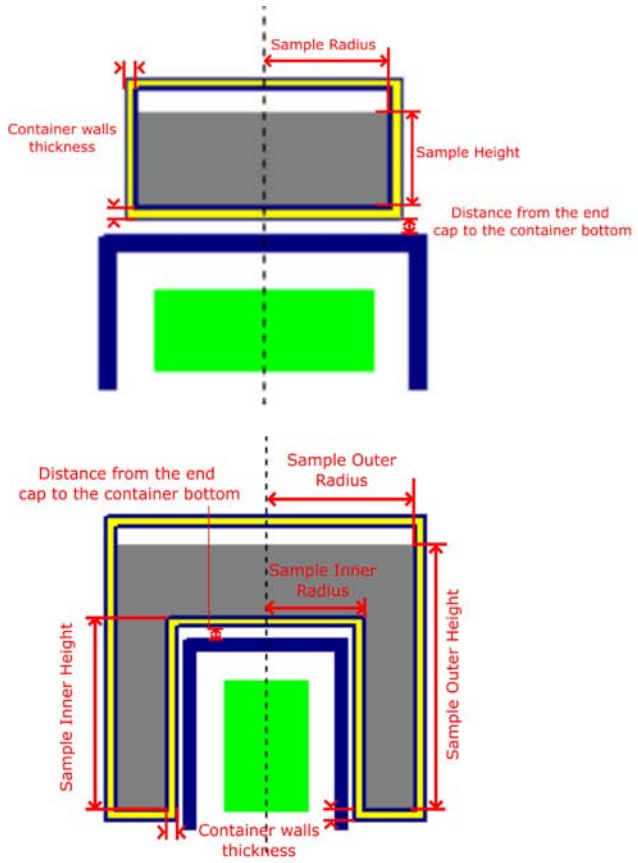

	5 GEO	50 GEO	100 GEO	250GEO
Sample Radius (cm)	0.603	3.925	4.032	4.247
Sample Height (cm)	4.554	1.199	2.363	4.895
Container Walls Thickness: (cm)	0.142	0.057	0.057	0.057
Container Walls Material	POLYPROP	POLYPROP	POLYPROP	POLYPROP
Container Walls Density (g/cm³)	9.0×10^{-1}	9.0×10^{-1}	9.0×10^{-1}	9.0×10^{-1}
Distance from the end cap to the bottom of the container (cm)	0.000	0.000	0.000	0.000

	500 GEO	1000 GEO
Sample Inner Radius (cm)	4.550	4.550
Sample Inner Height (cm)	7.600	7.600
Sample Outer Radius (cm)	6.500	8.500
Sample Outer Height (cm)	9.568	10.294
Container Walls Thickness: (cm)	0.201	0.185
Container Walls Material	POLYPROP	POLYPROP
Container Walls Density (g/cm³)	9.0×10^{-1}	9.0×10^{-1}
Distance from the end cap to the bottom of the container (cm)	0.000	0.000

Figure 2.2. Model ORM's cylinder and Marinelli geometries and associated parameters for input to GESPECOR. Polyprop, polypropylene.

2.2 X-ray/Computed Tomography Scan Characterisation of Selected Detectors

Although the above parameters represent a good starting point for modelling the detector, significant uncertainties usually remain regarding the active volume of individual detectors, the position of the crystal and the precise thicknesses of insensitive regions of the detectors, particularly the dead layers at the contacts. To verify important parameters such as crystal dimensions, position within the assembly and end cap to crystal distance, a selection of detectors were characterised using a combination of X-ray radiography and CT. All images were obtained using clinical equipment kindly made available to the project by staff at the Radiology Department in St Luke's Hospital (Rathgar). Four detectors (one n-type Gamma-X (GMX) detector, two p-type GEM detectors and one broad-energy germanium (BEGe) detector) were characterised in this way (Table 2.1).

To illustrate the characterisation process, the results obtained for one of the detectors (no. 12), a p-type coaxial HPGe detector with an 80% relative efficiency and an energy resolution (FWHM) of 1.87 keV at 1.33 MeV, are shown below. An X-ray image of detector 12, obtained using a GE Definium 6000 X-ray digital radiography system operating at 100 kV, is shown in Figure 2.3, together with the schematic of

Table 2.1. List of detectors characterised by X-ray/CT scan radiography

Detector number	Detector type	Manufacturer	Model number
9	n	Ortec	GMX-50220-P
11	p	Ortec	GEM-M7680P4-90-RB-S
12	p	Ortec	GEM-M7680P4-90-RB-S
13	BEGe	Canberra	BE5030

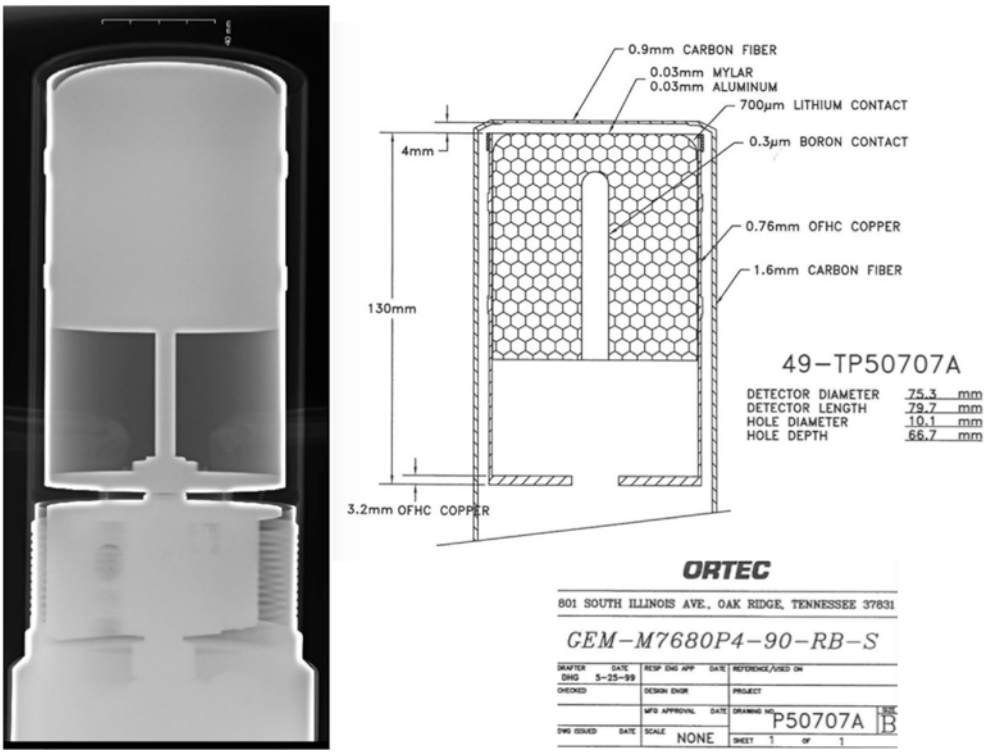

Figure 2.3. X-ray image of detector 12, together with manufacturer's schematic drawing and dimensions. Reprinted from Murphy *et al*. (2020). Copyright © 2019, with permission from Elsevier.

the detector provided by the manufacturer. The crystal, copper mounting cap (including the straps to secure the crystal) and the carbon fibre end cap are clearly visible in the image.

CT images of the detector assembly were obtained using a GE Lightspeed RT16 scanner set to axial mode with a slice thickness of 0.625 mm and operating at a tube voltage of 120 kV. Analysis of the DICOM (digital image and communications in medicine) image files obtained from X-rays and CT scans using the open source Medical Imaging Interaction Toolkit (MITK) software and in-house Python scripts allowed us to set realistic bound limits for 7 of the 12 required parameters, namely the end cap diameter, the outer contact crystal radius and length, the distance from the active face to entrance window, the detector holder side thickness, the end cap window thickness and the end cap side thickness (Table 2.2). Using the X-ray and CT images, it was not possible to verify the dimensions of the inner contact radius and length, the detector holder face thickness or the thickness of the dead layer active face or dead layer side face. For these parameters, realistic bounds based on the results reported by other researchers were used to restrict the parameter search space.

The end cap diameter was readily measured with a calliper and found to be 9.00 cm. Minimum and maximum values of 8.922 cm and 9.136 cm, respectively, were estimated from the CT scan images (Figure 2.4), and were consistent with the direct measurement. For the optimisation procedure, the value of the end cap diameter was kept fixed to its nominal value, as measured with the calliper.

The minimum and maximum values for the outer contact crystal radius were determined by assuming that the germanium crystal occupies the entire inner cavity formed by the detector holder. With this assumption, the minimum inner radius of the detector holder (and, thus, the minimum outer contact crystal radius) was estimated to be 3.638 cm from the CT images. The maximum value for the outer contact crystal radius was determined from the X-ray image of the detector. The validity of the measured dimensions obtained from the X-ray image was checked by determining the end cap diameter, which yielded a value of 9.03 cm, in excellent agreement with the value of 9.00 cm obtained by direct measurement. Analysis of the X-ray scan determined the maximum outer contact crystal radius to be 3.849 cm. This was achieved by measuring the detector holder diameter in

Table 2.2. Set of starting nominal parameters and constraints used for the optimisation search process for detector 12 (GEM-M7680P4-90-RB-S) based on the detector characterisation process

Parameter	Nominal	Minimum	Maximum	Basis of constraint
Outer contact crystal radius (cm)	3.80	3.64	3.85	X-ray/CT scan
Outer contact crystal length (cm)	8.37	8.18	8.36	X-ray/CT scan
Inner contact radius (cm)	0.455	0.432	0.478	±5% baseline
Inner contact length (cm)	6.37	6.05	6.69	±5% baseline
Thickness of dead layer active face (cm)	0.07	0.07	0.18	Literature
Thickness of dead layer side face (cm)	0.07	0.07	0.18	Literature
Distance from active face to entrance window (cm)	0.40	0.27	0.60	X-ray/CT scan
Detector holder face thickness (cm)	0.006	0.0054	0.0066	±10% baseline
Detector holder side thickness (cm)	0.076	0.068	0.152	X-ray/CT scan
Detector holder density ($g\,cm^{-3}$)	8.96	–	–	Fixed
End cap diameter (cm)	9.0	8.922	9.136	X-ray/CT scan
End cap window thickness (cm)	0.09	0.048	0.171	X-ray/CT scan
End cap density ($g\,cm^{-3}$)	1.49	–	–	Fixed
End cap side thickness (cm)	0.16	0.065	0.281	X-ray/CT scan
End cap side density ($g\,cm^{-3}$)	1.49	–	–	Fixed

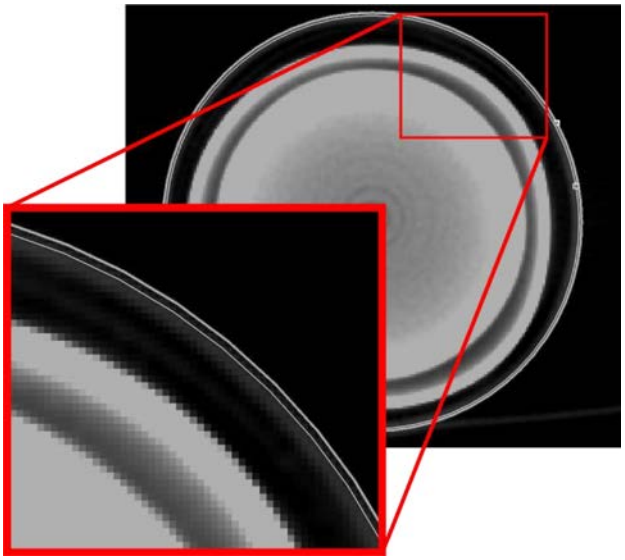

Figure 2.4. CT scan slice of detector 12. Two circles were fitted to the pixels that represent the end cap, placing limits on the end cap diameter value.

regions where the detector holder covered the crystal, but away from the straps used to support the detector holder (Figure 2.5). The detector holder thickness (as specified by the manufacturer) was subtracted from the estimated detector holder radius to yield the estimated outer contact crystal radius.

The minimum and maximum values for the outer contact crystal length were determined from the reconstructed CT image using the MITK line tool, which yielded values of 8.178–8.357 cm (Figure 2.6).

Analysis of the CT images showed that the face of the end cap is curved (Figure 2.7). This curvature cannot be accurately defined in GESPECOR geometry files. A maximum and minimum bound for the distance from active face to entrance window was defined based on the CT images. The value quoted by the manufacturer, 0.4 cm, lies in the range 0.271–0.604 cm found from the CT image.

The detector holder side thickness was estimated from the CT images to be in the range 0.068–0.152 cm. The thickness of the end cap window in the CT image did not appear to be uniform. A range from 0.049 cm (resolution of the CT scan) to 0.171 cm (based on the maximum value measured from the scan) was estimated from the images. The minimum and maximum values for the end cap size thickness was determined by fitting a double ellipse to the CT scan slices using the MITK software (Figure 2.8), which yielded a range of 0.065–0.281 cm.

2.3 Experimental Determination of Reference Full-energy Peak Efficiency Curves

Experimentally determined FEP efficiency curves were available for each of the operational detectors

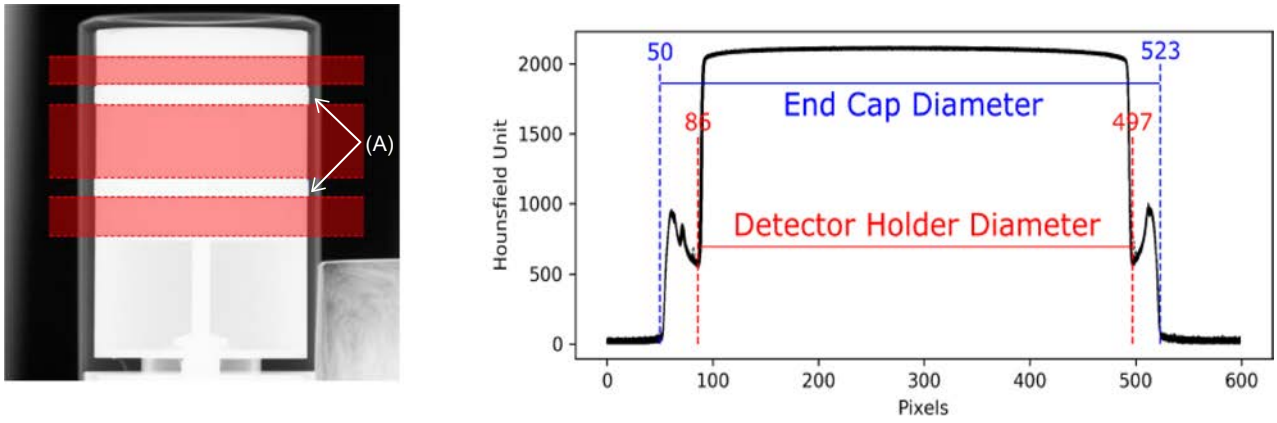

Figure 2.5. Left: X-ray scan of detector 12. Region A shows the straps. The red regions represent the slices used to determine the end cap diameter and detector holder diameter. Right: plot of Hounsfield units versus pixels corresponding to the red regions, showing the measurements used to estimate the crystal radius.

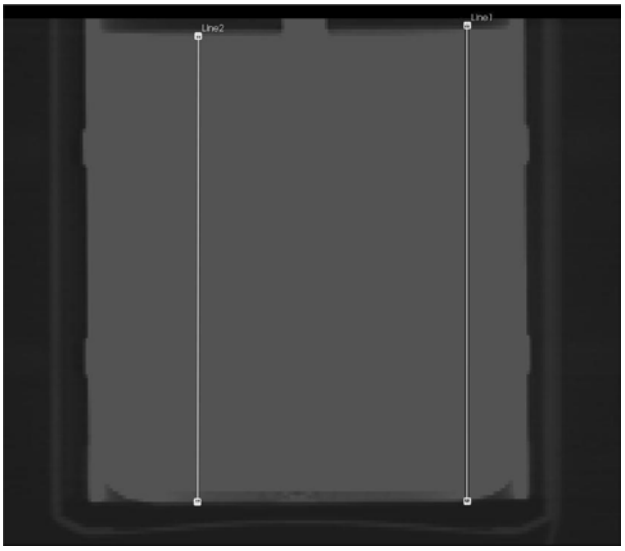

Figure 2.6. Reconstructed CT image from which the length of the crystal was determined. Reprinted from Murphy *et al*. (2020). Copyright © 2019, with permission from Elsevier.

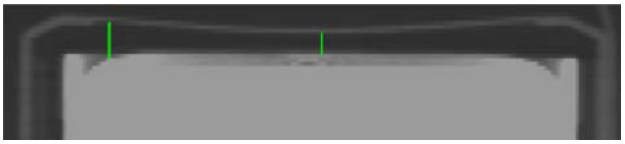

Figure 2.7. CT image of the detector, showing the curvature of the entrance window. Reprinted from Murphy *et al*. (2020). Copyright © 2019, with permission from Elsevier.

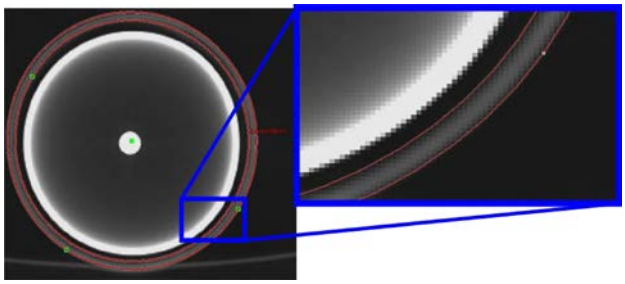

Figure 2.8. CT scan slice showing the determination of the side thickness of the end cap by fitting a double ellipse. Reprinted from Murphy *et al*. (2020). Copyright © 2019, with permission from Elsevier.

at the ORM at the start of the project. These had been obtained using certified calibration solutions containing ^{241}Am (59.54 keV), ^{109}Cd (88.03 keV), ^{57}Co (122.06 keV), ^{139}Ce (165.85 keV), ^{51}Cr (320.08 keV), ^{113}Sn (391.69 keV), ^{85}Sr (514.00 keV), ^{137}Cs (661.66 keV), ^{54}Mn (834.83 keV), ^{88}Y (898.83 keV and 1836.05 keV), ^{65}Zn (1115.53 keV) and ^{60}Co (1173.22 keV and 1332.49 keV). During the project, a ^{210}Pb (46.54 keV) calibration solution was acquired by ORM to extend the calibration to lower energies and the feasibility of using ^{137}Cs Kα and Kβ X-rays (in the energy range 32–37 keV) was also explored. An example of a typical experimental FEP efficiency curve for one of the detectors (using the 250 GEO geometry) is shown in Figure 2.9. It is worth mentioning that a number of the nuclides included in the standard

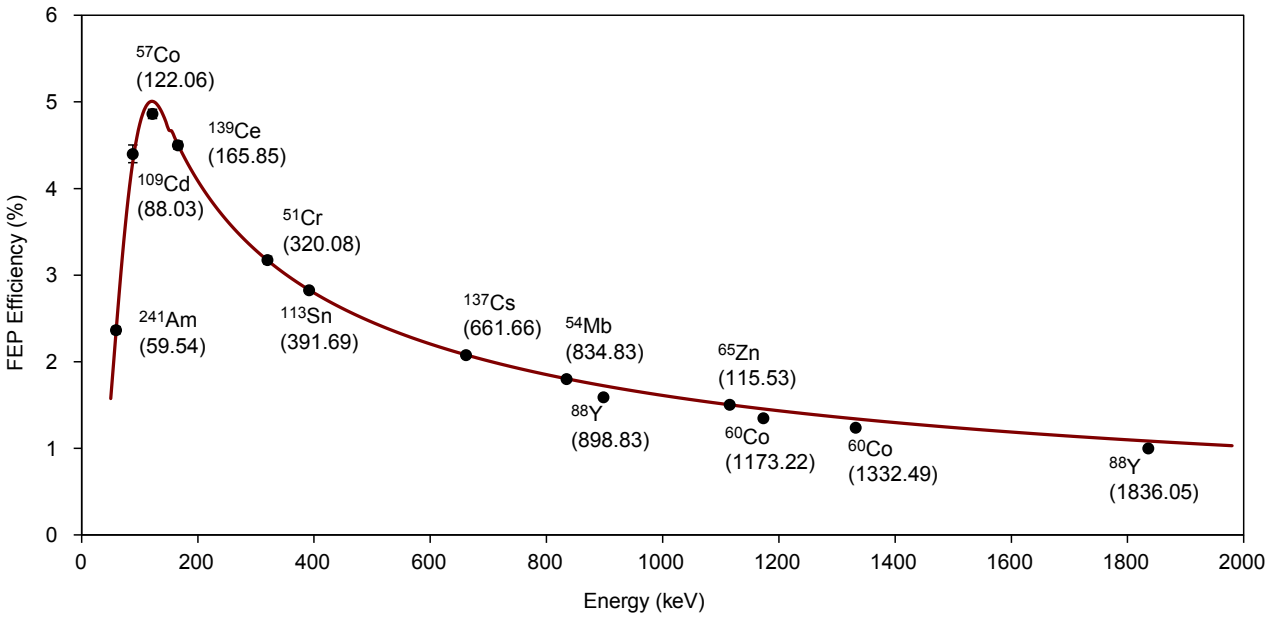

Figure 2.9. Empirical FEP efficiency curve for n-type detector using multi-nuclide calibration standard (250 GEO geometry).

(most notably ^{88}Y and ^{60}Co) are affected by true coincidence summing, particularly when counting is carried out under close geometry counting conditions. Furthermore, for n-type detectors, gamma/X-ray coincidence summing may also be expected for certain nuclides, which may affect the calibration. In Figure 2.9, the solid line was obtained by fitting the efficiencies only of nuclides not affected by coincidence summing. These experimental calibrations are required for the model optimisation process (see Chapter 3) and also for the evaluation of self-attenuation correction factors (see Chapter 4).

A new multi-gamma calibration standard was purchased from the UK's National Physical Laboratory (Id: A180138; National Physical Laboratory (NPL) code: R08-03-2018030327-1; EPA code: ES1800427) in August 2018. Following primary dilution, a number of calibration standards were prepared in a range of geometries, including the 50-mL (50 GEO), 100-mL (100 GEO) and 250-mL (250 GEO) tubs; the 500 mL (500 GEO) and 1000-mL (1000 GEO) Marinelli beakers; and the cylindrical vial geometry used for counting small samples inside the wells of well-type detectors (5 GEO).

The last geometry (5 GEO) was used to establish the FEP efficiency curves for the two well-type detectors currently in operation at the ORM laboratory (detectors 6 and 14). These efficiencies were required for the development of optimised models for each of these detectors. The measured FEP efficiencies are shown in Figures 2.10 and 2.11. In these plots, the solid line represents a non-linear polynomial best fit to the FEP efficiencies of nuclides not affected by coincidence summing. Note that, owing to the high detection efficiency achieved for samples counted inside the well, FEP efficiencies for nuclides affected by coincidence summing (^{60}Co, ^{88}Y and ^{139}Ce) show very large deviations (up to 43%) with respect to the FEP efficiencies expected from the coincidence-free curve. Inclusion of these nuclides in the optimisation process required the application of accurate true coincidence summing correction factors. These factors were computed based on a first iteration detector model derived by restricting the optimisation process to those nuclides in the calibration standard that are free of coincidence summing effects (see Chapter 3 for further details).

The three tub geometries and the two Marinelli beakers were used to establish the FEP efficiency curves for the other detectors, including detector 12 (Ortec model GEM-M7680P4-90-RB-S), which was one of the detectors characterised by X-radiography and CT during this project. The detector, which was not operational at the start of the project, was configured

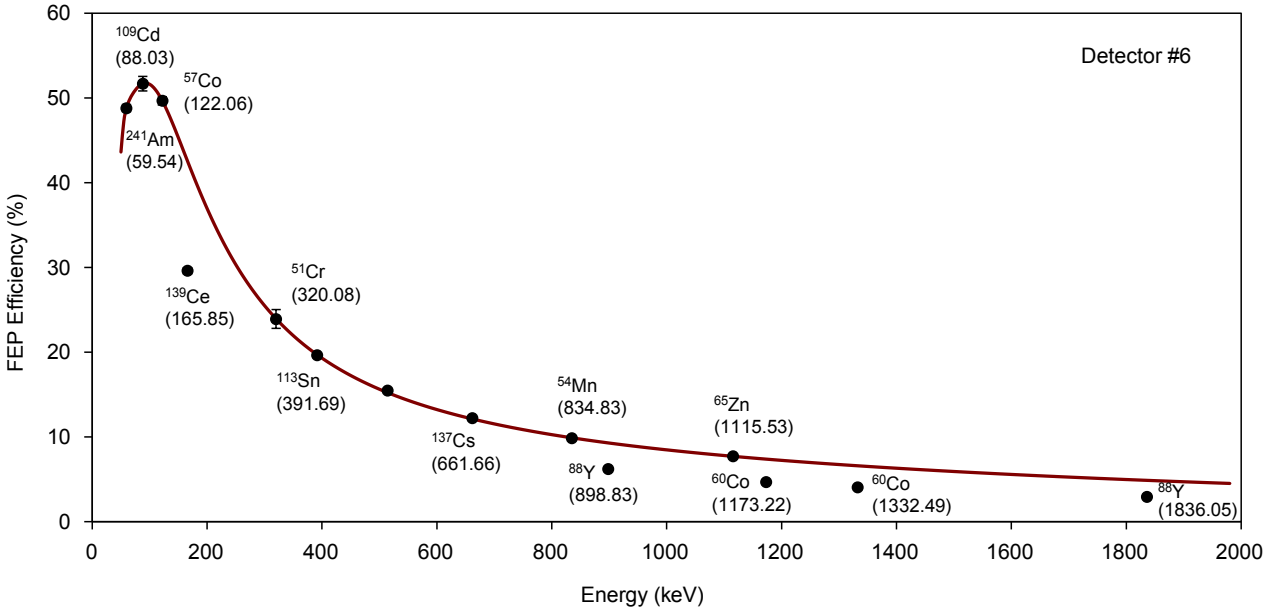

Figure 2.10. Experimental FEP efficiency curve for cylindrical vial geometry counted inside the well of ORM's detector 6. The solid line is a non-linear polynomial fit to the FEP efficiencies of nuclides not affected by true coincidence summing effects.

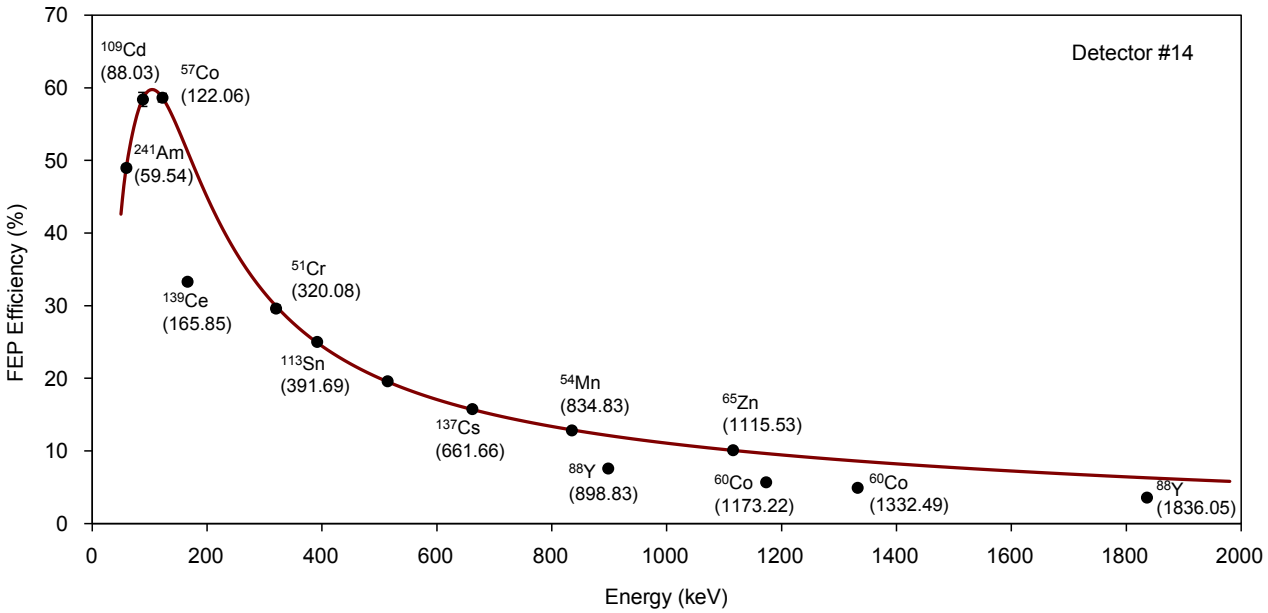

Figure 2.11. Experimental FEP efficiency curve for cylindrical vial geometry counted inside the well of ORM's detector 14. The solid line is a non-linear polynomial fit to the FEP efficiencies of nuclides not affected by true coincidence summing effects.

and set up for use. As detailed in Chapter 3, accurate models for each of the detectors were obtained using the measured FEP efficiency curves and the latest version of the optimisation programme developed during the project. A typical set of experimentally determined FEP efficiencies, used as input for the optimisation programme, are shown in Figure 2.12. The solid lines shown in the plot correspond to the fitting obtained using the Genie 2000 gamma analysis software.

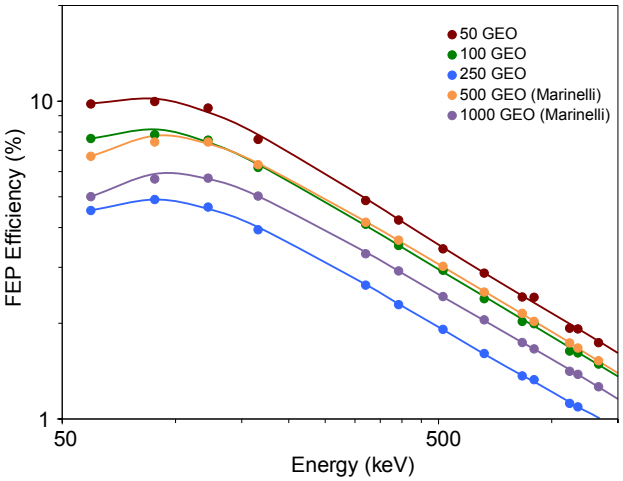

Figure 2.12. Experimentally determined FEP efficiencies for different geometries in detector 9.

Extension of the FEP efficiency curves for all operational detectors to lower energies by using a ^{210}Pb standard (46.5 keV) required the use of the tools developed to account for the differences in self-attenuation between the ^{210}Pb standard medium (2 M HNO_3) and the multi-gamma calibration standard medium (4 M HCl). The latter was chosen as the reference medium for all calibrations, simulations and matrix corrections performed at the EPA's ORM laboratory using GESPECOR. Some of the results for this task are discussed further in Chapter 4.

3 HPGe Sensitivity Analysis and Detector Model Optimisation

The next step was to develop an automated process for optimising HPGe detector model input parameters, so that experimentally determined FEP efficiency curves for a number of reference geometries could be accurately reproduced by Monte Carlo simulation using an optimised model of the detector, allowing for self-attenuation and coincidence summing effects to be corrected for. To this end, a user-friendly software application was developed that uses GESPECOR to conduct Monte Carlo simulations and yields an optimised model of the HPGe detector by applying suitable optimisation algorithms without requiring any further user intervention. The program developed is capable of simultaneously employing multiple experimental FEP efficiency curves for the parameter optimisation process. At the end of the process, a set of optimised parameters is obtained that can be used in GESPECOR to carry out self-attenuation, coincidence summing and efficiency transfer calculations.

3.1 Sensitivity Analysis of Important Input Parameters Using GESPECOR

Before developing the optimisation application, a sensitivity analysis program was developed to investigate the effect of modifying key input parameters on the FEP efficiency at different energies for different types of detectors and counting geometry arrangements. The program developed enables an automated one-at-a-time (OAT) sensitivity analysis to be performed with GESPECOR. A graphical user interface (GUI) constructed with the tkinter package in Python permits user-defined input of detector parameters, additional parameters and energy values. Figure 3.1 shows the GUI window of the program used for carrying out the sensitivity analysis.

Before running the program, the user inputs appropriate values for the detector parameters, additional parameters and energy values using

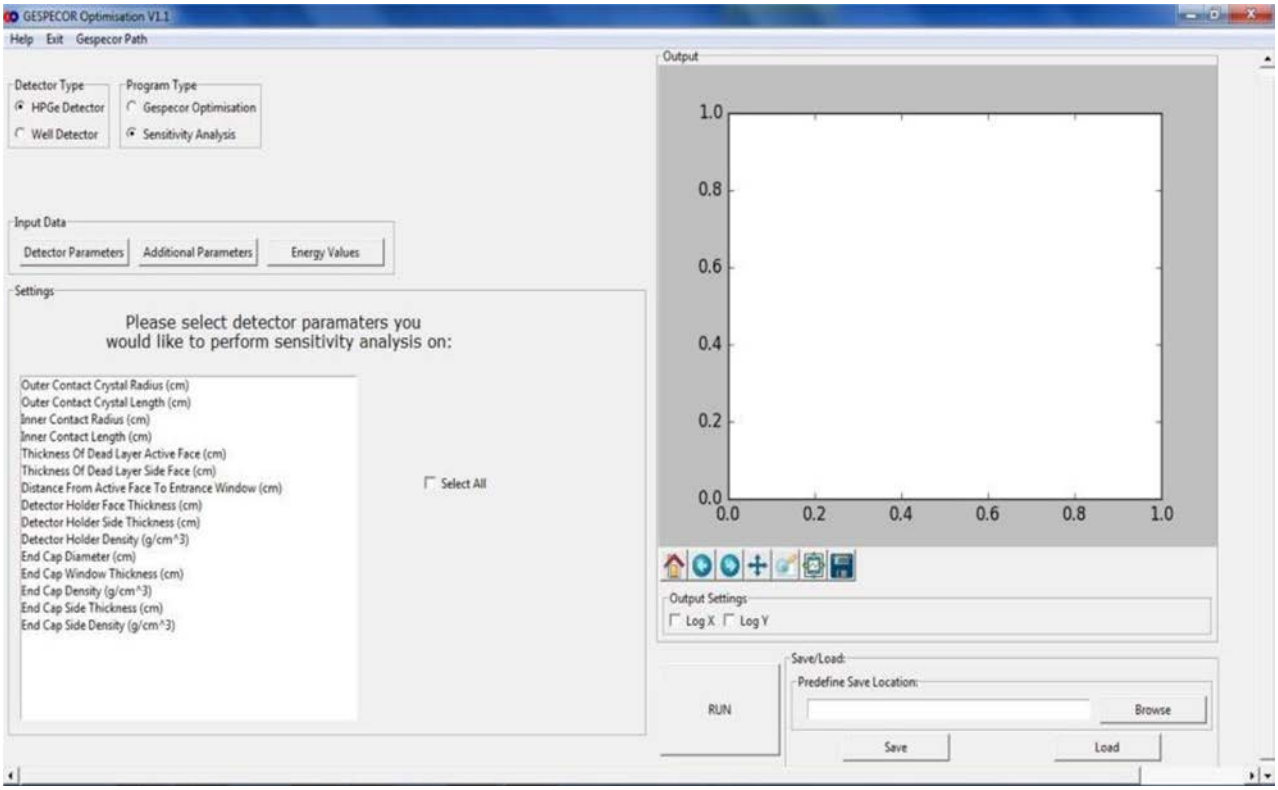

Figure 3.1. GUI for the sensitivity analysis component of the program.

the buttons in the "Input Data" box. The "Detector Parameter*"* button opens a window which allows the user to introduce baseline values for all detector parameters. The "Minimum", "Maximum" and "Division*"* values (specifying the range and number of values to be explored) are entered for those parameters for which the sensitivity analyses are to be carried out. The "Additional Parameters" button requests the name and path for the geometry, source matrix and shield files, which are required by GESPECOR and are retrieved directly from the appropriate GESPECOR directories. Finally, the *"*Energy Values" button opens a window in which the energies for those FEP efficiencies being calculated can be manually entered or loaded from a text file.

Once these input parameters have been introduced, the user can select the detector parameters to perform the sensitivity analysis on, and click "Run" to start the sensitivity analysis process. An array of detector parameters is created and used to generate the required detector files needed by GESPECOR, which is run multiple times using PyAutoIt 0.4, a Python binding for AutoIT (a scripting language designed for automating Windows GUIs). Once the sensitivity analysis calculation has finished, the user can select a detector parameter to view. The sensitivity analysis results are plotted in an interactive graph built using matplotlib (Figure 3.2). The user can save the results to a comma-separated values (csv) file for later viewing in the program or for further analysis in another application (e.g. Excel). A flow diagram of the program operation is shown in Figure 3.3.

A sensitivity analysis was carried out for generic coaxial HPGe and well-type detectors, with the minimum and maximum values for each parameter being determined by the ranges found among the EPA's ORM detectors, as taken from the manufacturer specifications. The default (nominal) parameters used to define the generic model for each type of detector have been taken as the minimum values found for each parameter.

For the HPGe coaxial detector, the sensitivity analysis was completed for three different cylindrical counting geometries (50 GEO, 100 GEO and 250 GEO), as well as the two Marinelli beakers (500 GEO and 1000 GEO), as defined in section 2.1. In all cases, the geometry was placed directly on top of the end cap. The source matrix was defined as water using the generic GESPECOR material file (watersol.mat) and one of the available shield files (shield10.shi) was used as a representative generic shield (note that the shield type does not contribute to the FEP efficiency calculation in GESPECOR). For the well-type detector, the sensitivity analysis was performed for the smallest cylindrical geometry (5 GEO), with the geometry placed inside the well.

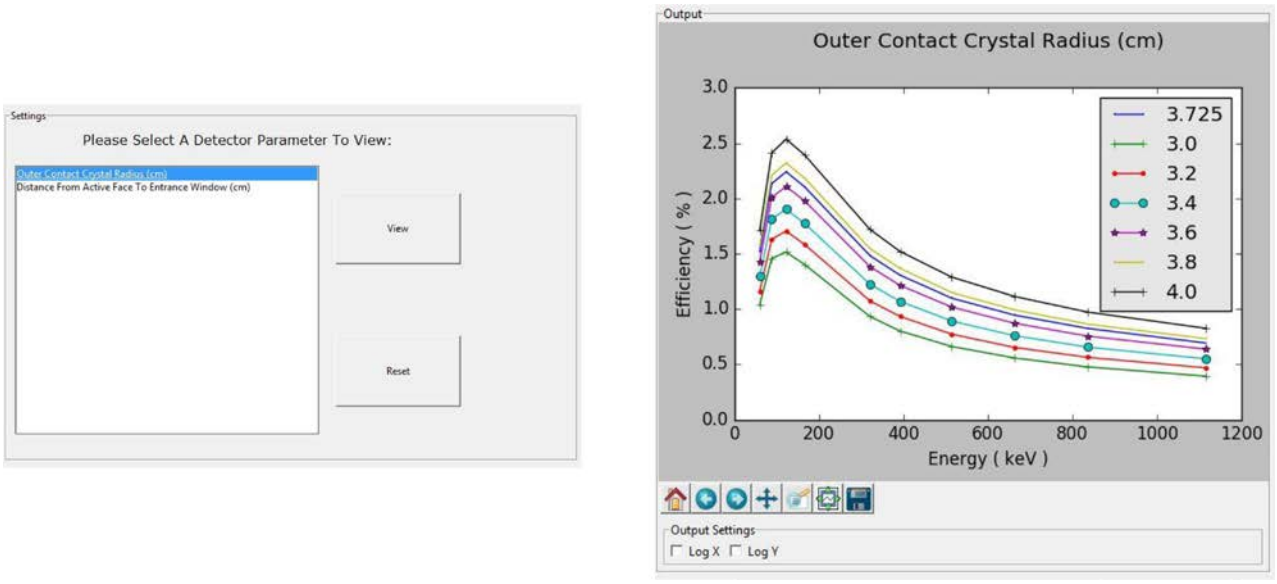

Figure 3.2. Example of sensitivity analysis carried out on the outer contact crystal radius parameter.

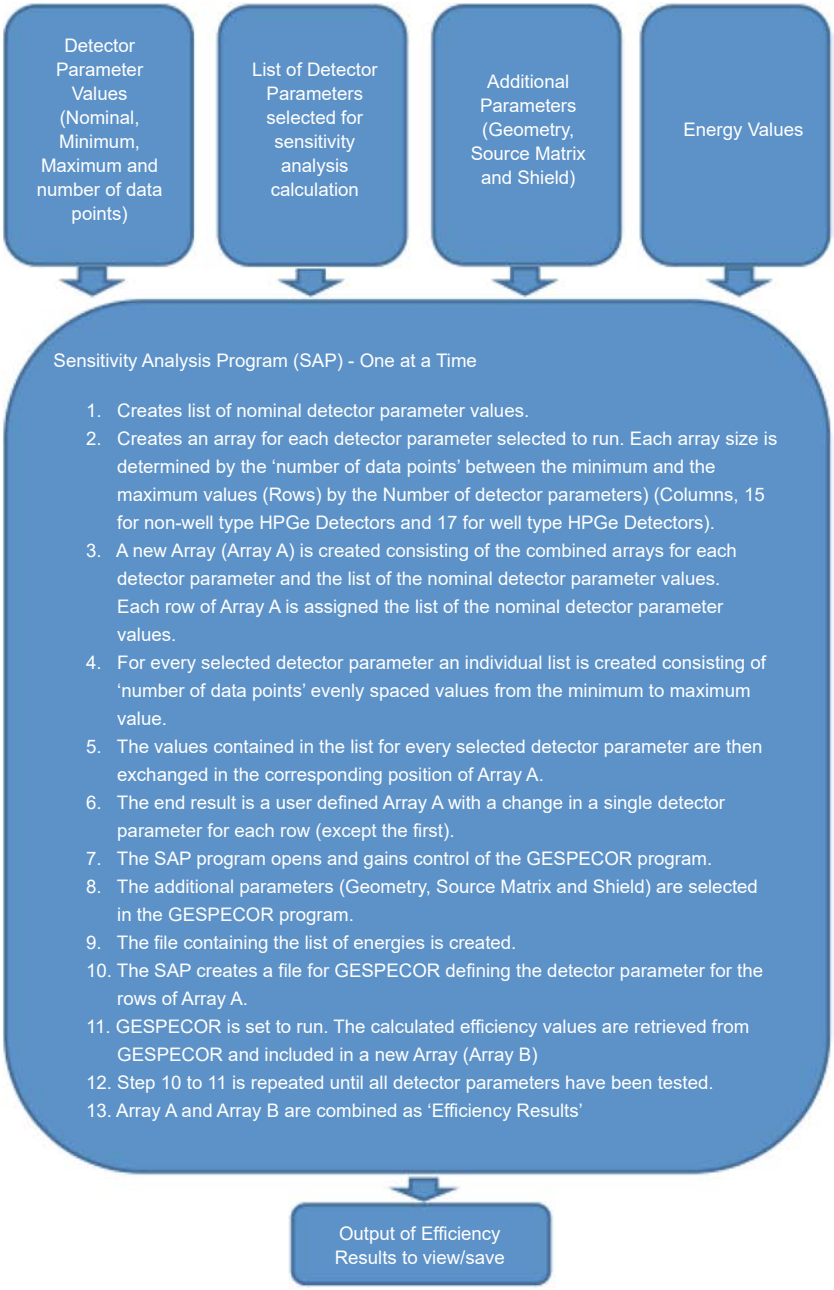

Figure 3.3. Flow chart of sensitivity analysis program (SAP).

For a given detector and counting geometry, the deviation in FEP efficiency associated with a given parameter, defined as:

$$\text{Deviation (frn)} = \frac{[\text{efficiency for minimum detector parameter}] - [\text{efficiency for maximum detector parameter}]}{[\text{efficiency for minimum detector parameter}]} \quad (3.1)$$

was calculated as a function of energy.

The results obtained for a typical cylindrical geometry (250 GEO) placed on top of a generic HPGe coaxial detector are shown in Figure 3.4. A number of parameters (grouped under band 1) do not strongly influence the efficiency and are of relatively little importance for the development of an accurate detector model in this counting set-up. These parameters include the end cap side density, end cap side thickness, end cap diameter, detector holder side thickness and detector holder face thickness. Another set of parameters (grouped under band 2)

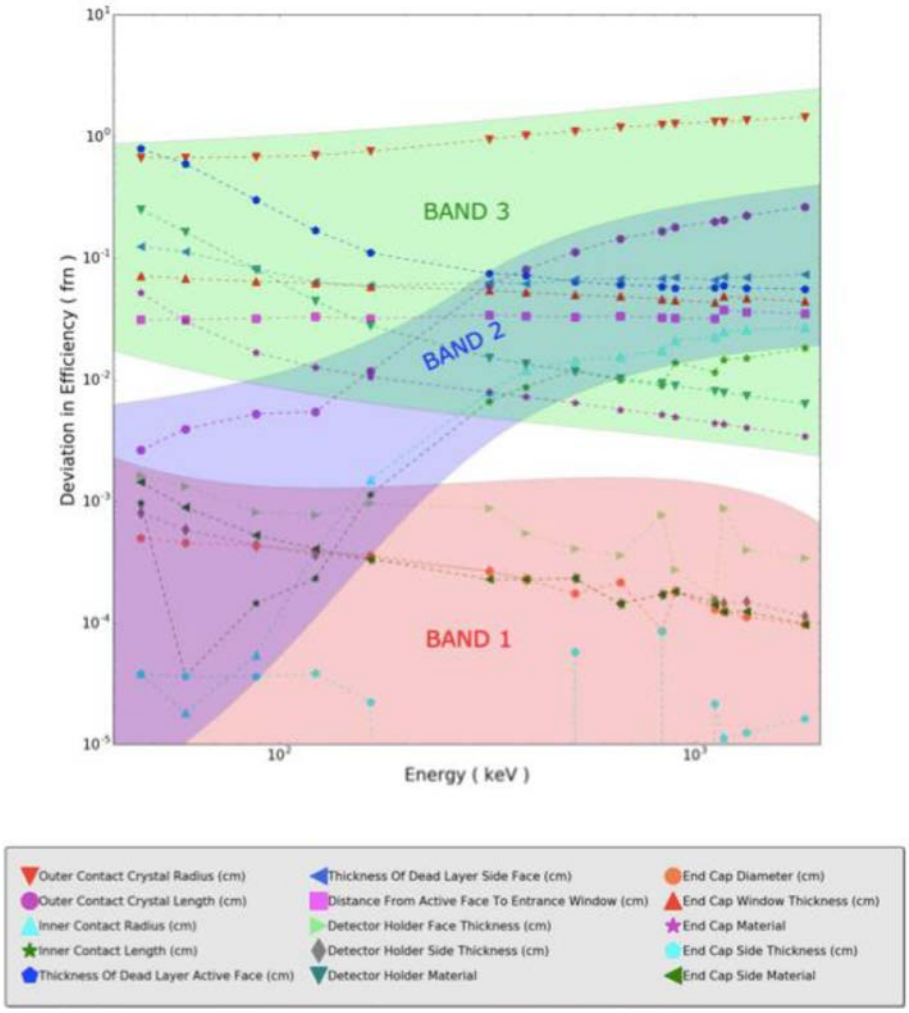

Figure 3.4. Sensitivity analysis for a generic HPGe coaxial detector (250 GEO).

has a stronger effect on the FEP efficiency for high-energy gamma rays. These parameters comprise the inner contact radius, inner contact length and outer contact crystal length. Finally, a third set of parameters (band 3), defining any materials/distances between the source and the crystal (end cap density, distance from active face to entrance window, detector holder density and end cap window thickness), as well as the size of the active volume of the detector (outer contact crystal radius, thickness of dead layer active face, thickness of dead layer side face), has a large effect on the efficiency, particularly for low-energy gamma rays.

The results are consistent with previous studies and show that, for this geometry set-up, three parameters (outer crystal radius, thickness of dead layer active face and outer contact crystal length) are of most importance in defining an accurate detector model, while detector parameters concerning the side of the germanium crystal (except for the thickness of dead layer side face, which also affects the active volume of the detector) are relatively insensitive to change and have little impact on the model's output for FEP efficiency.

The results of a sensitivity analysis for the same type of detector using a Marinelli beaker (where the source also surrounds the sides of the crystal) are shown in Figure 3.5. In contrast to the case of the cylindrical geometry placed directly on top of the end cap, the outer contact crystal length has a significant influence on FEP efficiencies at low energies, and other parameters that were relatively unimportant for the cylindrical geometry, such as the detector holder material and the thickness of dead layer side face, become important at such low energies. For this

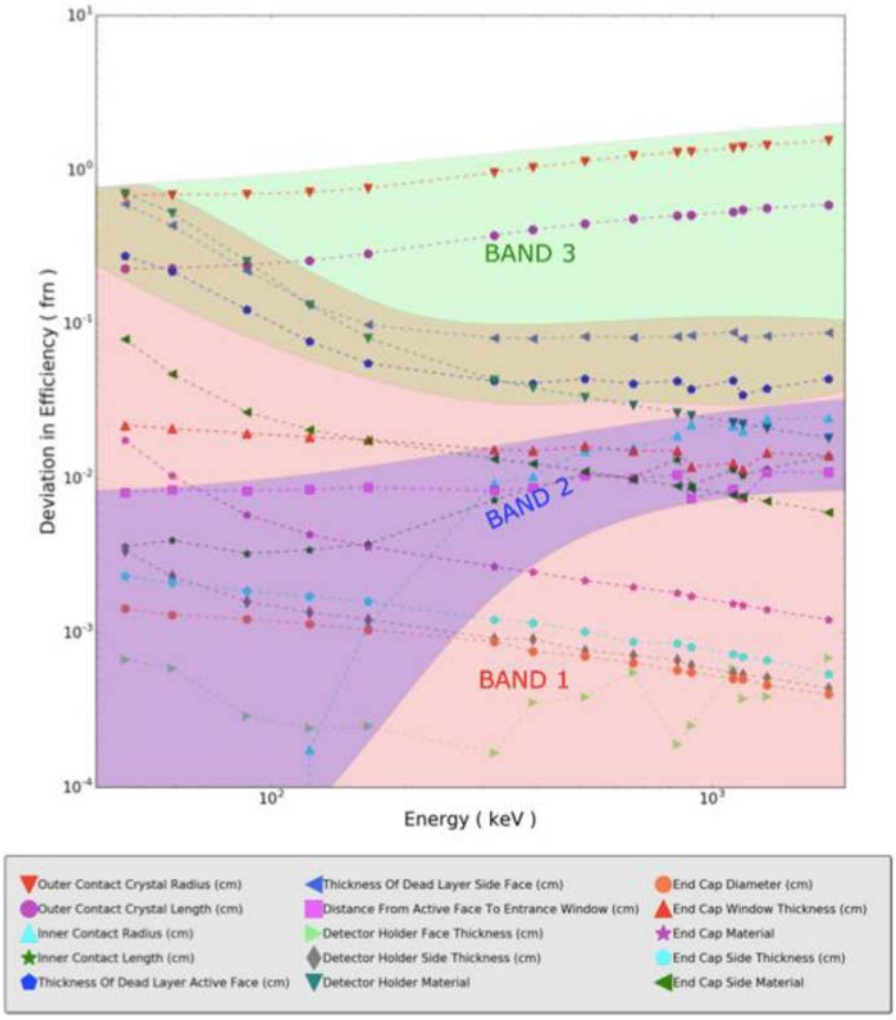

Figure 3.5. Sensitivity analysis for a generic HPGe coaxial detector (1000 GEO).

geometry arrangement, the most sensitive parameters are those that define the active volume of the detector, particularly the outer contact crystal radius and crystal length, as well as the thicknesses of the face and side dead layers.

For a well-type generic detector with a cylindrical geometry (5 GEO) placed inside the well, the most sensitive parameters affecting the FEP efficiency are the crystal well length and the distance from the bottom of the crystal well to the end cap bottom. At high energies, the outer contact crystal length and crystal well radius are important. In contrast, the end cap outside the well side thickness, the thickness of dead layer outside the well and the detector holder thickness outside the well are relatively insensitive to this particular counting arrangement (Figure 3.6).

3.2 Development of an Automated Software Application for Detector Model Optimisation

The optimisation program developed during this project, written in Python, acts as a front end for the GESPECOR software to conduct iterative runs and, using an optimisation algorithm, allows the use of several experimental FEP efficiency curves (corresponding to multiple geometries) in parallel, to optimise all (or selected) detector parameters. In this way, an optimised set of parameters is found that simultaneously fits all experimental curves and accounts for the sensitivity of various parameters under different counting geometry arrangements.

The program, which uses PyAutoIt 0.4 (Python binding for AutoItX3.dll) to enable the automation of

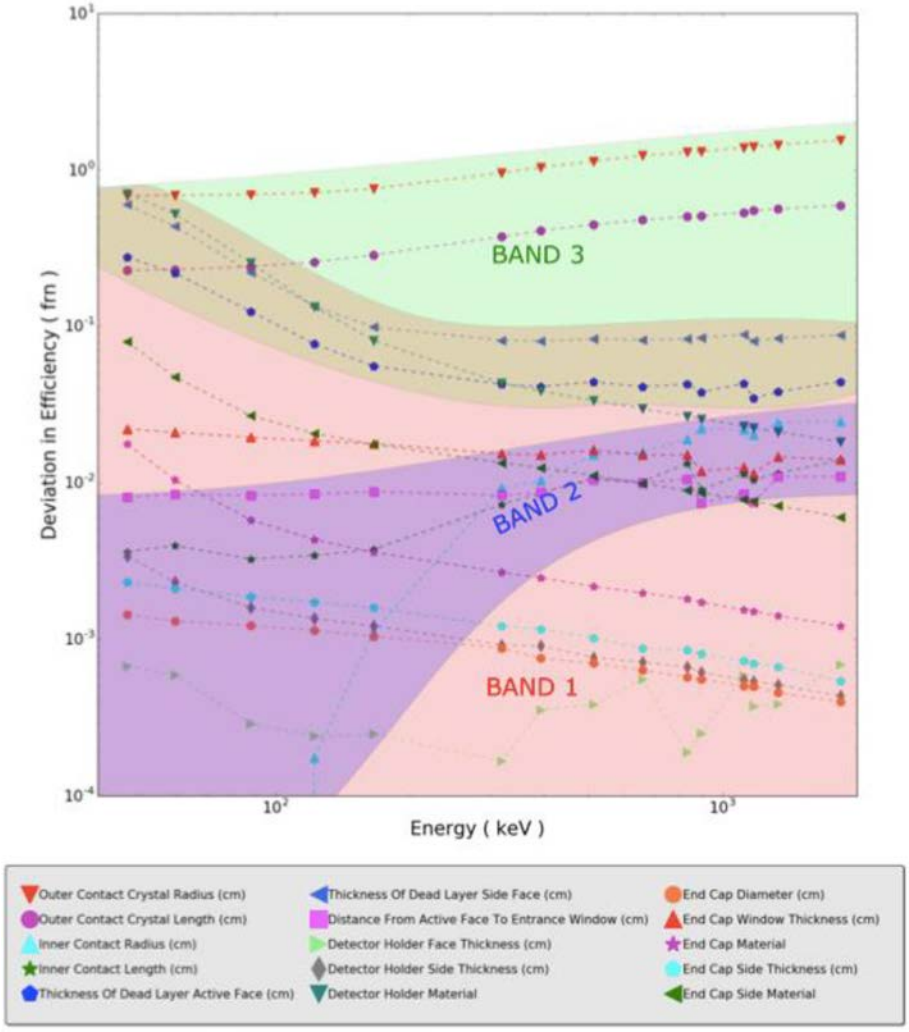

Figure 3.6. Sensitivity analysis for a generic well detector (5 GEO).

successive GESPECOR runs and tkinter to create a user-friendly GUI, allows the user to have control over the choice of optimisation algorithm. Although a differential evolution (DE) optimisation algorithm was initially used, a covariance matrix adaptation evolution strategy (CMAES) algorithm (Hansen *et al*., 2019), incorporated into the software from the pycma Python package, was found to provide a more effective, robust method of parameter optimisation, and was therefore selected as the default optimisation algorithm in the final version of the software. The CMAES is a stochastic derivative-free numerical optimisation algorithm developed for difficult optimisation problems in continuous search spaces.

To run the program, a set of nominal parameters and tolerances are introduced to define the search parameter space (Figure 3.7), together with information on the material composition of the detector's holder, the end cap window and the end cap side. Once this information has been entered, the user can input experimental FEP efficiency values for multiple geometries. For each of these geometries, a set of geometry, source matrix and shield files are specified (Figure 3.8), together with a list of the energy–FEP efficiency pairs obtained experimentally using appropriate calibration sources (Figure 3.9). With all the required inputs entered, the optimisation process is finally started by selecting an optimisation method and clicking the "RUN" button (Figure 3.10) without the need for further user intervention. The final set of optimised parameters and calculated FEP efficiencies for each of the geometries used in the process are saved and the efficiencies displayed graphically in a plot window. A flow chart of the program is shown in Figure 3.11. The optimisation process can take several hours to complete,

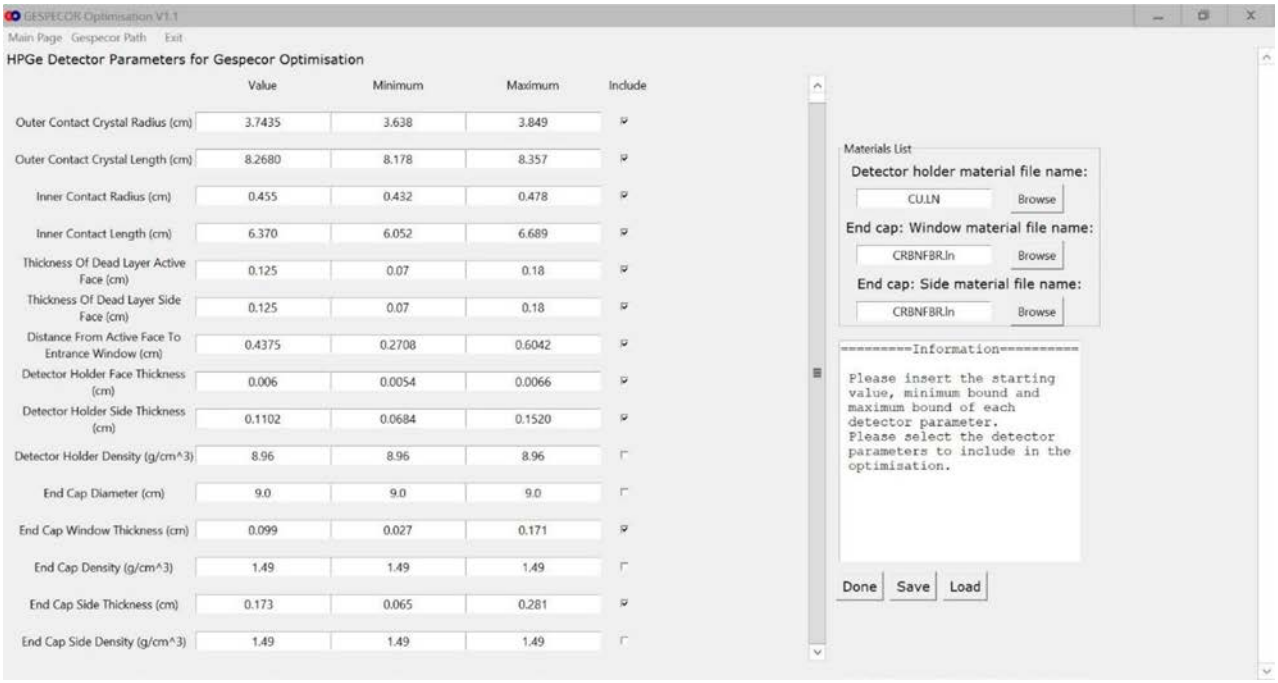

Figure 3.7. HPGe detector parameter input for the optimisation program.

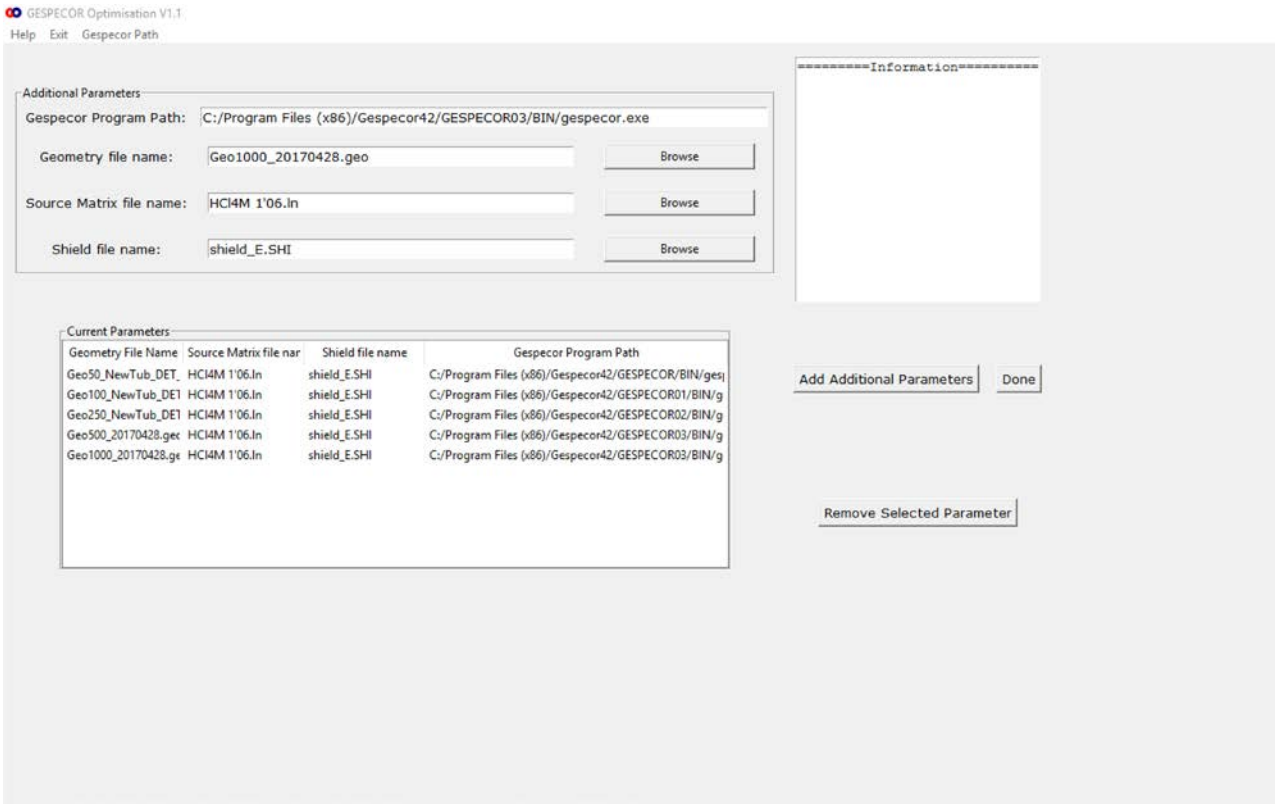

Figure 3.8. Additional parameters screen, used to enter and define the geometries used in the optimisation process.

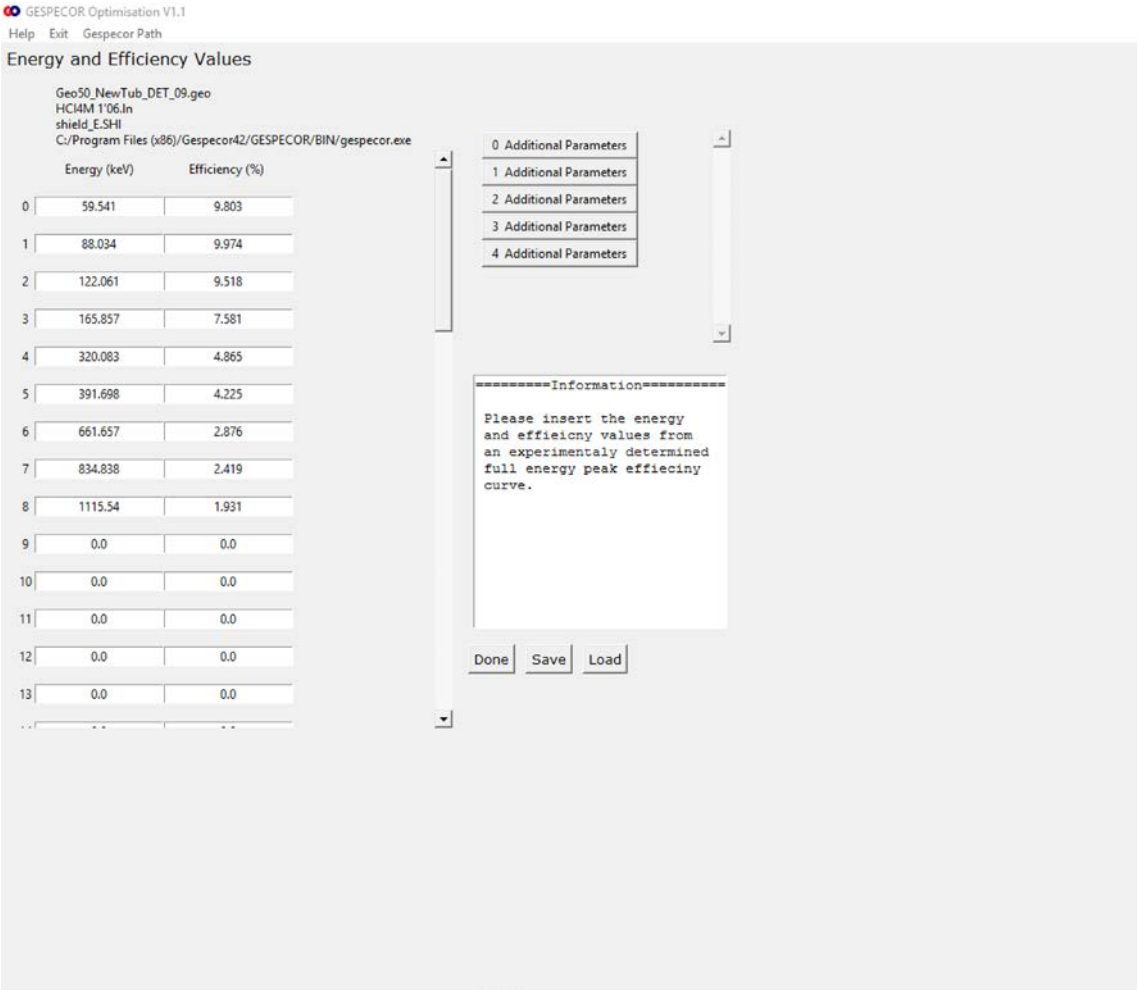

Figure 3.9. Energy and efficiency screen, used to input energy–FEP efficiency pairs determined experimentally for each of the geometries entered in the additional parameters screen.

depending on the number of experimental FEP curves employed.

The model optimisation software is initially run using only the experimental FEP efficiencies for radionuclides not affected by coincidence summing. The optimised model parameters obtained in this first iteration are used to correct the efficiencies of nuclides affected by coincidence summing, which are then included in a second, final, iteration of the optimisation process. The inclusion of these nuclides (most notably ^{60}Co and ^{88}Y, commonly present in multi-gamma calibration standards) increases the number of experimental efficiencies at high energies (> 1000 keV), extending the range over which the optimised model can reliably be used and enabling better optimisation of detector parameters that are particularly sensitive to high-energy gamma rays.

3.3 Optimisation of Detector Model Parameters for HPGe Detectors in Use at the EPA's ORM Analytical Laboratory

To illustrate the above detector optimisation process, we detail here the results obtained for one of the detectors used at the ORM's analytical laboratory (detector 12), a p-type coaxial HPGe detector (ORTEC GEM-M7680P4-90RB-S), and give a less detailed overview of the results obtained for other detectors. The nominal baseline parameters obtained from manufacturer specifications for detector 12 have already been presented in Table 2.2 (see section 2.2). Using these baseline parameters for FEP efficiency calculation showed mean absolute deviations between modelled and experimental efficiencies of ~30% for the three cylindrical geometries (50 GEO, 100 GEO

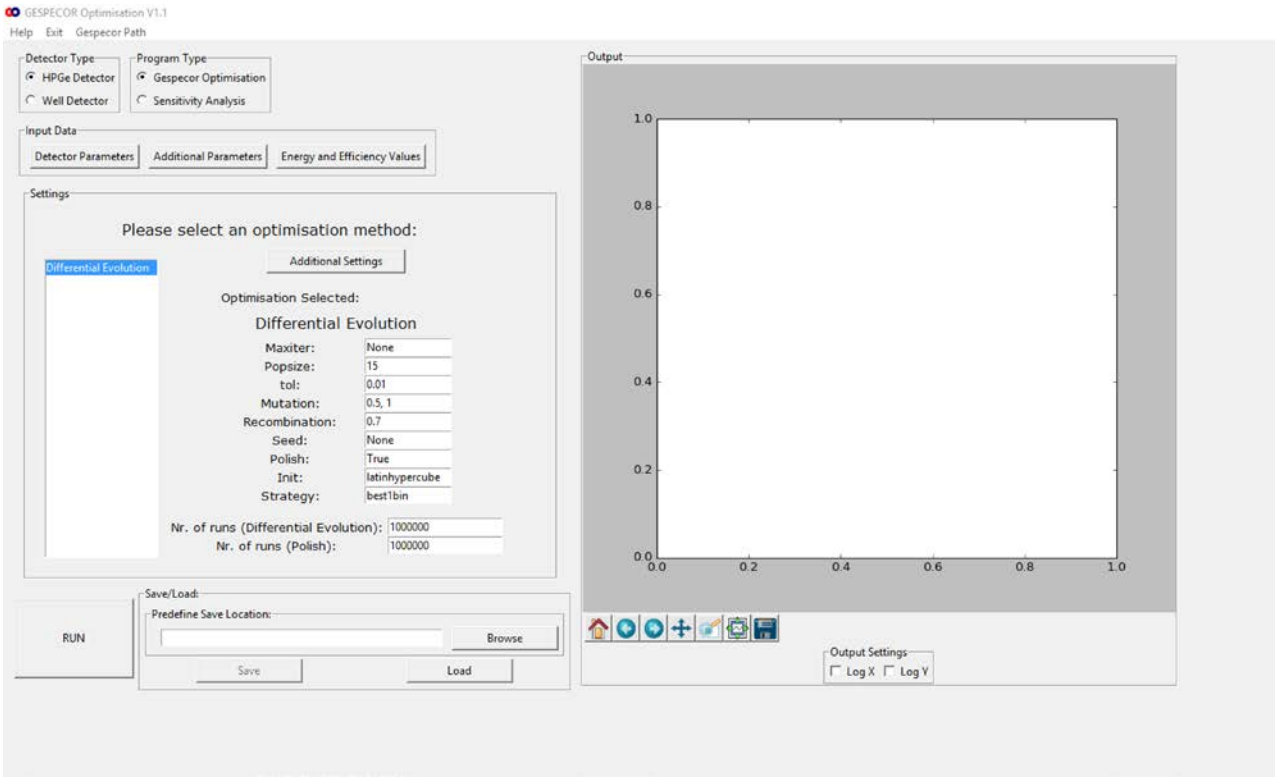

Figure 3.10. Optimisation screen used to run the optimisation program.

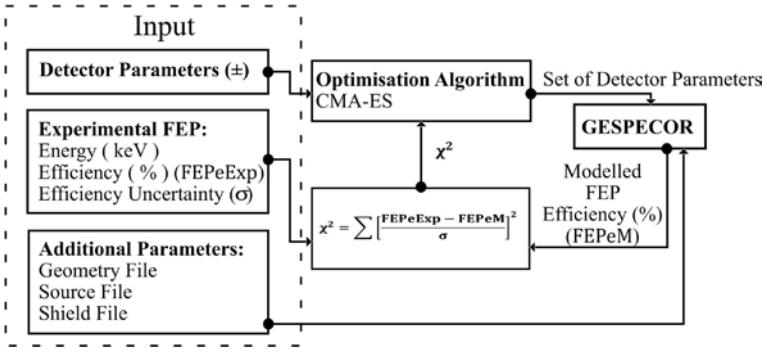

Figure 3.11. Flow chart for the optimisation program. Reprinted from Murphy *et al.* (2020). Copyright © 2019, with permission from Elsevier.

and 250 GEO) and ~45% for the two Marinelli beakers (500 GEO and 1000 GEO) over the energy range 59–1836 keV, with the highest discrepancies taking place at low energies.

As mentioned, a first iteration of the optimisation process was carried out using only those nuclides free of coincidence summing effects as input, giving a total of 40 experimental FEP efficiencies (eight per geometry multiplied by five geometries). The optimised model obtained in this way was used to derive appropriate true coincidence summing correction factors for ^{60}Co, ^{88}Y and ^{139}Ce. A second iteration of the optimisation program was carried out including the corrected efficiencies for these nuclides, increasing the number of experimental FEP efficiencies to 65 (13 per geometry). Following this second optimisation process, the mean absolute deviation between modelled and experimental efficiencies over the full energy range considered (59–1836 keV) was found to be < 2% for all geometries, with no individual absolute deviation higher than 4% (Figure 3.12).

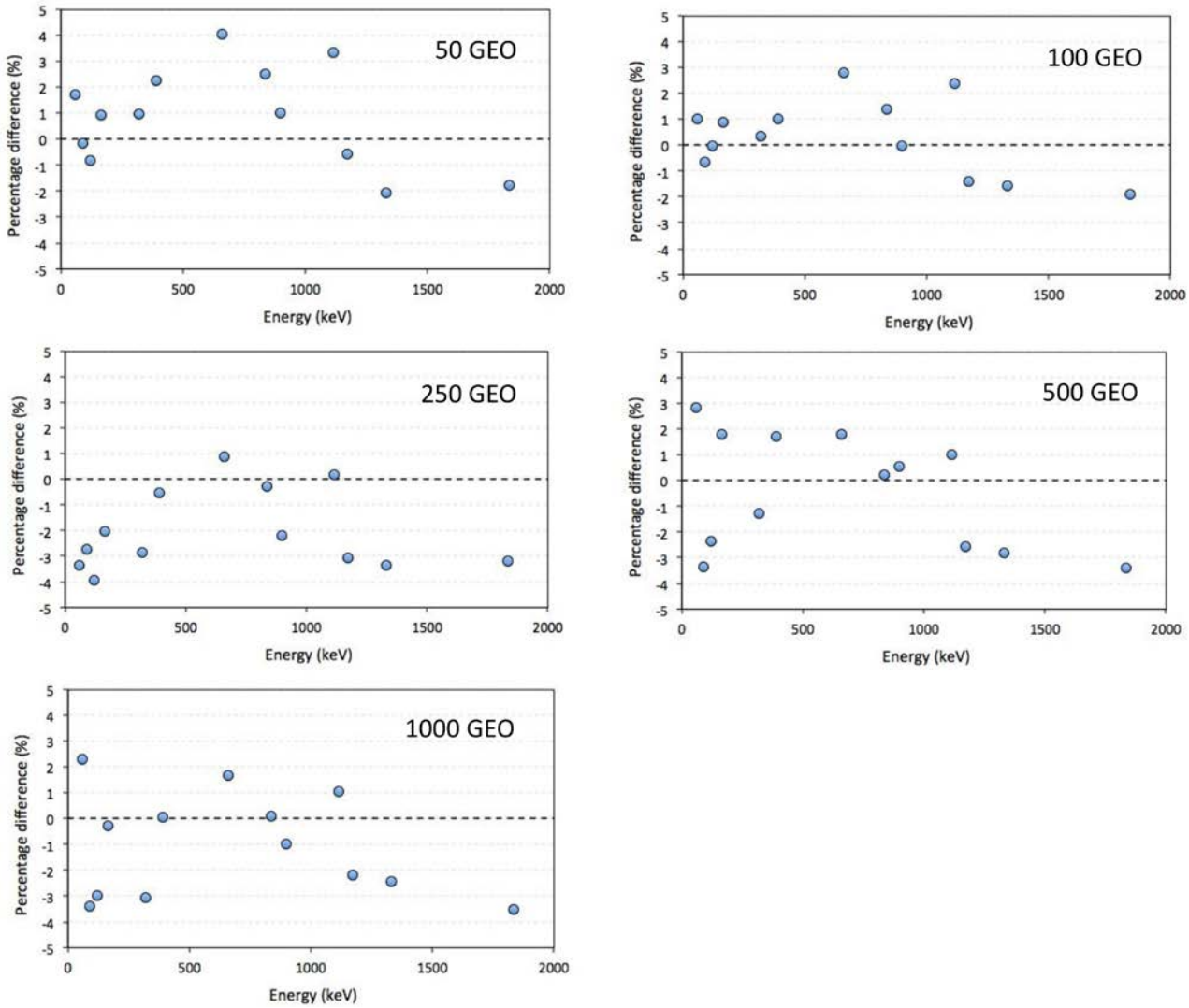

Figure 3.12. Percentage deviations between measured and modelled FEP efficiencies following model optimisation for detector 12. Reprinted from Murphy *et al*. (2020). Copyright © 2019, with permission from Elsevier.

The set of optimised model parameters for the detector are summarised in Table 3.1. Optimised crystal dimensions, comprising the outer and inner crystal radii and lengths, were well defined by the baseline parameters and remained relatively unchanged (within 5% of the specified values). In contrast, significant changes were required for other baseline parameters, including the dead layer face thickness, the distance from the active face to the entrance window, the end cap side and window thicknesses and the detector holder side thickness. Similar variation in dead layer(s) thicknesses and crystal position have been found during the optimisation of other detectors in our laboratories and have also been reported in the literature as being required to match experimental and modelled FEP efficiencies (Hardy *et al.*, 2002; Helmer *et al.*, 2003; Luís *et al.*, 2010; Hedman *et al.*, 2015; Novotny and To, 2015).

As another example of the level of agreement achieved between modelled and experimental data using this approach, the results obtained for one of the ORM's n-type detectors (detector 1, n-type ORTEC GMX 70230-S) using four FEP efficiency curves as input, corresponding to a 50 mL tub (50 GEO), a 100-mL tub (100 GEO), a 250-mL tub (250 GEO) and a 500 mL Marinelli beaker (500 GEO), are shown in Figure 3.13. In this figure, log–log plots of the FEP efficiencies for each of the geometries are presented. The plots show the modelled FEP efficiencies based on the baseline parameters provided by the

Table 3.1. Set of baseline and optimised parameters for detector 12 (GEM-M7680P4-90-RB-S)

Parameter	Baseline	Optimised
Outer contact crystal radius (cm)	3.80	3.64
Outer contact crystal length (cm)	8.37	8.26
Inner contact radius (cm)	0.455	0.475
Inner contact length (cm)	6.37	6.13
Thickness of dead layer active face (cm)	0.07	0.12
Thickness of dead layer side face (cm)	0.07	0.09
Distance from active face to entrance window (cm)	0.40	0.27
Detector holder face thickness (cm)	0.006	0.006
Detector holder side thickness (cm)	0.076	0.147
Detector holder density ($g\,cm^{-3}$)[a]	8.96	8.96
End cap diameter (cm)[a]	9.0	9.0
End cap window thickness (cm)	0.09	0.14
End cap density ($g\,cm^{-3}$)[a]	1.49	1.49
End cap side thickness (cm)	0.16	0.28
End cap side density ($g\,cm^{-3}$)[a]	1.49	1.49

[a]**These parameters are fixed and do not change during the optimisation process.**

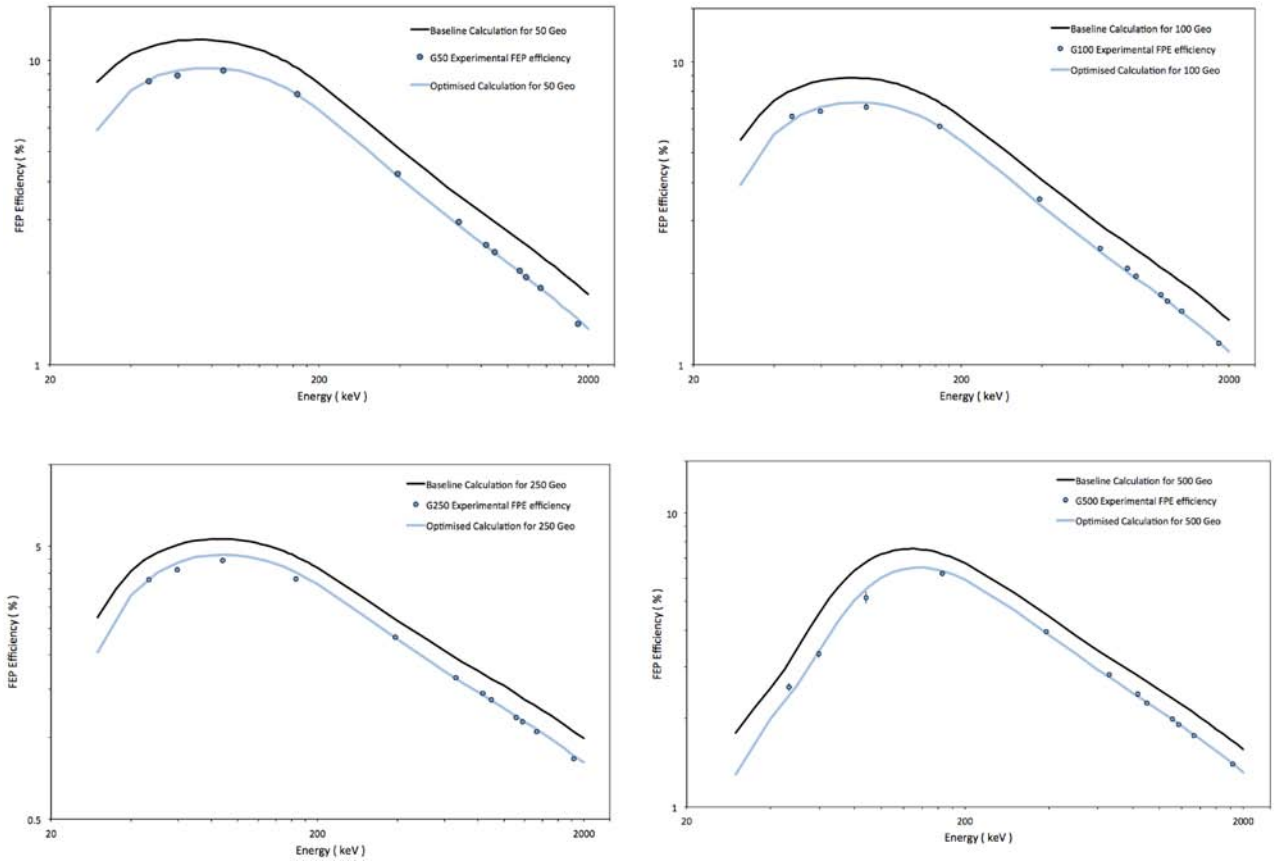

Figure 3.13. Experimental and modelled FEP efficiencies for detector 1 (GMX-70230-S) at the EPA's ORM laboratory for four geometries: 50 GEO (top left), 100 GEO (top right), 250 GEO (bottom left) and 500 GEO (bottom right). The solid black lines correspond to modelled efficiencies obtained using baseline parameters, while the blue lines show GESPECOR-computed efficiencies using the optimised detector model.

manufacturers and those obtained at the end of the optimisation process. In all cases, Monte Carlo simulations using baseline parameters overestimated FEP efficiencies at all energies, with values differing from the experimental values by as much as 36%. Following the optimisation process, however, mean deviations over the full energy range considered (40.5–1836 keV) were approximately 2% for all geometries, with differences between modelled and experimental efficiencies of less than 4% for 43 out of the 48 (90%) points. For the remaining five points, which correspond to low-energy emissions in the G500 and G250 geometries, the agreement between modelled and experimental efficiencies was still within 7%.

The application of the optimisation process to well-type detectors required modification of the Python program to take account of the different set of parameters needed to characterise this type of detector (see Figure 2.1). The required changes to the Python scripts were made and optimisation runs carried out for detectors 6 and 14 using only those nuclides not affected by true coincidence summing. Figure 3.14 shows the results of this optimisation process for detector 6. Excellent agreement was achieved between modelled and experimental FEP efficiencies, with a mean absolute deviation of < 1% and no individual absolute deviation higher than 2.2%.

The optimised model was used to estimate the true coincidence summing correction factors for those nuclides present in the calibration standard that are known to be affected by coincidence summing effects (^{60}Co, ^{88}Y and ^{139}Ce). As shown in Figure 3.15, application of these correction factors brought the efficiencies for these nuclides much closer to the "coincidence-free" efficiency curve, but corrected efficiencies remained 6–8% lower than those predicted by the optimised model and by the non-linear polynomial fit to the FEP efficiencies for the non-true coincidence summing nuclides. Although the uncertainty of the true coincidence summing correction factors for measurements carried out in well detectors is reported to be significant (3% for nuclides with simple decay schemes and 5–10% for nuclides with complex schemes), better agreement should be expected from an accurate model of the detector. The possible reasons for the observed discrepancy should be investigated in the future, with a better characterisation of the detectors and additional coincidence-free nuclides to better define the FEP efficiency curves.

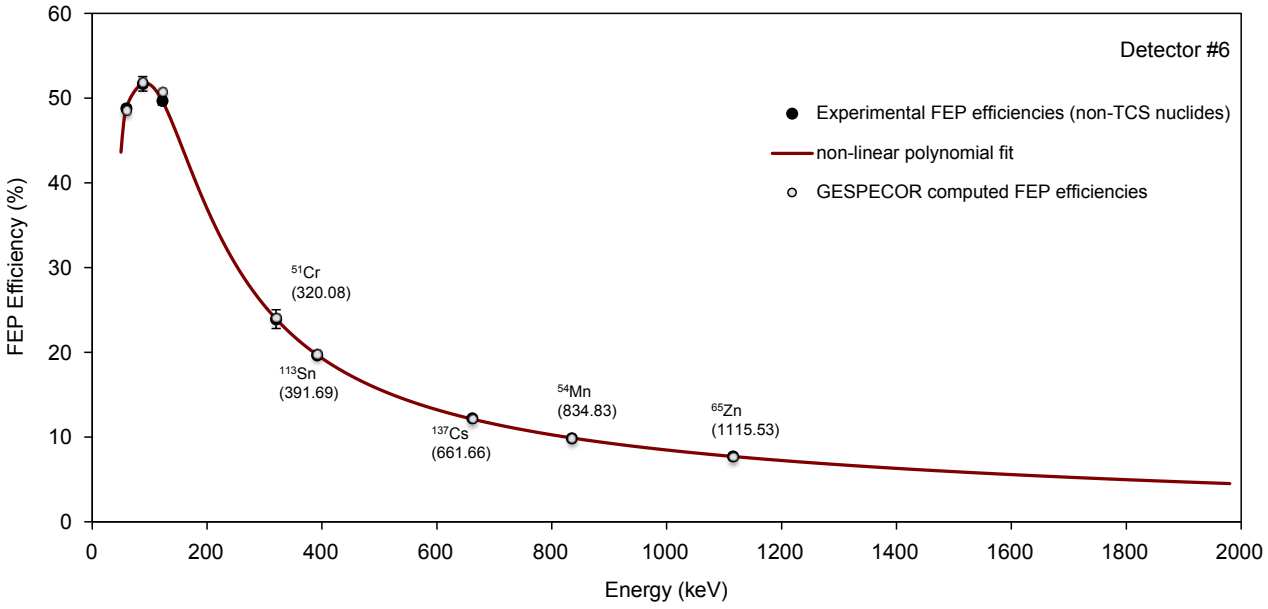

Figure 3.14. Experimental and GESPECOR-computed FEP efficiencies for the 5 GEO geometry following detector optimisation using only nuclides not affected by true coincidence summing effects. TCS, true coincidence summing.

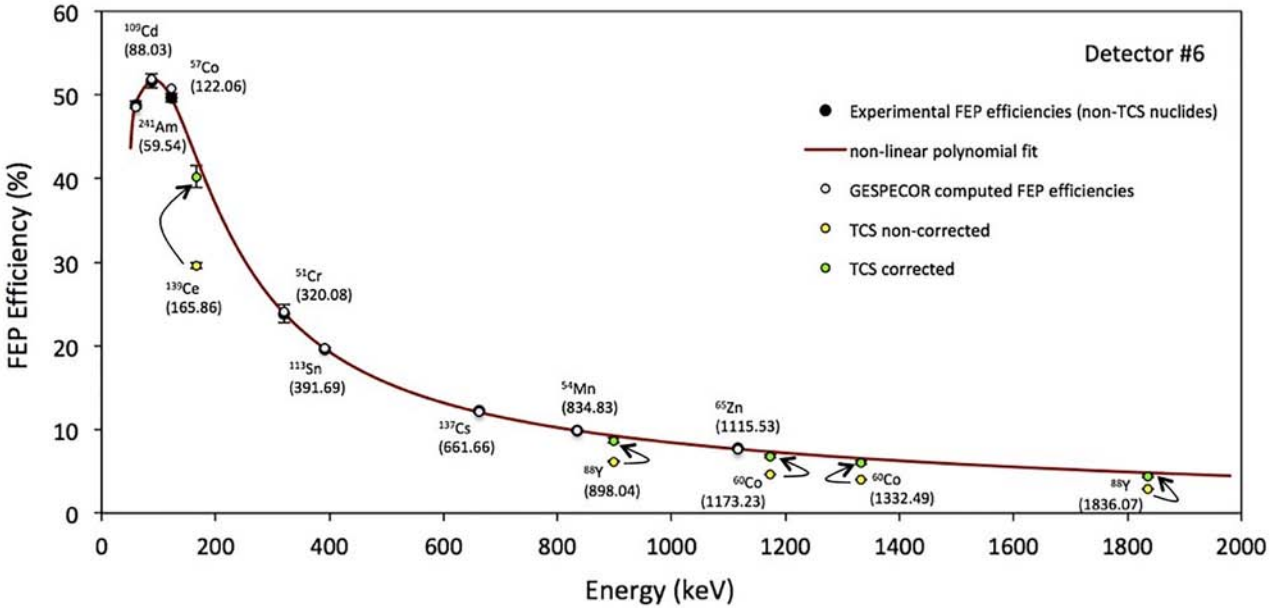

Figure 3.15. The effect of true coincidence summing corrections on the FEP efficiencies of ^{60}Co, ^{88}Y and ^{139}Ce, carried out using the optimised model for detector 6. In plotting the error bars, an uncertainty of 3% has been assumed for all computed true coincidence summing correction factors. TCS, true coincidence summing.

4 Self-attenuation Corrections

4.1 Determination of Approximate Generic Composition and Density for Common Environmental Materials Analysed by the EPA's ORM – Development of Methodologies for the Determination of Linear and Mass Attenuation Coefficients

The experimental and modelled FEP efficiency values obtained using the methodologies outlined in the previous chapters are only valid for measuring samples that have the same geometry and identical composition and density as the calibration standard (4 M HCl in our case). If, as is most often the case, the sample being measured differs from the calibration standard used for FEP efficiency calibration in terms of both matrix composition and density, a suitable correction factor must be introduced to evaluate the FEP efficiency for the sample of interest at a given photon energy *E*. This energy-dependent correction factor, known as the self-attenuation correction factor, F_{ca}, accounts for the difference in self-attenuation between the sample and the calibration standard, and depends on the sample geometry, the linear attenuation coefficients for both sample and calibration standard and, to a lesser extent, on the detector parameters. The relationship between the FEP efficiencies for the calibration standard and the measured sample is given in equation 4.1:

$$\varepsilon(E,\text{sample}) = F_{ca}(E,\text{sample/calibration standard}) \cdot \varepsilon(E,\text{calibration standard}) \quad (4.1)$$

Monte Carlo methods are used in GESPECOR to compute self-attenuation correction factors for any sample matrix with respect to the calibration source, so that reliable values of the efficiency for any matrix can readily be obtained by multiplying the computed correction factors by the experimental values of the efficiency, measured with a calibration source in the same experimental arrangement (geometry).

GESPECOR offers a number of different options to compute self-attenuation correction factors for a set of specified energies. In the standard procedure, a detailed knowledge of the chemical composition of both sample and calibration standard is required. Based on this information, linear attenuation coefficients are computed by GESPECOR using the XCOM photon cross-sections database (https://www.nist.gov/pml/xcom-photon-cross-sections-database). Alternatively, linear attenuation coefficients can be directly input by the user if the sample composition is not known but the linear attenuation coefficients have been measured by carrying out transmission experiments under "good geometry" conditions (i.e. collimated source). If not available, attenuation coefficients can also be directly evaluated by GESPECOR from transmission experiments using uncollimated sources. In each case, Monte Carlo simulations are performed only once for a given detector model and geometry set-up. The results are stored in an appropriate file specific for this measurement arrangement, so the subsequent computation of self-attenuation correction factors for other samples is very fast. A special procedure, involving full, independent Monte Carlo simulations for each matrix and energy, can be used if a high level of accuracy is required or if the self-attenuation is expected to be very high, provided a reliable model of the detector is in place.

As the exact chemical composition of the majority of matrices routinely analysed by the EPA's ORM laboratory is not known, a series of transmission experiments were carried out during the project to experimentally measure attenuation coefficients for commonly analysed materials (e.g. seaweed, fish flesh, honey, vegetation ash), so that appropriate self-attenuation correction factors can be calculated using GESPECOR. The experimental set-up, depicted in Figure 4.1, made use of collimated gamma-ray beams to measure transmission through an empty container and a container filled with the sample matrix of interest to a known height, *x*. The measured FEP count rates (R_1 and R_2) at a given energy (*E*) can be used, together with the density of the sample (ρ) to derive the linear (μ) and mass (μ_m) attenuation coefficient for that energy using the expressions in equations 4.2 and 4.3:

$$\mu(E) = \frac{1}{x} \ln\left(\frac{R_1(E)}{R_2(E)}\right) \quad (4.2)$$

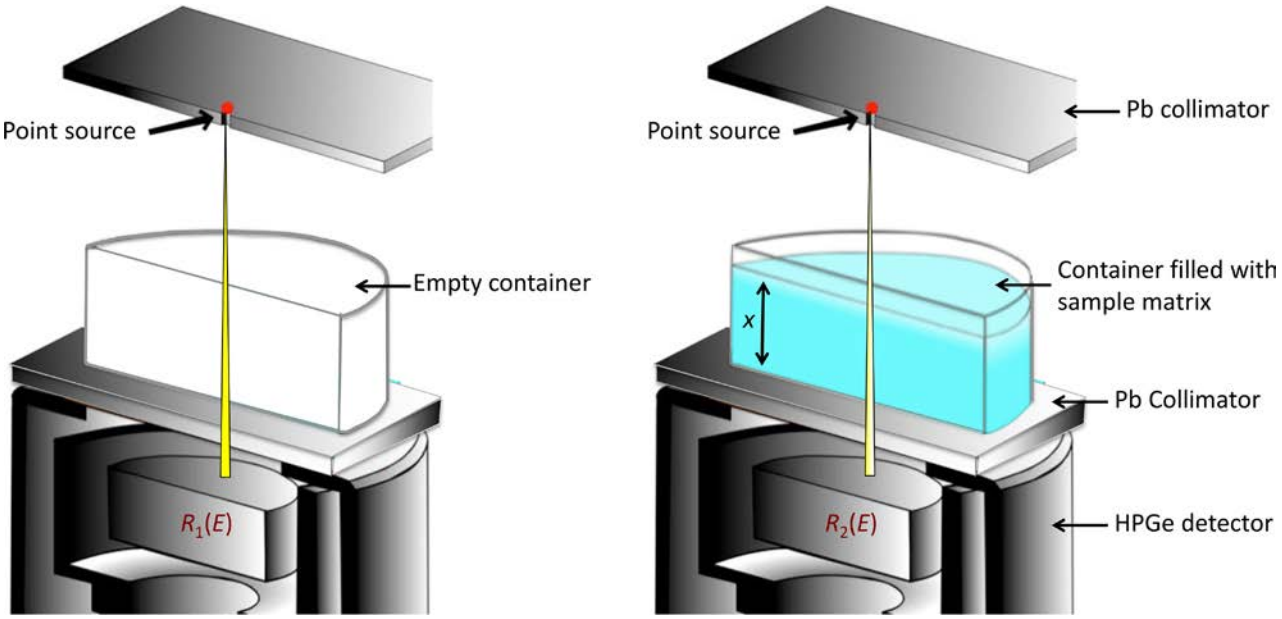

Figure 4.1. Experimental set-up for transmission experiments using collimated point sources.

$$\mu_m = \frac{\mu}{\rho} \qquad (4.3)$$

The validity of this approach was tested by the measurement of mass attenuation coefficients for sample matrices of known chemical composition (e.g. 2 M HNO_3, 4 M HCl, $CaHPO_4$, iron powder), and the comparison of the values obtained with those computed using the XCOM photon cross-sections database, based on the samples' chemical composition. The results, shown in Figure 4.2, confirm that accurate mass attenuation coefficients can be obtained from these transmission measurements even for high atomic number, high-density samples, such as iron powder, whose self-attenuation effects are very pronounced, especially at low photon energies.

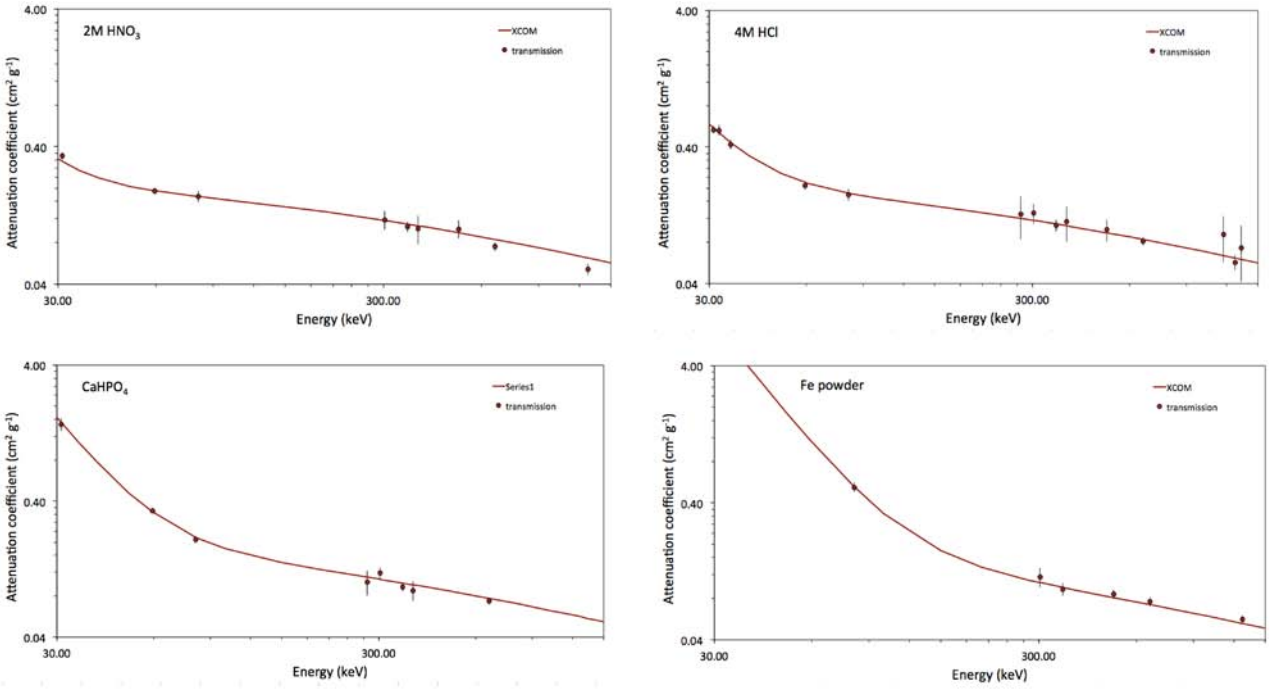

Figure 4.2. Mass attenuation coefficients for samples of known density and composition as determined by transmission experiments (•) and using the XCOM photon cross-sections database (—).

Attenuation coefficients for a number of environmental matrices of varying density and composition were determined using the validated transmission approach outlined above (Figure 4.3). For each matrix, a generic composition, based on elemental analysis data found in the literature for similar samples, was also used to generate attenuation coefficients using the XCOM photon cross-sections database. As Figure 4.3 shows, there is good agreement between the experimentally determined mass attenuation coefficients and those found based on generic composition. Because self-attenuation depends on sample composition and density only through the values of the linear attenuation coefficients, generic compositions that have been shown to match measured attenuation coefficients over a wide range of energies (especially low energies) could be used to derive appropriate self-attenuation correction factors using GESPECOR's standard method, even if their composition is not identical to the samples analysed.

As an alternative to the above transmission methods, a new GESPECOR module developed to directly compute linear attenuation coefficients based on uncollimated source transmission experiments was tested for a number of matrices, as this could be a faster, more convenient procedure than the conventional transmission experiments using collimated sources. As in the collimated source approach, the value of the linear attenuation coefficient at a given energy is obtained by comparing the measured count rates of a point source for an empty container and for a container filled with the sample matrix. In this case, however, the source is placed directly on top of the container without the need for collimation (Figure 4.4), thus reducing counting times and allowing the use of weaker sources. Calculation of the attenuation coefficient is complicated by the distribution of photon path lengths through the sample and the change in the detector's response to photons arriving at different incidence angles. These factors are taken into consideration by GESPECOR when deriving attenuation coefficients using this approach.

Some of the results obtained for matrices of known composition are shown in Figure 4.5. Although measured attenuation coefficients at high energies are in good agreement with those computed using XCOM, which are based on the sample's known elemental composition, significant differences were observed at lower energies (below 100 keV), with measured attenuation coefficients being consistently lower than those computed using XCOM, by as much as 25% in some cases. Further analyses will be required to

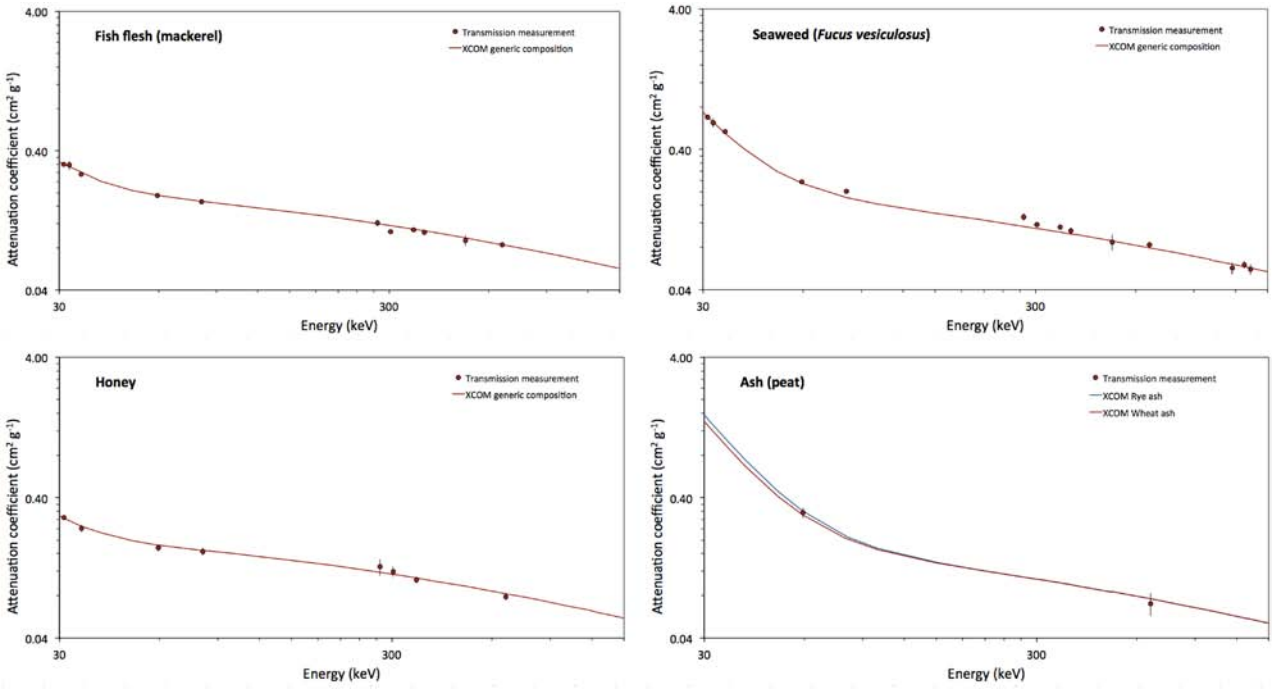

Figure 4.3. Mass attenuation coefficients for environmental samples of unknown composition as determined by transmission experiments (•) and using the XCOM photon cross-sections database (—) with sample generic composition.

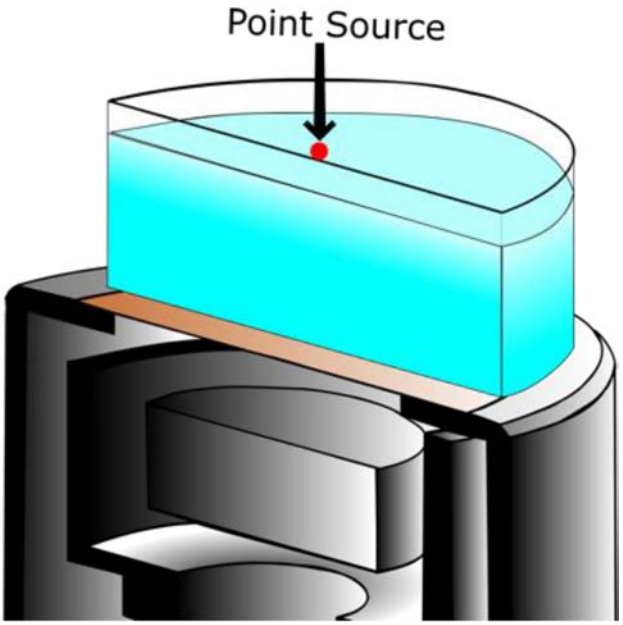

Figure 4.4. Experimental set-up for transmission experiments using uncollimated point sources.

determine if the source of these discrepancies lies in the approximations/assumptions made by the calculation algorithm used by GESPECOR, or if they can be attributed to systematic errors associated with the determination of FEP areas at low energies, particularly for X-ray emissions used for the calculation of some of the transmission factors used in the computation. However, with the new GESPECOR module making use of uncollimated transmission experiments, it provides a fast and convenient method for the determination of linear attenuation coefficients for energies above 100 keV if large variations in composition are expected within a given environmental matrix (e.g. soils, sediments) that prevent the use of generic compositions.

4.2 Determination of Self-attenuation Correction Factors

The attenuation coefficients obtained based on collimated source transmission experiments and/or sample elemental composition in the previous subtask, together with the optimised GESPECOR models for each of the detectors obtained in Chapter 3 can now be used to easily derive sets of self-attenuation correction factors (F_{ca}) for each geometry and sample matrix in a specific detector. Examples of the type of data generated are presented in Tables 4.1 and 4.2, which summarise the self-attenuation correction factors for seaweed (*Fucus vesiculosus*) and fish flesh (mackerel) matrices in different geometry arrangements for one of the detectors (detector 1).

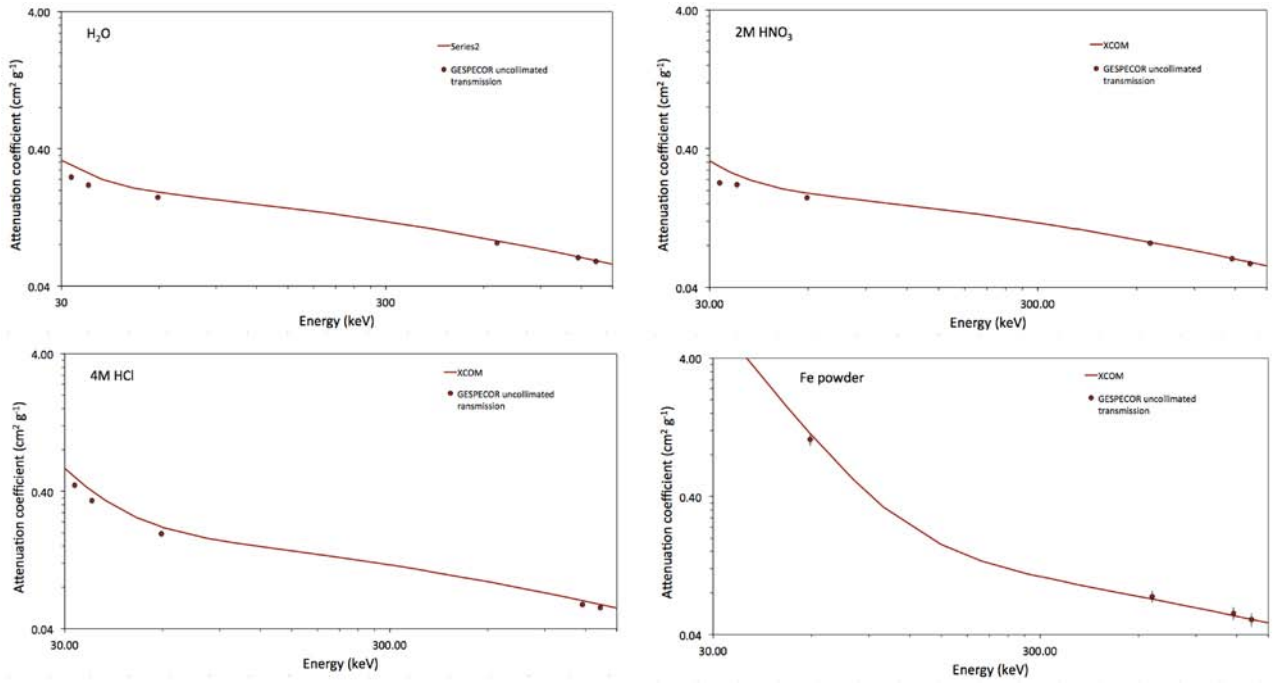

Figure 4.5. Mass attenuation coefficients for environmental samples of known composition as determined by uncollimated source transmission experiments (•) and using the XCOM photon cross sections database.

Table 4.1. Self-attenuation correction factors (F_{ca}) (relative to 4 M HCl standard) for seaweed (*F. vesiculosus*) samples counted in detector 1 using different counting geometries

		Geometry				
Nuclide	Energy |(keV)	50 GEO	100 GEO	250 GEO	500 GEO	1000 GEO
^{133}Ba	30.97	0.986	0.978	0.971	0.983	0.976
^{137}Cs	32.19	0.991	0.986	0.981	0.989	0.984
^{133}Ba	34.99	0.990	0.984	0.978	0.988	0.982
^{241}Am	59.54	1.019	1.033	1.053	1.024	1.037
^{133}Ba	80.99	1.015	1.026	1.042	1.019	1.029
^{133}Ba	276.39	1.010	1.017	1.029	1.013	1.019
^{133}Ba	302.85	1.016	1.029	1.049	1.021	1.032
^{133}Ba	356.01	1.013	1.024	1.041	1.018	1.028
^{133}Ba	383.85	1.016	1.028	1.047	1.020	1.031
^{22}Na	511.00	1.018	1.031	1.054	1.023	1.036
^{137}Cs	661.67	1.012	1.022	1.037	1.016	1.025
^{60}Co	1173.23	1.014	1.024	1.042	1.018	1.028
^{22}Na	1274.54	1.010	1.017	1.030	1.013	1.020
^{60}Co	1332.49	1.011	1.020	1.034	1.014	1.023

Table 4.2. Self-attenuation correction factors (F_{ca}) (relative to 4 M HCl standard) for fish flesh (mackerel) samples counted in detector 1 using different counting geometries

		Geometry				
Nuclide	Energy (keV)	50 GEO	100 GEO	250 GEO	500 GEO	1000 GEO
^{133}Ba	30.97	1.158	1.263	1.393	1.195	1.301
^{137}Cs	32.19	1.133	1.222	1.332	1.164	1.253
^{133}Ba	34.99	1.113	1.191	1.295	1.141	1.218
^{241}Am	59.54	1.025	1.043	1.070	1.032	1.049
^{133}Ba	80.99	1.014	1.024	1.039	1.018	1.027
^{133}Ba	276.39	1.004	1.006	1.010	1.005	1.007
^{133}Ba	302.85	1.012	1.020	1.034	1.015	1.023
^{133}Ba	356.01	1.005	1.009	1.014	1.006	1.010
^{133}Ba	383.85	1.005	1.009	1.015	1.007	1.010
^{22}Na	511.00	1.006	1.010	1.017	1.008	1.012
^{137}Cs	661.67	1.003	1.006	1.010	1.004	1.007
^{22}Na	1274.54	1.002	1.004	1.007	1.003	1.005

Note that, because low-energy linear attenuation coefficients for seaweed are quite similar to those for the 4 M HCl standard, self-attenuation correction factors remain close to unity for this matrix in all geometries, with corrected sample FEP efficiencies not differing significantly from those obtained using the calibration standard. In contrast, the lower linear attenuation coefficients for fish flesh (mackerel) at low energies result in self-attenuation correction factors that can be as high as 1.40 for certain geometries (e.g. 250 GEO). Failure to account for self-attenuation effects when quantifying low-energy gamma-emitting nuclides in this type of sample would clearly result in a significant overestimation of the activity concentrations, as the effective sample counting efficiencies are greater than those estimated based on the 4 M HCl standard.

As mentioned in Chapter 2, self-attenuation corrections were also used to extend existing FEP efficiency curves to lower energies by using a ^{210}Pb standard (46.5 keV). These corrections are required to account for the differences in self-attenuation between the ^{210}Pb standard medium (2 M HNO_3) and the multi-gamma calibration standard medium (4 M HCl). The effect of the applied corrections for different geometries in one of the characterised detectors (detector 1) is shown in Figure 4.6. The corrections bring the measured efficiencies for ^{210}Pb much closer to the values expected for the 4 M HCl calibration curve (used by the ORM laboratory as reference for all calculations in GESPECOR) based on the optimised detector model, providing validation of the model and emphasising the need to carry out self-attenuation corrections, particularly at low gamma energies.

4.3 Validation of Derived Self-attenuation Correction Factors Using Low-energy Radionuclides and Samples of Known Chemical Composition

As a further test of the validity of derived self-attenuation correction factors, an experiment was carried out to compare modelled and measured self-attenuation coefficients in samples of known composition. For this, a set of 0.1 M HNO_3 solutions containing increasing amounts of lead nitrate ($Pb(NO_2)_3$) were prepared in the 250 GEO geometry before addition of known activities of ^{210}Pb and ^{241}Am. As the mass of $Pb(NO_2)_3$ present in each solution was accurately known, it was possible to directly compute gamma attenuation coefficients with GESPECOR by specifying the composition for

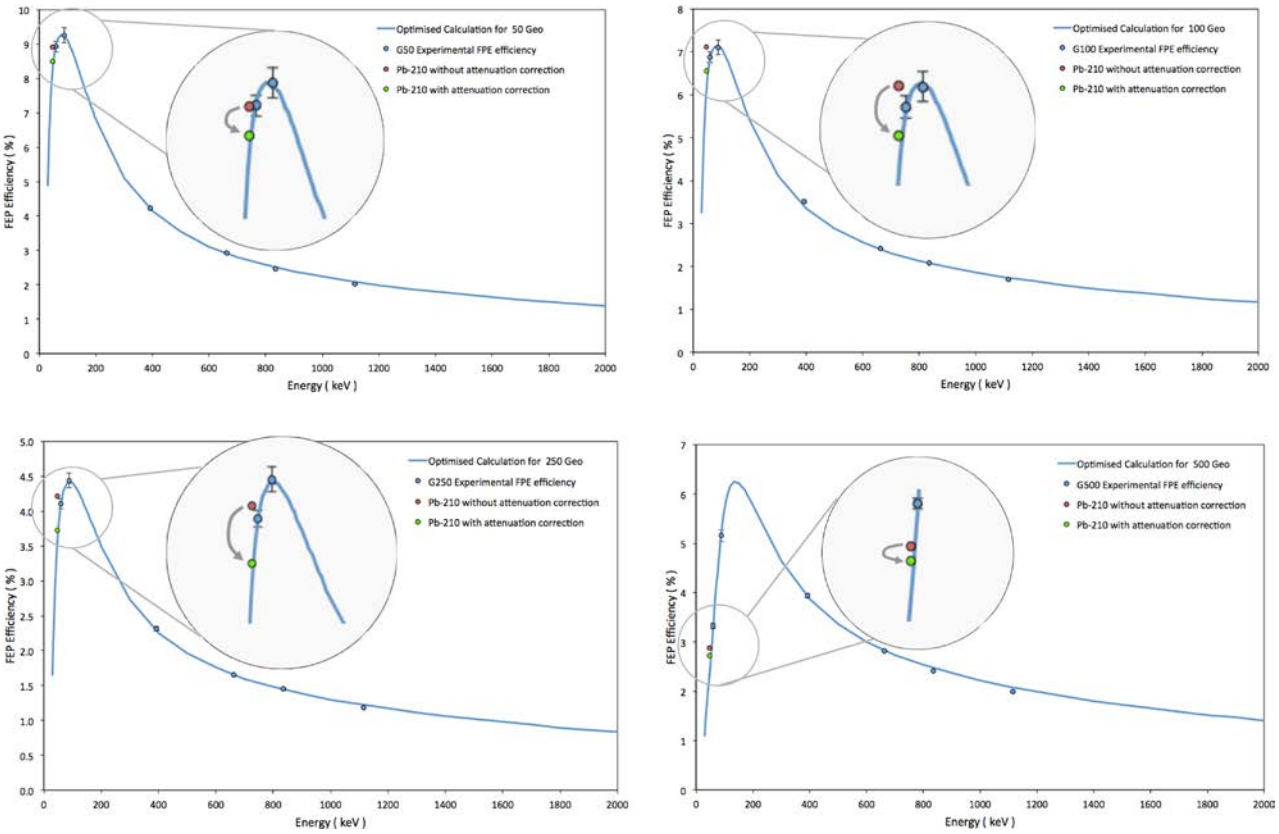

Figure 4.6. Extension of the 4 M HCl reference FEP efficiency curve for detector 1 to include ^{210}Pb (46.54 keV). The effect of self-attenuation caused by the difference in medium for the ^{210}Pb standard (2 M HNO_3) and the corrections achieved by applying computed self-attenuation correction factors is shown for each of the geometries: 50 GEO (top left), 100 GEO (top right), 250 GEO (bottom left) and 500 GEO (bottom right).

each sample (for example, see Figure 4.7). Taking the 0.1 M HNO_3 solution with no added $Pb(NO_2)_3$ as the reference medium, self-attenuation correction factors were computed by GESPECOR using the optimised model for detector 1, the measured sample densities and the specified compositions (Figure 4.8). The resulting self-attenuation correction factors obtained in this way, spanning quite a wide range of attenuation values, were then compared with those obtained experimentally by counting the samples in detector 1 and taking the ratio between the activities measured for a given sample and those for the reference sample (0.1 M HNO_3 solution containing no lead nitrate). For samples containing $Pb(NO_2)_3$, ^{210}Pb activities were corrected to take into account the activity of this nuclide present in the lead nitrate, which was quantified by counting each sample prior to the addition of the ^{210}Pb and ^{241}Am spikes.

The results of this comparison exercise are presented in Table 4.3. Excellent agreement was found between experimental and modelled self-attenuation correction factors (Figure 4.9), confirming the validity of the computed values even for cases where self-attenuation is so high as to decrease the measured FEP efficiency by a factor of 2. Uncertainties associated with the experimental correction factors were typically 2.5% and 1.2% for ^{210}Pb and ^{241}Am, respectively. Uncertainties of the self-attenuation correction factors computed by GESPECOR, even in samples showing large attenuation, have been reported to be better (and usually much better) than 5% for energies between 50 and 100 keV. For the purpose of comparison, a nominal uncertainty of 2% (of the same order as the experimental correction factors) was assigned to all computed self-attenuation correction factors.

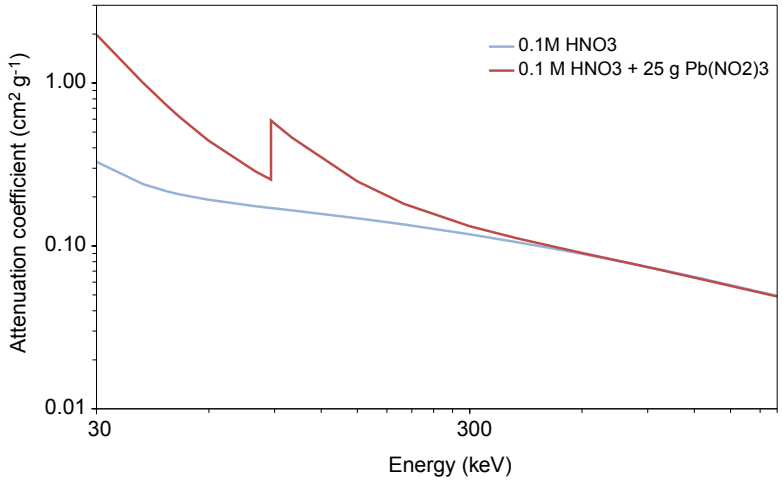

Figure 4.7. Mass attenuation coefficients for 0.1 M HNO_3 (reference solution) and the sample containing 25 g of $Pb(NO_2)_3$ using the XCOM photon cross-sections database.

Standard source composition file: 0.1MHNO3.mat Density: 1.00E+00 g/cm^3
Current sample composition file: 0.1MHNO3+25gPbN2O6 Density: 1.08E+00 g/cm^3

Energy	Mu(std)	Mu(sample)	Fa0	Fa1	Fca	Obs.
46.54	0.33687	0.89962	0.52767	0.26872	0.50926	
59.54	0.32477	0.61547	0.53788	0.36079	0.67077	

Figure 4.8. GESPECOR output for the self-attenuation correction factors (F_{ca}) of ^{210}Pb (46.54 keV) and ^{241}Am (59.54 keV) for the sample containing 25 g of $Pb(NO_2)_3$. Fa0 and Fa1 give the efficiency reduction factors for the calibration source and the sample at the given energy in comparison with an ideal source, measured in the same experimental arrangement, but without self-attenuation.

Table 4.3. Modelled and measured self-attenuation correction factors in 0.1 M HNO_3 solutions with increasing amounts of $Pb(NO_2)_3$. Modelled correction factors have been assigned a 2% uncertainty

	^{210}Pb self-attenuation correction (F_{ca})		^{241}Am self-attenuation correction (F_{ca})	
Amount of $Pb(NO_2)_3$ added (g)	Modelled	Experimental	Modelled	Experimental
	0.826±0.017	0.819±0.020	0.900±0.018	0.905±0.010
10	0.697±0.014	0.686±0.017	0.816±0.016	0.832±0.009
15	0.600±0.012	0.581±0.014	0.744±0.015	0.759±0.009
20	0.524±0.010	0.525±0.013	0.682±0.014	0.700±0.008
25	0.466±0.009	0.480±0.011	0.630±0.013	0.632±0.008

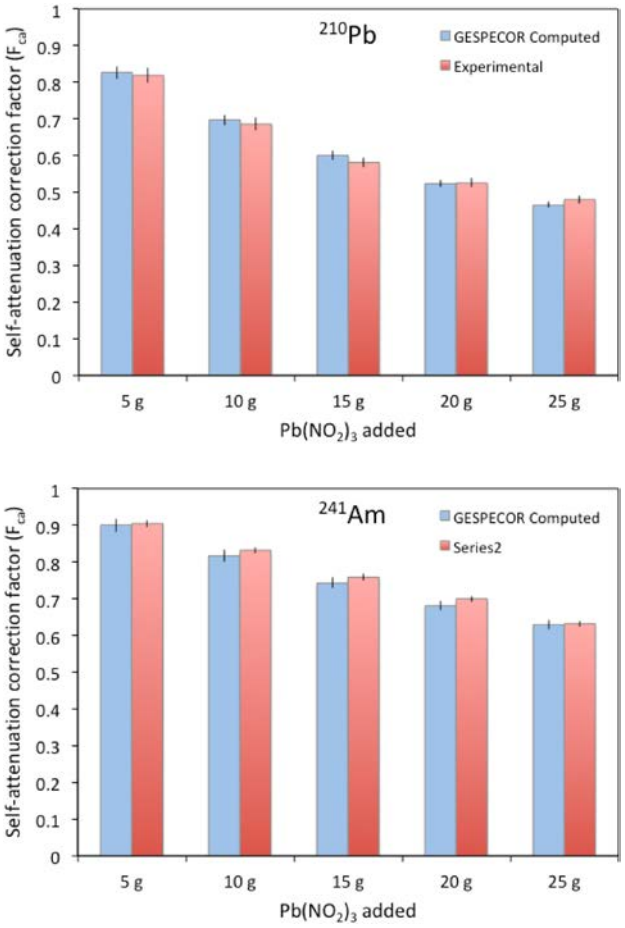

Figure 4.9. Modelled (blue) and measured (red) self-attenuation correction factors in 0.1 M HNO_3 solutions with increasing amounts of $Pb(NO_2)_3$.

4.4 Validation of Efficiency Transfer and Direct Monte Carlo Computation of Full-energy Peak Efficiency Curves in Large Samples of Different Matrix Composition

Changes in FEP efficiency resulting from changes in matrix composition can also be accounted for using the transfer method in GESPECOR. To test the validity of our optimised detector models, we studied the transfer of the experimental efficiencies computed in the calibration medium (4 M HCl) to a different matrix. Bituminous coal is used by the ORM as a high-performance absorbing medium for air sampling. The material (granule size 10 × 16 US mesh, surface area minimum 1050 m^2) is designed for the containment of radioactive gases, particularly ^{131}I. Recently, the ORM acquired a certified reference material for this matrix, which is arranged in the 500 GEO (Marinelli beaker) geometry. The nuclides present in the reference material are ^{54}Mn, ^{65}Zn, ^{85}Sr, ^{88}Y, ^{133}Ba, ^{137}Cs and ^{139}Ce, providing 14 calibration points over the energy range 80–1836 keV. The availability of a certified material in this medium offered an ideal opportunity to verify the validity of computed self-attenuation correction and true coincidence summing correction factors (see Chapter 5), and permitted the comparison of computed FEP efficiencies derived from direct Monte Carlo simulation or transferred efficiencies from the 4 M HCl reference calibration medium to bituminous coal with those measured directly using the coal certified reference material.

To achieve the transfer efficiency, the experimental FEP efficiencies obtained using the 4 M HCl calibration standard had to be corrected to account for the transfer from 4 M HCl to a bituminous coal medium. To achieve this, gamma attenuation coefficients for bituminous coal at different energies were determined from transmission measurements using collimated sources. A generic composition that matched the experimental attenuation coefficients was established by considering the average elemental composition of bituminous coal reported in the literature (77% carbon, 5% hydrogen, 5% oxygen, 1.5% nitrogen, 0.5% sulfur and 11% ash) (Vignesh, 2018) and taking the ash composition as that reported by Suzin *et al*. (1998) for

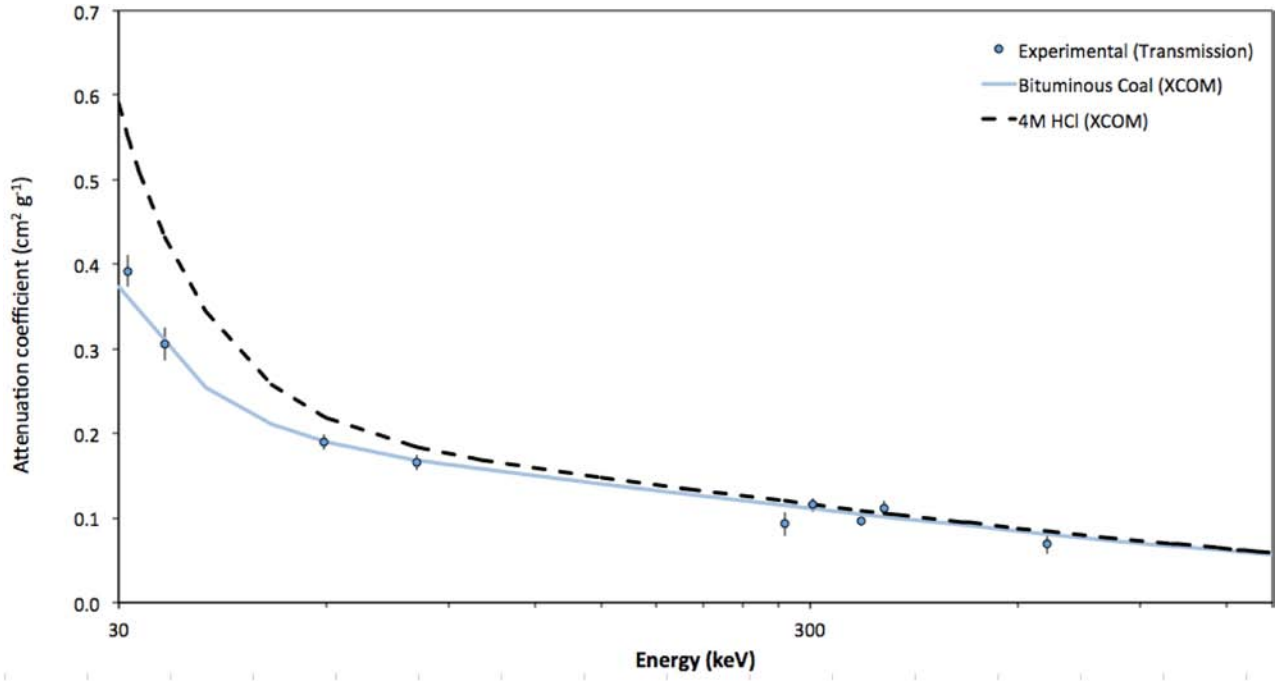

Figure 4.10. Mass attenuation coefficients for bituminous coal determined by transmission experiments (•) and using the XCOM photon cross-sections database (—). The mass attenuation coefficients for 4 M HCl (—) are also shown.

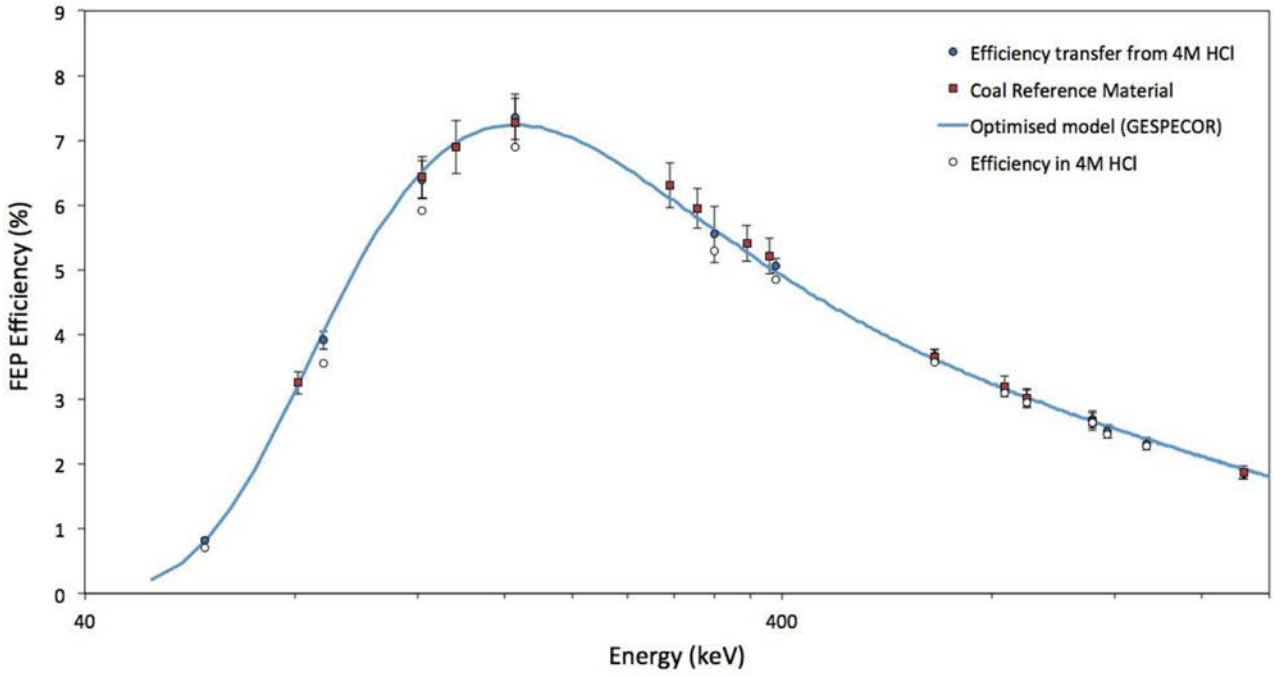

Figure 4.11. Efficiency transfer from a 4 M HCl matrix (reference calibration standard) to bituminous coal. The solid red squares correspond to experimental FEP efficiencies determined from the certified coal reference material. The solid blue dots are the FEP efficiencies transferred from the original 4 M HCl calibration (shown as empty dots) using derived self-attenuation correction factors. The blue solid line is the FEP efficiency curve generated by GESPECOR using the optimised detector model and the generic composition for bituminous coal. All efficiencies have been corrected for coincidence summing effects and thus represent coincidence-free FEP efficiencies. Expanded uncertainties are shown with a coverage factor of $k = 2$. Reprinted from Murphy *et al.* (2020). Copyright © 2019, with permission from Elsevier.

bituminous coal granular carbon. The experimentally determined mass attenuation coefficients and those obtained based on the assumed generic composition using the XCOM photon cross-sections database are shown in Figure 4.10. Also shown in this figure is the mass attenuation coefficient for 4 M HCl.

The mass attenuation coefficients obtained in this way, together with the measured density of the bituminous coal ($\rho = 0.47$ g cm^{-3}) and the optimised detector model, were used in GESPECOR to compute the self-attenuation correction factors to account for the differences between the two media. These correction factors were applied to the experimental efficiencies for the 500 GEO obtained using the 4 M HCl reference calibration standard and the resulting efficiencies plotted against those directly determined from the coal reference material. In addition, the FEP efficiency curve for bituminous coal, generated in GESPECOR by Monte Carlo simulation using the optimised detector model, was computed to test the ability of the Monte Carlo simulation to reproduce the experimental efficiencies. The results, presented in Figure 4.11, confirm the validity of the efficient transfer process and suggest that reliable FEP efficiencies can be readily generated for any sample matrix in this geometry if the experimental or modelled attenuation coefficients for that matrix are known. In the cases of nuclides that were present in both the reference calibration standard and the coal reference material, the mean absolute deviation between the FEP efficiencies was < 1%, with a maximum observed difference of approximately 1.5%.

5 True Coincidence Summing Corrections

5.1 Derivation of True Coincidence Correction Factors for Different Geometries and Detectors Used by the EPA's ORM

Using the GESPECOR software and the optimised detector models developed in Chapter 3, it was possible to derive appropriate true coincidence summing correction factors for a variety of nuclides that decay through a cascade of successive photon emissions, for which coincidence summing effects can be important, particularly when measured in high-efficiency, close-geometry conditions. Under these conditions, "summing-in" and "summing-out" effects, caused by the simultaneous arrival of more than one photon into the detector, can alter the number of counts in the FEP of a particular energy. This leads to an apparent loss or gain of efficiency relative to single photon-emitting nuclides, which do not present coincidence summing effects.

The coincidence summing effects depend, in a complex way, on the decay scheme of the nuclide, the sample geometry and composition, the detector efficiency and the shielding and materials surrounding the sample and detector. In GESPECOR, coincidence summing effects are evaluated by Monte Carlo simulation. Monte Carlo runs are performed for every peak of each nuclide, taking into consideration the sample composition (matrix) and counting arrangement (geometry). The output of these simulations is a set of true coincidence summing correction factors, F_c, for each of the nuclides of interest. For a nuclide affected by coincidence summing, the coincidence summing correction factor for a gamma emission at energy E is defined as the ratio of the apparent efficiency at that energy for the nuclide in question to that obtained at the same energy for a nuclide not affected by coincidence summing, see equation 5.1 (i.e. the efficiency value established from a calibration curve derived with nuclides with negligible coincidence summing effects):

$$F_c = \frac{\varepsilon(E,\text{TCS})}{\varepsilon(E,\text{TCS free})} \tag{5.1}$$

True coincidence summing correction factors were routinely computed for several nuclides present in the multi-gamma calibration standard used for the determination of the experimental FEP efficiency curves in Chapter 2 which are affected by true coincidence summing. As mentioned earlier, these nuclides (namely ^{60}Co, ^{88}Y and ^{139}Ce) were not included in the first iteration of the optimisation process, which was restricted to nuclides free of coincidence summing effects; however, they were included in a second iteration of the optimisation process after applying appropriate correction factors obtained from the model and derived using coincidence-free nuclides. Following the second optimisation, true coincidence summing correction factors were recalculated based on the final optimised model. Examples of the correction factors obtained for detector 1 for each of the relevant energies of ^{60}Co, ^{88}Y and ^{139}Ce, using 4 M HCl as the sample matrix, are given in Table 5.1.

Table 5.1. True coincidence summing correction factors for ^{60}Co, ^{88}Y and ^{139}Ce computed in different geometries using the optimised model for detector 1. A 4 M HCl medium (corresponding to the calibration standard) has been assumed for all computations

		Geometry			
Nuclide	Energy (keV)	50 GEO	100 GEO	250 GEO	500 GEO
^{139}Ce	165.86	0.940	0.953	0.964	0.986
^{88}Y	898.04	0.926	0.934	0.946	0.916
^{60}Co	1173.23	0.922	0.930	0.943	0.910
^{60}Co	1332.49	0.921	0.929	0.941	0.906
^{88}Y	1836.05	0.917	0.926	0.940	0.907

For the nuclides considered in Table 4.3, failure to account for coincidence summing effects can result in the underestimation of activity concentrations by up to 10% under the counting arrangements considered.

As in the case of the self-attenuation correction factors, the optimised models derived in Chapter 3 can be (and are) used by EPA's ORM staff to derive appropriate true coincidence summing correction factors for a range of geometries and sample matrices for any of the detectors.

5.2 Validation of Derived True Coincidence Summing Correction Factors by Participation in Proficiency Tests

The accuracy of the self-attenuation and coincidence summing correction factors computed by GESPECOR using the optimised detector models derived during the project was tested by participating in the analysis of proficiency samples distributed by the UK's NPL as part of its annual environmental radioactivity proficiency test exercise in 2017. The sample (code: GL) was a 500-g solution of dilute 1 M HNO_3 containing ^{210}Pb, ^{241}Am and ^{134}Cs. The activities per unit mass for each nuclide present in this sample were traceable to national standards of radioactivity in the UK and, therefore, to the international measurement system.

In addition to the self-attenuation corrections required to account for the difference in medium between the sample (1 M HNO_3) and the reference calibration solution (4 M HCl) used for efficiency determination, quantification of ^{134}Cs required the determination of true coincidence summing correction factors, as this nuclide is affected by coincidence summing effects. The calculated self-attenuation and true coincidence summing correction factors for the sample, which were counted in the 250 GEO geometry, are given in Table 5.2. It is evident from these data that, while self-attenuation corrections are critical for the accurate quantification of ^{210}Pb and ^{241}Am, a significant true coincidence summing correction is required for each of the three main emission lines of ^{134}Cs.

The data were analysed using the same methods as in previous proficiency exercises, as described in Dean *et al.* (2018). The deviation (D) from the assigned value and its standard uncertainty (u_D) were calculated from:

$$D = \frac{L-N}{N} = \left(\frac{L}{N} - 1\right) u_D = \frac{L}{N}\sqrt{\left(\frac{u_L}{L}\right)^2 + \left(\frac{u_N}{N}\right)^2}, \qquad (5.2)$$

where L is the participant's value, N is the NPL assigned value, u_L is the standard uncertainty ($k=1$) of the participant's value and u_N is the standard uncertainty ($k=1$) of the assigned value.

The quantities zeta (ζ), the relative uncertainty of the participant's value (R_L) and the z-score were calculated from:

$$\xi = \frac{L-N}{\sqrt{u_L^2 + u_N^2}} \qquad (5.3)$$

$$R_L = \frac{u_L}{L} \qquad (5.4)$$

$$z = \frac{L-N}{\sigma_p} = \frac{L-N}{0.05823\ N} \qquad (5.5)$$

where σ_p is the standard uncertainty for proficiency assessment, corresponding to a level of performance that NPL want laboratories to be able to achieve. The value chosen corresponds to a deviation D of 15% (at a 99% confidence level), so that any result with a deviation (D) smaller than ±15% will pass the test.

Table 5.2. Self-attenuation and true coincidence summing correction factors used for the quantification of the GL sample as part of the NPL's proficiency test exercise in 2017

Nuclide	Energy (keV)	Intensity (%)	Self-attenuation correction factor, F_{ca}	True coincidence summing correction factor, F_c
^{210}Pb	46.54	4.25	0.88842	1.00000
^{241}Am	59.54	35.92	0.94163	1.00000
^{134}Cs	569.33	15.37	0.99568	0.87296
^{134}Cs	604.72	97.63	0.99579	0.92267
^{134}Cs	795.86	85.47	0.99625	0.92072

Table 5.3. Measured activity concentrations for the NPL proficiency test exercise in 2017 (GL sample)

Nuclide	NPL-assigned activity concentration (Bq g^{-1})	PMWM[a] (Bq g^{-1})	Activity concentration (Bq g^{-1})[b]	
			Corrected	Uncorrected
^{210}Pb	16.11 ± 0.17	16.86 ± 0.38	16.72 ± 1.68	18.82 ± 1.89
^{241}Am	2.3943 ± 0.0078	2.518 ± 0.041	2.68 ± 0.21	2.86 ± 0.21
^{134}Cs	18.78 ± 0.15	18.14 ± 0.14	17.76 ± 0.39	16.27 ± 0.54

[a]PMWM based on the results submitted by all the participants.

[b]The activity concentrations reported here are slightly different from those submitted to the NPL by ORM, being based on the mean of repeated (×4) measurements of the same sample rather than a single measurement.

The zeta (ξ) and *z*-scores were used to determine whether or not the difference between the participant's value and the assigned value is significantly different from zero. Results for which the absolute values of the zeta score and the *z*-score are both ≤ 2.576 and for which R_L is not significantly larger than the other values in the data set are taken to mean that the participant's value is "in agreement" with the assigned value. If R_L is significantly larger than the other values in the data set, or the result passes the zeta test but not the *z*-test (or vice versa), the participant's value is classified as "questionable". If the absolute values of both the zeta and *z*-scores are > 2.576, then the participant's value is classified as "discrepant", regardless of the value of R_L.

The measured activity concentrations for each nuclide with and without applying the self-attenuation and true coincidence summing corrections are given in Table 5.3, together with the assigned NPL values and the power-moderated weighted mean (PMWM) based on the results submitted by all the participants. The quoted corrected and uncorrected values for ^{134}Cs were calculated as a weighted mean of the results obtained using the three main emission lines (569.33 keV, 604.72 keV and 795.86 keV), with the standard uncertainty estimated as the highest of the internal (pooled) or external (weighted) variance.

A plot of the deviations (*D*) of measured concentrations from the NPL-assigned values (Figure 5.1) clearly highlights the need to apply the corrections. Classification of the results according to the zeta and *z*-scores indicates that although corrected results can be considered to be "in agreement" with the assigned values (Table 5.4), uncorrected values would have been classified as "questionable" (Table 5.5), failing to pass either the zeta or *z*-score test. The results not only highlight the need for applying the self-attenuation and true coincidence summing corrections, but further confirm the validity of the correction factors obtained using the optimised detector models in GESPECOR. It is interesting to note that for all nuclides the corrected activity concentrations were closer to the PMWM values than to the NPL-assigned values.

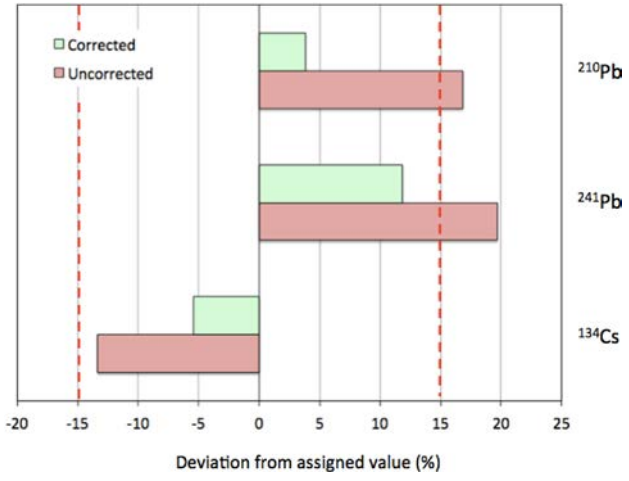

Figure 5.1. Deviations of measured activity concentrations from the NPL-assigned values for the NPL proficiency test exercise in 2017 (GL sample).

Table 5.4. Classification of corrected activity concentrations (Bq g^{-1}) for the NPL proficiency test exercise in 2017 (GL sample) based on the zeta and *z*-scores

Nuclide	Measured activity concentration	NPL-assigned activity concentration	Deviation (%)	Zeta	*z*-score	Classification
^{210}Pb	16.72 ± 1.68	16.11 ± 0.17	3.8	0.36	0.65	In agreement
^{241}Am	2.68 ± 0.21	2.3943 ± 0.0078	11.85	1.38	2.03	In agreement
^{134}Cs	17.62 ± 0.44	18.78 ± 0.15	–5.45	–2.45	–0.94	In agreement

Table 5.5. Classification of uncorrected activity concentrations (Bq g^{-1}) for the NPL proficiency test exercise in 2017 (GL sample) based on the zeta and *z*-scores

Nuclide	Measured activity concentration	NPL-assigned activity concentration	Deviation (%)	Zeta	*z*-score	Classification
^{210}Pb	18.82 ± 1.89	16.11 ± 0.17	16.84	1.43	2.89	Questionable
^{241}Am	2.86 ± 0.21	2.3943 ± 0.0078	19.67	2.21	3.38	Questionable
^{134}Cs	16.26 ± 0.57	18.78 ± 0.15	–13.35	–7.17	–2.29	Questionable

Note: numbers in red indicate measurements that failed the corresponding statistical test.

6 Evaluation of Uncertainties in Gamma Spectrometry

6.1 Uncertainties Associated with Experimental and Computed Full-energy Peak Efficiencies

Gamma spectrometry software packages such as Genie 2000 or GammaVision often use non-linear fitting functions to interpolate between experimentally measured FEP efficiencies, establishing a FEP efficiency curve from which FEP efficiencies can be calculated for any required energy. Estimation of uncertainties in the computed efficiencies must take account of possible correlations between fitting parameters. By calculating the variance–covariance matrix for the non-linear least squares fit, it is possible to define a confidence interval for the interpolated efficiencies using an appropriate coverage factor. As well as defining the uncertainty associated with the interpolated FEP efficiencies, this interval also defines a range within which any Monte Carlo computed efficiencies that accurately simulate the detector's response (such as those calculated by GESPECOR based on the optimised models) would be expected to fall.

Python scripts were written that allow determination, for a given geometry, of the 95% confidence interval (coverage factor $k = 2$) associated with the FEP efficiency curve generated by non-linear fitting of a set of experimental energy (E)–FEP efficiency (ε) pairs to the following function (equation 6.1), commonly used for HPGe detectors by gamma analysis packages:

$$\ln\varepsilon = a_1 E + a_2 + \frac{a_3}{E} + \frac{a_4}{E^2} + \frac{a_5}{E^3} + \frac{a_6}{E^4} \qquad (6.1)$$

The confidence intervals for all geometries obtained for detector 12 are shown in Figure 6.1, plotted as red bands around the best least squares non-linear fit. Also plotted in Figure 6.1 are the experimental FEP efficiencies (black points) and the FEP efficiencies computed by GESPECOR based on the optimised model for this detector (green crosses). Analysis of the plots shows that 58 out of the 65 (89%) Monte Carlo computed efficiencies fell within the predicted 95% confidence interval, with the remaining seven points (11%) lying just outside it. The GESPECOR-computed efficiencies are, therefore, consistent with the experimental confidence interval, giving us further confidence in the validity of the optimised detector model.

Replicate measurements of selected calibration standards were carried out to establish whether or not the peak area uncertainty given by the software analysis package (Genie PC) was consistent with the variability encountered from the statistical analysis of the replicate measurements. The results indicate that this is the case; therefore, experimental uncertainties calculated by error propagation based on the reported uncertainties for the primary calibration standard solution and required nuclear data, as well as the uncertainties associated with the dilution process and the preparation of the standards and those associated with the counting statistics, are considered to yield accurate estimates of the total uncertainty. In the case of nuclides affected by true coincidence summing, the uncertainty in the applied correction factors (taken from typical values quoted in the GESPECOR manual or estimated by simulation) must also be included.

6.2 Validation of Direct Monte Carlo Computation of Full-energy Peak Efficiency Curves for Sources in Different Geometry Arrangements

FEP efficiencies computed by Monte Carlo simulation are quite sensitive to any inaccuracies in the detector model. Therefore, the robustness of the optimised parameters was investigated by using GESPECOR to compute the FEP efficiency curves for geometries differing significantly from those used in the optimisation process using a full Monte Carlo simulation and comparing the results with those obtained experimentally.

Two different geometry arrangements, namely point source (POINT) and filter (1 GEO) geometries, were chosen to perform these analyses. For the point source measurements, single radionuclide activity standards of ^{241}Am, ^{133}Ba, ^{137}Cs and ^{60}Co (Amersham, UK) were placed at a distance of 9.05 cm from the end cap entrance window using a special Perspex holder. The filter source (QCRB19846, 2017, Eckert & Ziegler,

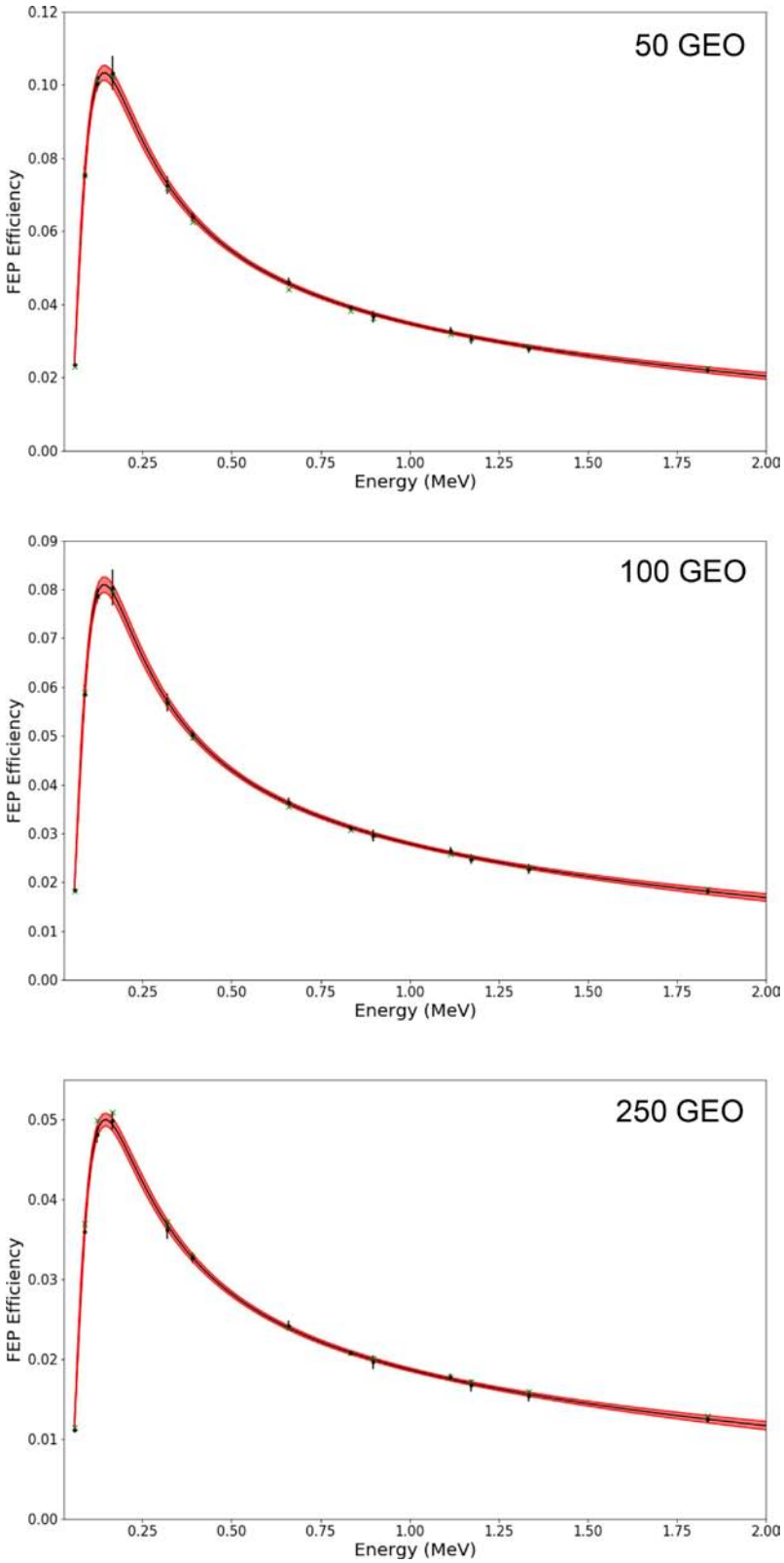

Figure 6.1. Estimated 95% confidence interval (red band; coverage factor $k=2$) for measured experimental FEP efficiencies (black points) in detector 12. The green crosses are the FEP efficiencies computed by GESPECOR based on the optimised model for this detector. Uncertainties in FEP experimental efficiencies are shown with a coverage factor of $k=2$. Reprinted from Murphy *et al*. (2020). Copyright © 2019, with permission from Elsevier.

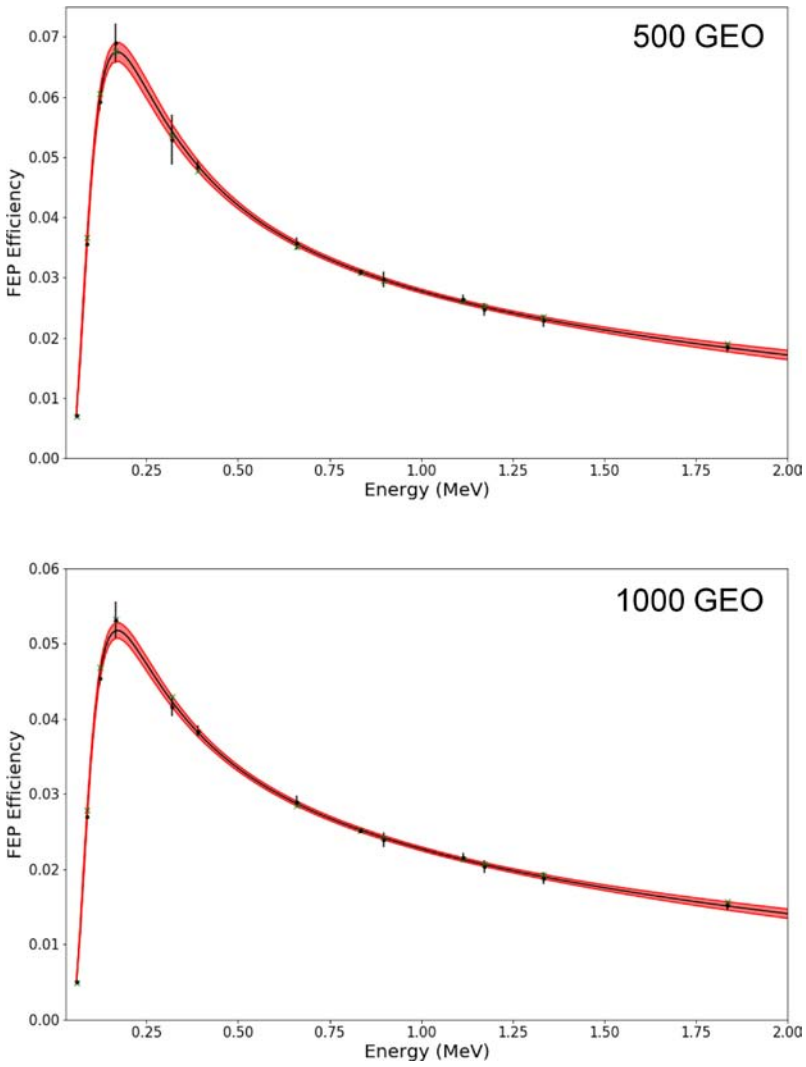

Figure 6.1. Continued.

Germany) consisted of a glass fibre disc (diameter (∅) 47 mm, height 0.2 mm) containing ^{241}Am, ^{109}Cd, ^{57}Co, ^{139}Ce, ^{113}Sn, ^{137}Cs, ^{88}Y and ^{60}Co placed inside a polypropylene holder and was counted at a distance of 6.8 mm from the end cap entrance window.

The results obtained for both geometries are shown in Figures 6.2 and 6.3. In all cases, experimental FEP efficiencies were corrected for true coincidence summing effects using the optimised model in GESPECOR. For the point sources, the mean absolute deviation between computed and experimental efficiencies over the whole energy range was < 3%, although a significant difference was seen in the case of ^{241}Am, for which the computed FEP efficiency was ~13% higher than that determined experimentally. It should be noted, however, that the uncertainties associated with the certified source activities were quite large, yielding relative uncertainties for the experimental FEP efficiencies that were more than 10% (k = 2) in most cases. For the filter geometry, the relative uncertainties for all the experimental FEP efficiencies were smaller than for the point geometry, at 3–5% (k = 2), and the mean absolute deviation between computed and experimental FEP efficiencies over the whole energy range was again < 3%, with a maximum deviation of 4.1% for ^{109}Cd. The results obtained demonstrate that the optimised model can be used reliably to compute FEP efficiencies in other geometries, even when these differ significantly from those employed in the optimisation process.

6.3 Benchmarking of GESPECOR Monte Carlo Computed Efficiencies

As part of the investigation on the uncertainties associated with gamma spectrometry, the FEP

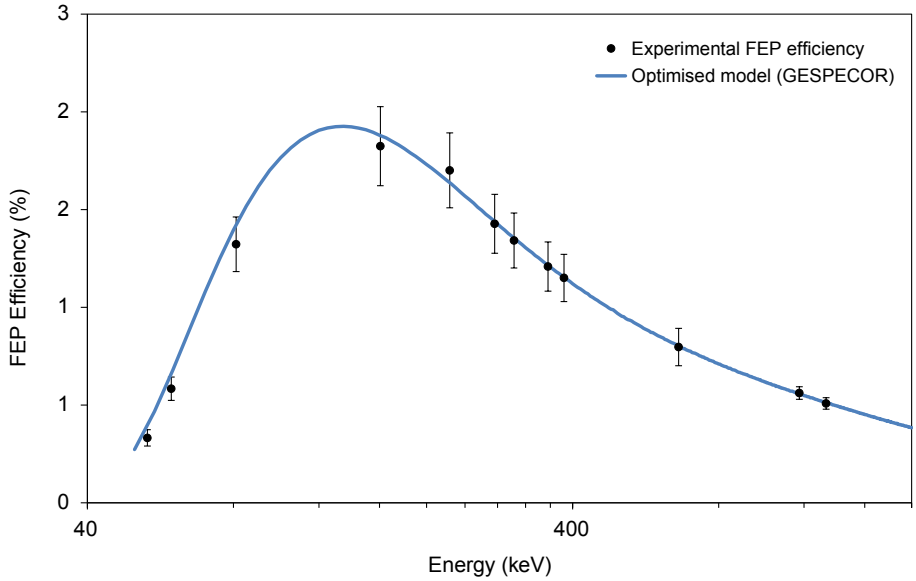

Figure 6.2. Experimental and modelled FEP efficiencies for the point source geometry. Expanded uncertainties shown with $k=2$. Reprinted from Murphy *et al*. (2020). Copyright © 2019, with permission from Elsevier.

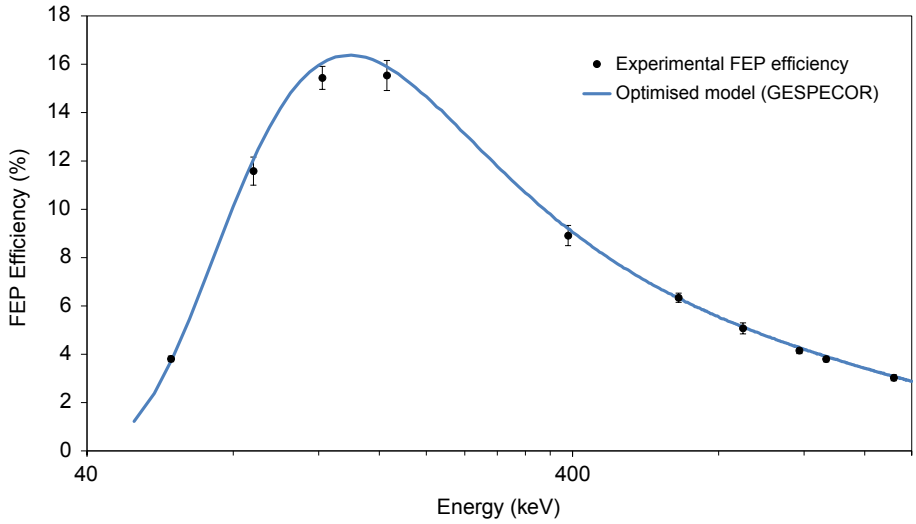

Figure 6.3. Experimental and modelled FEP efficiencies for the filter source geometry (1 GEO). Expanded uncertainties shown with $k=2$. Reprinted from Murphy *et al*. (2020). Copyright © 2019, with permission from Elsevier.

efficiencies generated by GESPECOR were benchmarked against those obtained by other Monte Carlo codes. This was achieved by comparing the computed FEP and total efficiencies generated by GESPECOR with those obtained independently using the electron gamma shower (EGSnrc) Monte Carlo software for two generic detectors defined in a recent benchmark exercise organised by the ICRM's Gamma-Ray Spectrometry Working Group (ICRM-GSWG). As the results of this exercise became available during the reporting period, a comparison between GESPECOR and the mean efficiency values obtained by all the participants in the exercise using a variety of Monte Carlo codes (EGSnrc, GEANT4, MCNP and PENELOPE) was also possible. When applied to a precisely defined detector/geometry/shield configuration, differences in the computed efficiencies between different Monte Carlo packages can be attributed to different approaches to particle tracking and the nuclear and material data employed by each

individual package. These differences can be treated as intrinsic uncertainties and can provide useful information and general guidelines for the uncertainty that may be assigned to such efficiencies.

Two simple detector models were defined in the ICRM-GSWG exercise, which incorporate the main components of typical coaxial HPGe detectors. In both cases, the detector consisted of a germanium crystal (length (L) = 60 mm, ∅ = 60 mm) with an inner hole of 40 mm in length and 10 mm in diameter. The only difference between the two detectors was the size of the top and side dead layers, which was set to 0 mm for one of the detectors (to simulate an n-type detector) and 1 mm for the other (to simulate a p-type detector). In each case, the crystal was enclosed by a 1-mm thick aluminium housing (L = 80 mm, ∅ = 80 mm), and the crystal-to-window distance was set to 5 mm. Four different types of sources (one point source and three volumetric sources) were modelled, placed 1 mm above the detector window. The volumetric sources were defined as cylinders (with no walls) made of three different materials, namely water, silicon dioxide and cellulose, to represent aqueous, soil and filter counting geometries. Each detector with the corresponding source was placed inside a 50-mm-thick lead shield (L = 400 mm, ∅ = 400 mm). A schematic of the detector/geometry set-up and the dimensions for one of the modelled detectors (p-type) is shown in Figure 6.4.

Models of each detector arrangement were created in GESPECOR, and FEP and total efficiencies were computed by direct Monte Carlo calculation for five different energies (50 keV, 100 keV, 200 keV, 500 keV and 1000 keV), as specified by the ICRM-GSWG exercise. Models were also created in the EGSnrc software, and the egs_spectrum application (kindly made available to the project by the code developers) was used to score the energy deposited by each emitted gamma ray in the crystal and to derive the FEP and total efficiencies. An example of the models created using the EGSnrc software (displaying some of the trajectories and interactions for a selections of the simulated photons) are shown in Figure 6.5.

The computed FEP and total efficiencies using GESPECOR and EGSnrc, as well as the mean value and standard deviation reported for the participants in the ICRM-GSWG action (based on the outputs of EGSnrc, GEANT4, MCNP and PENELOPE), are summarised in Tables 6.1–6.4. For the FEP efficiencies, excellent agreement was found between the values computed by GESPECOR and those reported for other codes, for both detectors, with

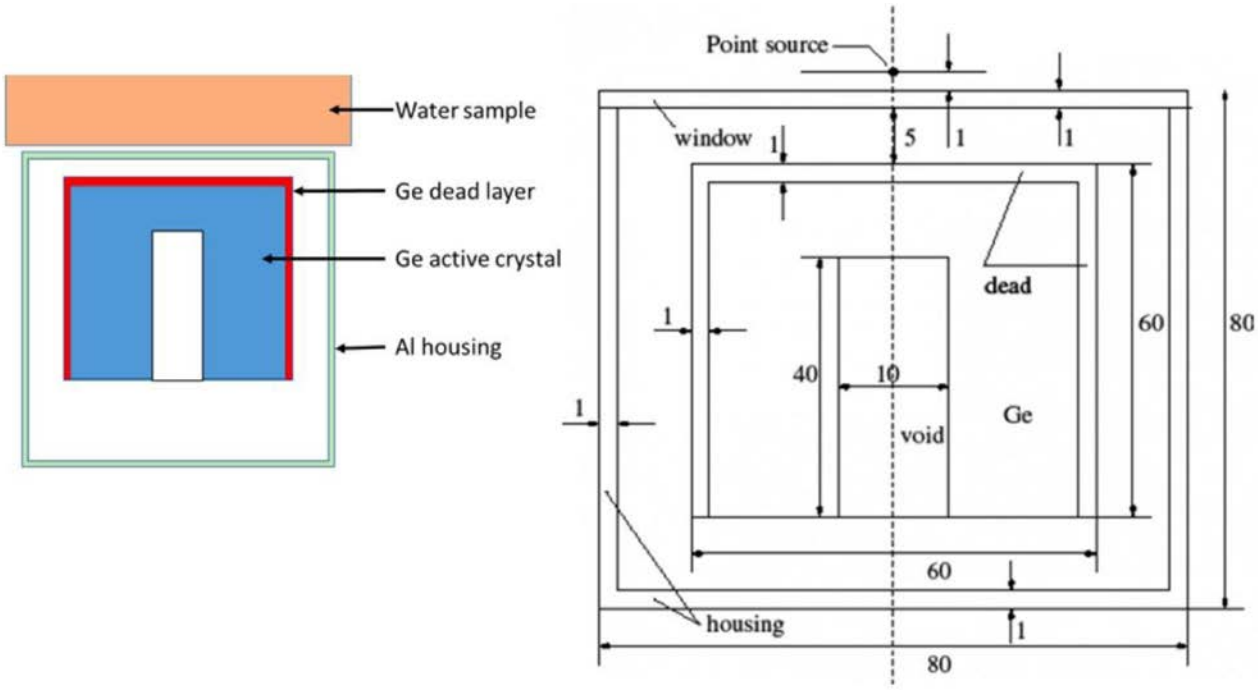

Figure 6.4. Schematic of the ICRM-GSWG model detector (p-type) configuration.

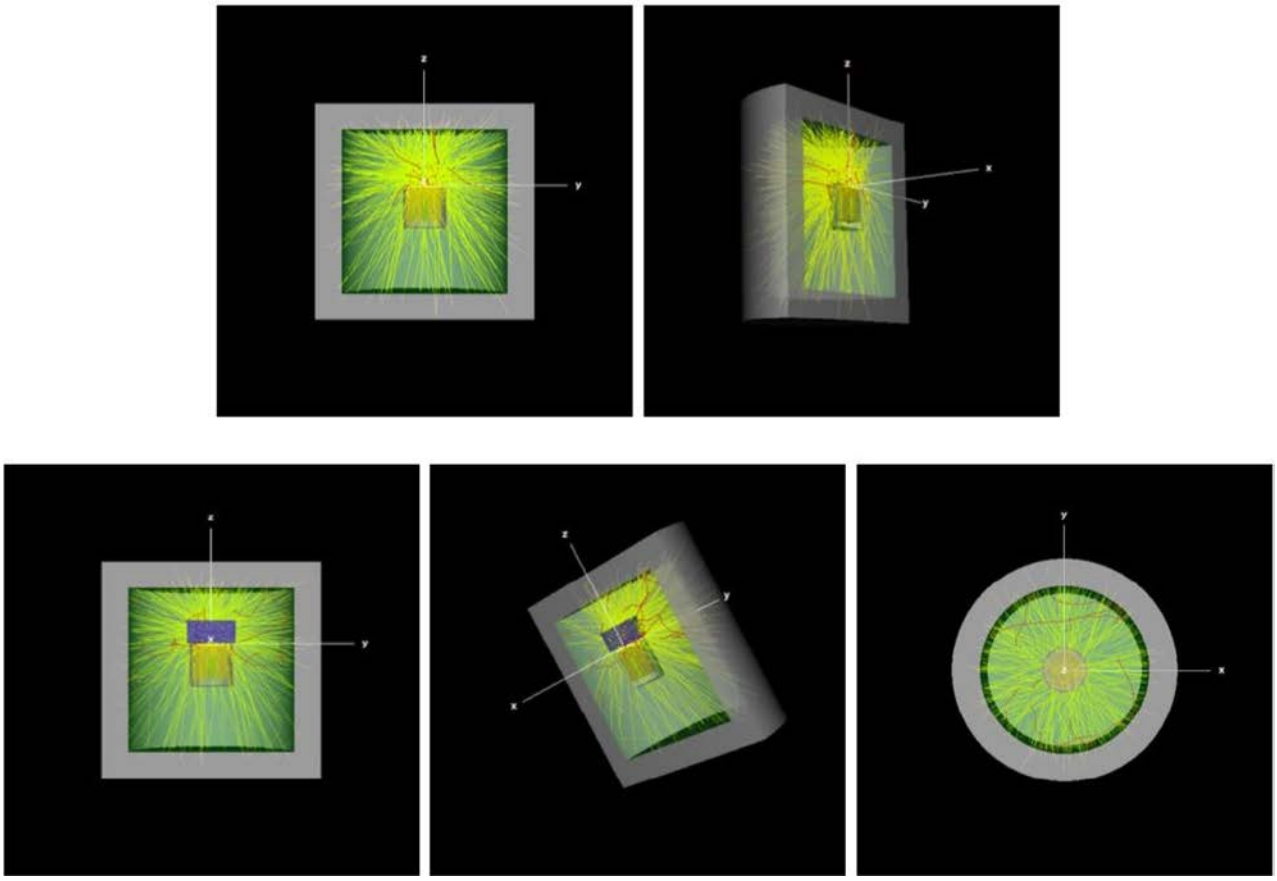

Figure 6.5. HPGe detector modelled with EGSnrc for (top) point source and (bottom) water source geometry. Photon trajectories are shown in yellow and electron trajectories are shown in red.

values differing by less than (and in most cases much less than) 4% for all sources and energies (mean absolute deviation was 1.5% for the p-type detector and 0.8% for the n-type).

In the case of the total efficiencies, good agreement was also found in the case of the n-type detector, with deviations from the ICRM-GSWG mean of < 5% in all cases and a mean absolute deviation of 3%. Nevertheless, GESPECOR values were consistently lower than those obtained by the other Monte Carlo codes. For the p-type detector, deviations of < 6% were found above 100 keV, with a mean absolute deviation of 4%. However, large discrepancies were apparent for 50 keV, with the GESPECOR computed total efficiencies being 40–70% higher than those obtained using other Monte Carlo codes. This large discrepancy, which is likely to arise from differences in the implementation of the physical interaction processes or the material data employed by GESPECOR, could potentially affect the values for the true coincidence summing correction factors at low (< 50 keV) energies.

To complete the comparison between the computed efficiencies by GESPECOR and EGSnrc, an EGSnrc model of detector 12 was created using the optimised model parameters found for this detector by applying the automated process developed in GESPECOR. The EGSnrc model was then used to compute the FEP efficiencies for the point sources described in section 6.2 and the results compared with those obtained in GESPECOR. As shown in Figure 6.6, good agreement was found between the results obtained using both codes, considering that the composition of the carbon fibre holder and end cap window was modelled as graphite in EGSnrc. The EGSnrc software thus potentially provides a useful alternative to model HPGe detectors and to benchmark the underlying radiation transport codes and correction factor used by GESPECOR.

Table 6.1. Comparison of computed FEP efficiencies (%) for a generic p-type detector using GESPECOR and other Monte Carlo codes

				GESPECOR relative difference (%)	
Energy (keV)	ICRM	EGSnrc	GESPECOR	ICRM	EGSnrc
Point source					
50	2.44±0.05	2.46	2.47	1.11	0.22
100	19.80±0.04	19.79	19.83	0.14	0.19
200	18.93±0.10	18.94	18.80	–0.71	–0.77
500	8.56±0.11	8.53	8.43	–1.47	–1.07
1000	4.81±0.09	4.79	4.71	–2.14	–1.65
Water source					
50	0.57±0.02	0.57	0.58	1.47	1.88
100	4.08±0.03	4.03	4.13	1.31	2.61
200	4.08±0.02	4.11	4.10	0.58	–0.19
500	2.08±0.01	2.06	2.06	–0.99	–0.04
1000	1.26±0.01	1.28	1.24	–1.51	–2.80
Filter source					
50	1.27±0.03	1.29	1.31	3.37	1.93
100	10.09±0.03	10.08	10.29	1.95	2.05
200	9.93±0.03	9.87	9.94	0.08	0.63
500	4.71±0.05	4.61	4.67	–0.79	1.36
1000	2.73±0.04	2.75	2.67	–2.33	–3.04
Soil source					
50	1.12±0.02	1.23	1.10	–0.86	–9.87
100	8.20±0.11	8.18	8.10	–1.22	–0.94
200	7.72±0.09	7.65	7.60	–1.57	–0.63
500	3.70±0.05	3.70	3.64	–1.76	–1.65
1000	2.18±0.03	2.18	2.12	–2.66	–2.65

Table 6.2. Comparison of computed total efficiencies (%) for a generic p-type detector using GESPECOR and other Monte Carlo codes

				GESPECOR relative difference (%)	
Energy (keV)	ICRM	EGSnrc	GESPECOR	ICRM	EGSnrc
Point source					
50	2.67±0.07	2.66	4.34	62.39	62.92
100	22.89±0.17	23.00	23.16	1.18	0.68
200	27.11±0.12	27.24	26.01	–4.08	–4.53
500	22.76±0.10	22.76	21.54	–5.37	–5.38
1000	19.38±0.09	19.43	18.32	–5.46	–5.71
Water source					
50	0.760±0.008	0.763	1.18	55.68	55.05
100	6.48±0.011	6.54	6.62	2.81	1.91
200	8.21±0.07	8.31	7.93	–3.38	–4.59
500	7.28±0.04	7.28	6.99	–4.00	–4.06
1000	6.32±0.03	6.37	6.04	–4.43	–5.13
Filter source					
50	1.42±0.04	1.42	2.38	67.60	67.35
100	12.16±0.16	12.32	12.46	2.48	1.11
200	15.06±0.06	15.17	14.42	–4.22	–4.90
500	13.22±0.07	13.30	12.55	–5.07	–5.62
1000	11.51±0.06	11.61	10.88	–5.47	–6.29
Soil source					
50	1.36±0.01	1.84	1.96	43.87	6.57
100	11.72±0.13	11.85	11.86	1.20	0.07
200	14.07±0.12	14.12	13.55	–3.68	–4.01
500	12.05±0.09	12.07	11.53	–4.37	–4.52
1000	10.31±0.08	10.32	9.76	–5.36	–5.41

Table 6.3. Comparison of computed FEP efficiencies (%) for a generic n-type detector using GESPECOR and other Monte Carlo codes

				GESPECOR relative difference (%)	
Energy (keV)	ICRM	EGSnrc	GESPECOR	ICRM	EGSnrc
Point source					
50	31.8±0.3	32.2	31.6	–0.63	–1.86
100	32.6±0.4	32.7	32.6	0.00	–0.31
200	23.1±0.3	23.3	23.1	0.00	–0.86
500	10.1±0.2	10.1	10.0	–0.99	–0.99
1000	5.62±0.09	5.65	5.58	–0.71	–1.24
Water source					
50	6.4±0.2	6.38	6.27	–2.07	–1.73
100	6.76±0.05	6.72	6.74	–0.35	0.19
200	5.07±0.02	5.02	5.05	–0.34	0.70
500	2.48±0.01	2.47	2.45	–1.08	–0.76
1000	1.49±0.01	1.50	1.48	–0.99	–1.58
Filter source					
50	17.91±0.12	18.01	17.76	–0.85	–1.40
100	17.91±0.05	17.78	17.90	–0.04	0.69
200	12.65±0.06	12.66	12.59	–0.44	–0.53
500	5.70±0.06	5.68	5.63	–1.30	–0.95
1000	3.26±0.05	3.24	3.22	–1.30	–0.81
Soil source					
50	11.3±0.2	11.6	11.1	–2.02	–4.88
100	12.98±0.07	13.00	12.93	–0.40	–0.55
200	9.42±0.03	9.43	9.36	–0.69	–0.82
500	4.37±0.01	4.38	4.32	–1.03	–1.22
1000	2.55±0.01	2.57	2.52	–1.00	–1.77

Table 6.4. Comparison of computed total efficiencies (%) for a generic n-type detector using GESPECOR and other Monte Carlo codes

				GESPECOR relative difference (%)	
Energy (keV)	ICRM	EGSnrc	GESPECOR	ICRM	EGSnrc
Point source					
50	34.49±0.06	34.47	34.05	–1.28	–1.23
100	36.50±0.2	36.69	35.48	–2.79	–3.30
200	31.34±0.13	31.62	30.38	–3.06	–3.92
500	25.02±0.06	25.12	24.33	–2.75	–3.14
1000	21.25±0.10	21.33	20.51	–3.48	–3.84
Water source					
50	10.15±0.03	10.10	10.03	–1.18	–0.69
100	11.50±0.2	11.62	10.96	–4.70	–5.68
200	10.06±0.13	10.14	9.65	–4.08	–4.83
500	8.18±0.05	8.24	7.95	–2.81	–3.52
1000	7.02±0.04	7.09	6.81	–2.99	–3.95
Filter source					
50	19.98±0.01	20.11	19.45	–2.65	–3.28
100	20.9±0.2	21.15	19.88	–4.79	–6.02
200	18.06±0.11	18.38	17.29	–4.32	–5.96
500	14.85±0.07	14.95	14.26	–3.97	–4.60
1000	12.88±0.06	12.91	12.26	–4.81	–5.06
Soil source					
50	15.06±0.04	15.83	14.88	–1.20	–6.00
100	19.20±0.2	19.56	18.66	–2.91	–4.60
200	16.74±0.14	16.97	16.29	–2.72	–4.04
500	13.39±0.06	13.51	13.04	–2.62	–3.41
1000	11.40±0.03	11.44	11.06	–2.96	–3.30

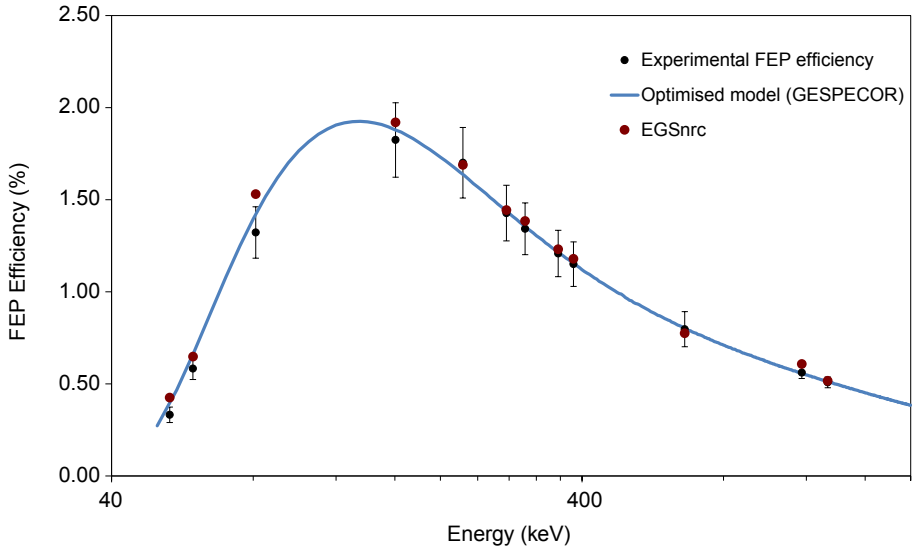

Figure 6.6. Measured and computed FEP efficiencies for point sources in detector 12 using the optimised detector model in GESPECOR (blue line) and EGSnrc (red dots).

7 Conclusions

As outlined in the introduction, the main goal of this project (as specified in the EPA's Sustainability Research Call 2015 – Health and Wellbeing Theme – Project 33) was to develop and implement suitable Monte Carlo methods for the assay of natural and artificial radionuclides using high-resolution gamma spectrometry with HPGe detectors at the EPA's ORM analytical laboratory, so that self-attenuation and true coincidence summing effects can be corrected for, and detector efficiencies established for a variety of geometries and sample matrices without the need to carry out multiple, time-consuming and expensive measurements using certified calibration standards.

To achieve this goal, an automated optimisation method was developed during this project for the characterisation of HPGe detectors. Starting with a set of nominal (but realistic) input parameters and experimentally determined FEP efficiencies for multiple calibration standard solutions in a variety of counting geometries (e.g. cylindrical tubs and Marinelli beakers), this method uses the GESPECOR software to arrive at an optimised model of the detector by applying suitable optimisation algorithms without any further user intervention.

Application of this optimisation method to each of the seven HPGe detectors currently in operation at the EPA's ORM has shown that, with relatively little effort from the user, it is possible to achieve excellent agreement between experimental FEP efficiencies and Monte Carlo calculations, with mean absolute deviations between modelled and experimental efficiencies of $< 2\%$ for all geometries, and individual absolute deviation no higher than 4%.

Through a comprehensive set of validation experiments, it has been demonstrated that the optimised models can be used to confidently predict FEP efficiencies for arbitrary source geometries by direct Monte Carlo simulation, to perform efficiency transfer from one matrix to another and to compute accurate values for self-attenuation and true coincidence summing correction factors.

Practical methodologies have been developed for the accurate determination of linear attenuation coefficients required for self-attenuation corrections, and the techniques applied to a number of environmental matrices routinely analysed by the EPA's ORM for the determination of appropriate self-attenuation correction factors. Participation in international environmental radioactivity proficiency test exercises has allowed validation of the accuracy of derived self-attenuation and coincidence summing correction factors. Furthermore, the accuracy of FEP and total efficiencies generated by GESPECOR has also been benchmarked against those obtained by other Monte Carlo codes such as EGSnrc, GEANT4, PENELOPE and MCNP.

The methodology developed in this project provides a simple solution for the development of accurate HPGe detector models which can be used for the accurate determination of FEP efficiencies and self-attenuation and coincidence summing correction factors. Indeed, the models and methods described in this report are now being used at the EPA's ORM for the determination of suitable self-attenuation and true coincidence summing, and to compute FEP detector efficiencies for a variety of geometries and sample matrices without the need to carry out multiple, time-consuming and expensive measurements using certified calibration standards. Over the next 3 years, these methods described will also be used for the analysis of natural radionuclides as part of another EPA-funded project, Radioactivity in the Irish Coastal Environment (2019-HW-MS-17).

References

Britton, R. and Davies, A.V., 2015. Characterisation of a SAGe well detector using GEANT4 and LABSOCS. *Nuclear Instruments and Methods in Physics Research A* 786: 12–16.

Budjás, D., Heisel, M., Maneschg, W. and Simgen, H., 2009. Optimisation of the MC-model of a p-type Ge-spectrometer for the purpose of efficiency determination. *Applied Radiation and Isotopes* 67: 706–710.

Cunningham, J.D., MacNeill, G. and Pollard, D., 1987. *Chernobyl: Its Effects on Ireland*. Nuclear Energy Board, Dublin.

Dababneh, S., Al-Nemri, E. and Sharaf, J., 2014. Application of Geant4 in routine close geometry gamma spectrometry for environmental samples. *Journal of Environmental Radioactivity* 134: 27–34.

Dean, J., Aitken-Smith, P., Collins, S. and Keightley, L., 2018. *Environmental Radioactivity Proficiency Test Exercise 2017 – Final Report.* NPL Report IR 47. National Physical Laboratory, Middlesex, UK.

García-Talavera, M., Neder, H., Daza, M.J. and Quintana, B., 2000. Towards a proper modeling of detector and source characteristics in Monte Carlo simulations. *Applied Radiation and Isotopes* 52: 777–783.

Gasparro, J., Hult, M., Johnston, P.N. and Tagziria, H., 2008. Monte Carlo modeling of germanium crystals that are tilted and have rounded edges. *Nuclear Instruments and Methods in Physics Research A* 594: 196–201.

Guerra, J.G., Rubiano, J.G., Winter, G., Guerra, A.G., Alonso, H., Arnedo, M.A., Tejera, A., Gil, J.M., Martel, P. and Bolivar, J.P., 2015. A simple methodology for characterization of germanium coaxial detectors by using Monte Carlo simulation and evolutionary algorithms. *Journal of Environmental Radioactivity* 149: 8–18.

Hansen, N., Akimoto, Y. and Baudis, P., 2019. CMA-ES/pycma on Github (Version r2.6.0). https://doi.org/10.5281/zenodo.2559634

Hardy, J.C., Iacob, V.E., Sanchez-Vega, M., Effinger, R.T., Lipnik, P., Mayes, V.E., Willis, D.K. and Helmer, R.G., 2002. Precise efficiency calibration of an HPGe detector: source measurements and Monte Carlo calculations with sub-percent precision. *Applied Radiation and Isotopes* 56: 65–69.

Hedman, A., Bahar Gogani, J., Granström, M., Johansson, L. and Andersson, J.S., 2015. Characterization of HPGe detectors using computed tomography. *Nuclear Instruments and Methods in Physics Research A* 785: 21–25.

Helmer, R.G., Hardy, J.C., Iacob, V.E., Sanchez-Vega, M., Neilson, R.G. and Nelson, J., 2003. The use of Monte Carlo calculations in the determination of a Ge detector efficiency curve. *Nuclear Instruments and Methods in Physics Research A* 511: 360–381.

Hurtado, S., García-León, M. and García-Tenorio, R., 2004. Monte Carlo simulation of the response of a germanium detector for low-level spectrometry measurements using GEANT4. *Applied Radiation and Isotopes* 61: 139–143.

Lépy, M.C., Pearce, A. and Sima, O., 2015. Uncertainties in gamma-ray spectrometry. *Metrologia* 52: S123–S145.

Luís, R., Benito, J., Carvalhal, G., Nogueira, P., Silva, L., Teles, P. and Vaz, P., 2010. Parameter optimisation of a planar BEGe detector using Monte Carlo simulations. *Nuclear Instruments and Methods in Physics Research A* 623: 1014–1019.

Lutter, G., Hult, M., Marissens, G., Stroh, H. and Tzika, F., 2018. A gamma-ray spectrometry analysis software environment. *Applied Radiation and Isotopes* 134: 200–204.

McCrory, A., 2011. Coincidence summing corrections in high resolution gamma spectrometry: a practical approach. MSc Thesis. National University of Ireland, Ireland.

McGinnity, P., Currivan, L., Dowdall, A., Hanley, O., Kelleher, K., McKittrick, L., Pollard, D., Somerville, S., Wong, J. and McMahon, C., 2012a. *Radioactive Monitoring of the Irish Environment 2010–2011.* RPII 12/02. Radiological Protection Institute of Ireland, Dublin.

McGinnity, P., Currivan, L., Duffy, J., Hanley, O., Kelleher, K., McKittrick, L., O'Colmain, M., Organo, C., Smith, K., Somerville, S., Wong, J. and McMahon, C., 2012b. *Assessment of the Impact on Ireland of the 2011 Fukushima Nuclear Accident.* RPII 12/01. Radiological Protection Institute of Ireland, Dublin.

Maidana, N.L., Vanin, V.R., García-Alvarez, J.A., Hermida-López, M. and Brualla, L., 2016. Experimental HPGe coaxial detector response and efficiency compared to Monte Carlo simulations. *Applied Radiation and Isotopes* 108: 64–74.

Mitchell, P.I., Sánchez-Cabeza, J.A., Ryan, T.P., McGarry, A.T. and Vidal-Quadras, A., 1990. Preliminary estimates of cumulative caesium and plutonium deposition in the Irish terrestrial environment. *Journal of Radioanalytical and Nuclear Chemistry* 138(2): 241–256.

Murphy, N.M., León Vintró, L., Burbidge, C.I. and Currivan, L., 2020. An automated programme for the optimisation of HPGe detector parameters using an evolutionary algorithm with GESPECOR. *Applied Radiation and Isotopes* 156: 108883.

Novotny, S. and To, D., 2015. Characterization of a high-purity germanium (HPGe) detector through Monte Carlo simulation and nonlinear least squares estimation. *Journal of Radioanalytical and Nuclear Chemistry* 304: 751–761.

O'Connor, C., Currivan, L., Cunningham, N., Kelleher, K., Lewis, M., Long, S., McGuinnity, P., Smith, V. and McMahon, C., 2014. *Radiation Doses Received by the Irish Population*. RPII 14/02. Radiological Protection Institute of Ireland, Dublin.

Peyres, V. and García-Toraño, E., 2007. Efficiency calibration of an extended-range Ge detector by a detailed Monte Carlo simulation. *Nuclear Instruments and Methods in Physics Research A* 580: 296–298.

Sima, O. and Arnold, D., 2002. Transfer of the efficiency calibration of germanium gamma-ray detectors using the GESPECOR software. *Applied Radiation and Isotopes* 56: 71–75.

Sima, O. and Dovlete, C., 1997. Matrix effects in the activity measurement of environmental samples – implementation of specific corrections in a gamma-ray spectrometry analysis program. *Applied Radiation and Isotopes* 48(1): 59–69.

Sima, O., Arnold, D. and Dovlete, C., 2001. GESPECOR: a versatile tool in gamma-ray spectrometry. *Journal of Radioanalytical and Nuclear Chemistry* 248(2): 359–364.

Suzin, Y., Buettner, L.C. and LeDuc, C.A., 1998. Behaviour of impregnated activated carbons heated to the point of oxidation. *Carbon* 36(11): 1557–1566.

Venkataraman, R., Croft, S. and Russ, W.R., 2005. Calculation of peak-to-total ratios for high purity germanium detectors using Monte-Carlo modeling. *Journal of Radioanalytical and Nuclear Chemistry* 264(1): 183–191.

Vidmar, T., Aubineau-Laniece, I., Anagnostakis, M.J., Arnold, D., Brettner-Messler, R., Budjas, D., Capogni, M., Dias, M.S., De Geer, L.-E., Fazio, A., Gasparro, J., Hult, M., Hurtado, S., Jurado Vargas, M., Laubenstein, M., Lee, K.B., Lee, Y.-K., Lépy, M.C., Maringer, F.-J., Medina Peyeres, V., Mille, M., Moralles, M., Nour, S., Plenteda, R., Rubio Montero, P., Sima, O., Tomei, C. and Vidmar, G., 2008. An intercomparison of Monte Carlo codes in gamma-ray spectrometry. *Applied Radiation and Isotopes* 66: 764–768.

Vignesh, S., 2018. Ultimate analysis – constituents of coal. Fossil Fuel Engineering ERG-252. Available online: https://www.slideshare.net/vigneshsekaran520/ultimate-analysis-of-coal (accessed 22 July 2018).

Abbreviations

BEGe	Broad-energy germanium
CMAES	Covariance matrix adaptation evolution strategy
COGER	Coordinated Group in Environmental Radioactivity
CT	Computed tomography
EGSnrc	Electron gamma shower
FEP	Full-energy peak
GUI	Graphical user interface
HPGe	High-purity germanium
ICRM	International Commission for Radionuclide Metrology
IRRS	Irish Radiation Research Society
MITK	Medical Imaging Interaction Toolkit
NPL	National Physical Laboratory
ORM	Office of Radiation Protection and Environmental Monitoring
PMWM	Power-moderated weighted mean

Appendix 1 Reporting and Dissemination of Results

During the project, the project partners attended eight conferences/meetings/workshops with a range of target audiences to disseminate the results and outputs of the research undertaken. At some of these, oral presentations and/or posters were delivered by Mr Niall Murphy, the PhD researcher associated with the project. A list of these is given below.

A1.1 Irish Radiation Research Society Annual Meeting, 11–12 November 2016 (Dublin, Ireland) – Oral Presentation

The Irish Radiation Research Society (IRRS) Annual Meeting was held on 11–12 November 2016 at the Trinity Centre for Health Science, St James's Hospital, Dublin. The IRRS is an all-Ireland organisation for researchers in the field of ionising and non-ionising radiation. The membership of IRRS is drawn from academic institutions, health research groups and statutory agencies. As part of the communication plan, Mr Murphy gave a talk on the project (Figure A1.1), and received one of two prizes awarded to the best student presentation.

A1.2 Coordinated Group in Environmental Radioactivity Open Meeting, 10–12 April 2017 (Portsmouth, UK) – Presentation

Mr Murphy attended the Coordinated Group in Environmental Radioactivity (COGER) Open Meeting, which was held in Portsmouth (UK) from 10 to 12 April 2017. At the meeting, he gave a 20-minute talk entitled "Automatising the determination of optimal HPGe detector model parameters in GESPECOR", in which he presented the background and objectives of his research project to an audience mainly comprising other PhD students in the field of environmental radioactivity.

Figure A1.1. Project presentation at the IRSS.

A1.3 International Conference on Radionuclide Metrology, 15–19 May 2017 (Buenos Aires, Argentina) – Attendance

Mr Murphy attended the 21st International Conference on Radionuclide Metrology and its Applications (ICRM 2017), held in Buenos Aires from 15 to 19 May 2017. Although not presenting at the meeting, Mr Murphy benefited from a number of sessions dealing with gamma spectrometry and also had useful discussions with some of the researchers involved in the development of the GESPECOR software, gaining access to some recent extensions to the software.

A1.4 Educational Symposium on Radiation and Health, 23–24 September 2017 (Hirosaki, Japan) – Poster and Talk

Mr Murphy attended the 4th Educational Symposium on Radiation and Health (ESRAH2017), which was held in Hirosaki (Japan) on 23–24 September 2017. At the symposium, he presented a poster and gave a short talk entitled "Optimisation and application of Monte Carlo models for self-attenuation corrections in HPGe gamma spectrometry", in which he outlined the objectives of his research project and presented some of the results achieved.

A1.5 Irish Radiation Research Society Annual Meeting, 10–11 November 2017 (Wexford, Ireland) – Presentation

Mr Murphy presented a poster at the IRSS Annual Meeting, which was held on 10–11 November 2017 at the EPA's headquarters in Wexford.

A1.6 Coordinated Group in Environmental Radioactivity Open Meeting, 11–13 April 2018 (Manchester, UK) – Presentation

Mr Murphy attended the COGER Open Meeting in Manchester from 11 to 13 April 2018. At the meeting, Mr Murphy gave an oral presentation titled "Determination of self-attenuation correction factors for environmental samples analysed by HPGe detectors" to an audience mainly comprising other PhD students working in the field of environmental radioactivity.

A1.7 International Conference on Radionuclide Metrology's Gamma Spectrometry Working Group, 12–14 June 2018 (Paris, France) – Course Attendance and Participation in the Working Group

Mr Niall Murphy and Associate Professor Luis León Vintró attended the "Gamma Spectrometry Training Course" organised by the ICRM-GSWG, which was held at the Laboratoire National de Métrologie et d'Essais in Paris (France) on 12–13 June 2018. The meeting, attended by 29 researchers, covered a wide range of topics of direct interest to this project, including self-attenuation and efficiency transfer methods, uncertainties and the application of GUM to gamma spectrometry, low-level instrumentation, Monte Carlo principles, peak and efficiency curve fitting techniques, radioactive equilibrium in gamma samples, coincidence summing and effects of volume sources, and Monte Carlo techniques applied to uncertainty calculation. Speakers at the meeting included Professor Octavian Sima (Bucharest University and developer of the GESPECOR software), Dr Marie-Christine Lépy (CEA-LNHB), Dr Philippe Cassette (CEA-LNHB) and Dr Mikael Hult (Joint Research Centre-Geel). Mr Murphy and Associate Professor León Vintró also attended the meeting of the GSWG-ICRM, which was held at the same location on 14 June 2018. At the meeting, ongoing and future actions on methods for the evaluation of coincidence summing corrections in the case of volume samples and facilitating the use of Monte Carlo simulation software were discussed, and some preliminary results presented.

A1.8 International Conference on Radionuclide Metrology, 27–31 May 2019 (Salamanca, Spain) – Presentation

Mr Niall Murphy delivered an oral presentation at the 22nd International Conference on Radionuclide Metrology and its Applications (ICRM 2019), which

was held in Salamanca (Spain) from 27 to 31 May 2019. The accompanying research publication, detailing the optimisation and validation methodologies developed in this project, was submitted to the conference organisers in February 2019 and has now been published in the international journal *Applied Radiation and Isotopes*.

A meeting of the ICRM-GSWG was also held during the conference, which allowed further dissemination of the project's main findings.

AN GHNÍOMHAIREACHT UM CHAOMHNÚ COMHSHAOIL
Tá an Ghníomhaireacht um Chaomhnú Comhshaoil (GCC) freagrach as an gcomhshaol a chaomhnú agus a fheabhsú mar shócmhainn luachmhar do mhuintir na hÉireann. Táimid tiomanta do dhaoine agus don chomhshaol a chosaint ó éifeachtaí díobhálacha na radaíochta agus an truaillithe.

Is féidir obair na Gníomhaireachta a roinnt ina trí phríomhréimse:

Rialú: *Déanaimid córais éifeachtacha rialaithe agus comhlíonta comhshaoil a chur i bhfeidhm chun torthaí maithe comhshaoil a sholáthar agus chun díriú orthu siúd nach gcloíonn leis na córais sin.*

Eolas: *Soláthraímid sonraí, faisnéis agus measúnú comhshaoil atá ar ardchaighdeán, spriocdhírithe agus tráthúil chun bonn eolais a chur faoin gcinnteoireacht ar gach leibhéal.*

Tacaíocht: *Bímid ag saothrú i gcomhar le grúpaí eile chun tacú le comhshaol atá glan, táirgiúil agus cosanta go maith, agus le hiompar a chuirfidh le comhshaol inbhuanaithe.*

Ár bhFreagrachtaí

Ceadúnú
Déanaimid na gníomhaíochtaí seo a leanas a rialú ionas nach ndéanann siad dochar do shláinte an phobail ná don chomhshaol:
- saoráidí dramhaíola *(m.sh. láithreáin líonta talún, loisceoirí, stáisiúin aistrithe dramhaíola)*;
- gníomhaíochtaí tionsclaíocha ar scála mór *(m.sh. déantúsaíocht cógaisíochta, déantúsaíocht stroighne, stáisiúin chumhachta)*;
- an diantalmhaíocht *(m.sh. muca, éanlaith)*;
- úsáid shrianta agus scaoileadh rialaithe Orgánach Géinmhodhnaithe *(OGM)*;
- foinsí radaíochta ianúcháin *(m.sh. trealamh x-gha agus radaiteiripe, foinsí tionsclaíocha)*;
- áiseanna móra stórála peitril;
- scardadh dramhuisce;
- gníomhaíochtaí dumpála ar farraige.

Forfheidhmiú Náisiúnta i leith Cúrsaí Comhshaoil
- Clár náisiúnta iniúchtaí agus cigireachtaí a dhéanamh gach bliain ar shaoráidí a bhfuil ceadúnas ón nGníomhaireacht acu.
- Maoirseacht a dhéanamh ar fhreagrachtaí cosanta comhshaoil na n-údarás áitiúil.
- Caighdeán an uisce óil, arna sholáthar ag soláthraithe uisce phoiblí, a mhaoirsiú.
- Obair le húdaráis áitiúla agus le gníomhaireachtaí eile chun dul i ngleic le coireanna comhshaoil trí chomhordú a dhéanamh ar líonra forfheidhmiúcháin náisiúnta, trí dhíriú ar chiontóirí, agus trí mhaoirsiú a dhéanamh ar leasúchán.
- Cur i bhfeidhm rialachán ar nós na Rialachán um Dhramhthrealamh Leictreach agus Leictreonach (DTLL), um Shrian ar Shubstaintí Guaiseacha agus na Rialachán um rialú ar shubstaintí a ídíonn an ciseal ózóin.
- An dlí a chur orthu siúd a bhriseann dlí an chomhshaoil agus a dhéanann dochar don chomhshaol.

Bainistíocht Uisce
- Monatóireacht agus tuairisciú a dhéanamh ar cháilíocht aibhneacha, lochanna, uiscí idirchriosacha agus cósta na hÉireann, agus screamhuiscí; leibhéil uisce agus sruthanna aibhneacha a thomhas.
- Comhordú náisiúnta agus maoirsiú a dhéanamh ar an gCreat-Treoir Uisce.
- Monatóireacht agus tuairisciú a dhéanamh ar Cháilíocht an Uisce Snámha.

Monatóireacht, Anailís agus Tuairisciú ar an gComhshaol
- Monatóireacht a dhéanamh ar cháilíocht an aeir agus Treoir an AE maidir le hAer Glan don Eoraip (CAFÉ) a chur chun feidhme.
- Tuairisciú neamhspleách le cabhrú le cinnteoireacht an rialtais náisiúnta agus na n-údarás áitiúil *(m.sh. tuairisciú tréimhsiúil ar staid Chomhshaol na hÉireann agus Tuarascálacha ar Tháscairí)*.

Rialú Astaíochtaí na nGás Ceaptha Teasa in Éirinn
- Fardail agus réamh-mheastacháin na hÉireann maidir le gáis cheaptha teasa a ullmhú.
- An Treoir maidir le Trádáil Astaíochtaí a chur chun feidhme i gcomhair breis agus 100 de na táirgeoirí dé-ocsaíde carbóin is mó in Éirinn.

Taighde agus Forbairt Comhshaoil
- Taighde comhshaoil a chistiú chun brúnna a shainaithint, bonn eolais a chur faoi bheartais, agus réitigh a sholáthar i réimsí na haeráide, an uisce agus na hinbhuanaitheachta.

Measúnacht Straitéiseach Timpeallachta
- Measúnacht a dhéanamh ar thionchar pleananna agus clár beartaithe ar an gcomhshaol in Éirinn *(m.sh. mórphleananna forbartha)*.

Cosaint Raideolaíoch
- Monatóireacht a dhéanamh ar leibhéil radaíochta, measúnacht a dhéanamh ar nochtadh mhuintir na hÉireann don radaíocht ianúcháin.
- Cabhrú le pleananna náisiúnta a fhorbairt le haghaidh éigeandálaí ag eascairt as taismí núicléacha.
- Monatóireacht a dhéanamh ar fhorbairtí thar lear a bhaineann le saoráidí núicléacha agus leis an tsábháilteacht raideolaíochta.
- Sainseirbhísí cosanta ar an radaíocht a sholáthar, nó maoirsiú a dhéanamh ar sholáthar na seirbhísí sin.

Treoir, Faisnéis Inrochtana agus Oideachas
- Comhairle agus treoir a chur ar fáil d'earnáil na tionsclaíochta agus don phobal maidir le hábhair a bhaineann le caomhnú an chomhshaoil agus leis an gcosaint raideolaíoch.
- Faisnéis thráthúil ar an gcomhshaol ar a bhfuil fáil éasca a chur ar fáil chun rannpháirtíocht an phobail a spreagadh sa chinnteoireacht i ndáil leis an gcomhshaol *(m.sh. Timpeall an Tí, léarscáileanna radóin)*.
- Comhairle a chur ar fáil don Rialtas maidir le hábhair a bhaineann leis an tsábháilteacht raideolaíoch agus le cúrsaí práinnfhreagartha.
- Plean Náisiúnta Bainistíochta Dramhaíola Guaisí a fhorbairt chun dramhaíl ghuaiseach a chosc agus a bhainistiú.

Múscailt Feasachta agus Athrú Iompraíochta
- Feasacht chomhshaoil níos fearr a ghiniúint agus dul i bhfeidhm ar athrú iompraíochta dearfach trí thacú le gnóthais, le pobail agus le teaghlaigh a bheith níos éifeachtúla ar acmhainní.
- Tástáil le haghaidh radóin a chur chun cinn i dtithe agus in ionaid oibre, agus gníomhartha leasúcháin a spreagadh nuair is gá.

Bainistíocht agus struchtúr na Gníomhaireachta um Chaomhnú Comhshaoil
Tá an ghníomhaíocht á bainistiú ag Bord lánaimseartha, ar a bhfuil Ard-Stiúrthóir agus cúigear Stiúrthóirí. Déantar an obair ar fud cúig cinn d'Oifigí:
- An Oifig um Inmharthanacht Comhshaoil
- An Oifig Forfheidhmithe i leith cúrsaí Comhshaoil
- An Oifig um Fianaise is Measúnú
- Oifig um Chosaint Radaíochta agus Monatóireachta Comhshaoil
- An Oifig Cumarsáide agus Seirbhísí Corparáideacha

Tá Coiste Comhairleach ag an nGníomhaireacht le cabhrú léi. Tá dáréag comhaltaí air agus tagann siad le chéile go rialta le plé a dhéanamh ar ábhair imní agus le comhairle a chur ar an mBord.

EPA Research Report 416

Development and Application of Monte Carlo Models for High-purity Germanium Gamma Spectrometry

Authors: Luis León Vintró and Niall Murphy

Identifying Pressures

The aim of this research project was to develop and implement suitable Monte Carlo calibration methods for the assay of natural and artificial radionuclides using HPGe gamma spectrometers, so that self-attenuation and true coincidence summing effects can be corrected for, and detector efficiencies established for a variety of geometries and sample matrices without the need to carry out multiple, time-consuming and expensive measurements using certified calibration standards.

The accurate detector models needed to conduct these Monte Carlo simulations to compute the required corrections were obtained for each of the detectors at the EPA's radiometric laboratory using an automated software application based on GESPECOR. This is a dedicated Monte Carlo software package specifically developed for the efficiency calibration of HPGe gamma-ray spectrometers.

Informing Policy

The accurate calibration of the HPGe detectors in use at the EPA's ORM radiometric laboratory and the development of robust, well-validated methods to correct for self-attenuation and true coincidence summing effects in gamma spectrometry are essential to fulfil the EPA's advisory and information provision functions following an emergency under the National Emergency Plan for Nuclear Accidents (NEPNA) and the Major Emergency Framework (MEF) protocol for multi-agency response to a nuclear emergency.

Furthermore, given the importance of agriculture and aquaculture to the Irish economy, the ability to quickly produce accurate results in the aftermath of an accident, so that the levels can be assessed and compared with EU or international action levels in foodstuffs, is of significant national strategic importance.

Developing Solutions

A software application was developed as part of this project. The application makes use of a set of nominal input parameters describing an HPGe detector, together with experimentally determined full-energy peak efficiencies for a range of radionuclides in a variety of counting geometries, to produce an optimised model of the detector by applying suitable optimisation algorithms without any further user intervention.

Application of this optimisation approach to each of the HPGe detectors currently in operation at the EPA's ORM has shown that it is possible to achieve excellent agreement between experimental full-energy peak efficiencies and Monte Carlo calculations, with mean absolute deviations between modelled and experimental efficiencies of < 2% for all geometries and individual absolute deviation no higher than 4%.

Through a comprehensive set of characterisation and validation experiments, it has been demonstrated that the optimised models obtained can be used to confidently predict full-energy peak efficiencies for arbitrary source geometries by direct Monte Carlo simulation, to perform efficiency transfer from one matrix to another and to compute accurate values for self-attenuation and true coincidence summing correction factors.

EPA Research: McCumiskey House,
Richiew, Clonskeagh, Dublin 14.

Phone: 01 268 0100
Twitter: @EPAResearchNews
Email: research@epa.ie